Studies on synthesis characteristics and mechanism of cuprous oxide nanoparticles by plasma-assisted electrolysis

Jiandi LIU

English Engineering Program (e3)

Laboratory of Plasma Processing for Environmental Technologies

Division of Quantum Science and Engineering

Graduate School of Engineering

Hokkaido University

TABLE OF CONTENTS

Chapter 1 General Introduction 2
1.1 Plasma-liquid interaction 2
1.2 Nanomaterial synthesis by the plasma-liquid interaction 4
1.3 Plasma electrolysis 6
1.4 The synthesis of Cu_2O nanoparticles 12
1.5 Objectives and importance of this study 14
1.6 Outline of this study 14
Chapter 2 Facile synthesis of cuprous oxide nanoparticles by atmospheric-pressure argon plasma electrolysis 22
2.1 Introduction 22
2.2 Experimental Procedure 23
2.3 Results and Discussion 25
2.4 Conclusion 31
Chapter 3 The effect of the surfactants on the plasma electrolytic synthesis of cuprous oxide nanoparticles and their visible-light photocatalytic abilities 35
3.1 Introduction 35
3.2 Experimental Procedure 36
3.3 Results and Discussion 38
3.3.1 Comparison of the effects between glucose and ascorbic acid 38
3.3.2 The effects of the surfactant of CTAB 43
3.3 The effect of surfactant on the synthesis of Cu_2O nanoparticles 47
3.4 Conclusion 49
Chapter 4 Study on the influence factors affects the synthesis of Cu_2O nanoparticles by plasma electrolysis 53
4.1 Introduction 53
4.2 Experimental Procedure 54
4.3 Results and Discussion 56
4.3.1 Effect of NaCl concentration 56
4.3.2 Effect of dissolved oxygen 59
4.3.3 Effect of electrolyte temperature 62

4.3.4 Effect of pH value 65
4.4 Conclusions 69
Chapter 5 Study on the synthesis mechanism of Cu_2O nanoparticles synthesis and the comparison between plasma electrolysis and conventional electrolysis 73
5.1 Introduction 73
5.2 Synthesis mechanism of Cu_2O nanoparticles by plasma electrolysis 74
5.3 Cu_2O nanoparticles synthesized by conventional electrolysis 83
5.4 Comparison between Cu_2O nanoparticles synthesized by plasma and conventional electrolysis 88
5.5 Conclusion 89
APPENDIX EXPERIMENTS 92
Chapter 6 General Conclusions 95
6.1 Achievement of this study 95
6.2 Challenges and outlook for the future 97
ACHIVEMENTS 98
ACKNOWLEDGEMENT 100

Chapter 1 General Introduction

Chapter 1 General Introduction

1.1 Plasma-liquid interaction

Plasmas are regarded as the fourth fundamental states of matter immediately followed by solids, liquids and gases, which are closely related to human life and modern industry (figure 1.1). Discharge plasma is an electrically neutral medium of unbound positive and negative particles, accompanied by many highly reactive species, such as excited atoms and molecules, reactive radicals, ultraviolet (UV) photons, and so on. Because of its highly reactive compositions, it has presented powerful abilities in modern industry such as surface modification of materials and surface processing in the integrated circuits processing [1]. In these applications, plasma reacts either with gas or solid, but none of them are with liquids.

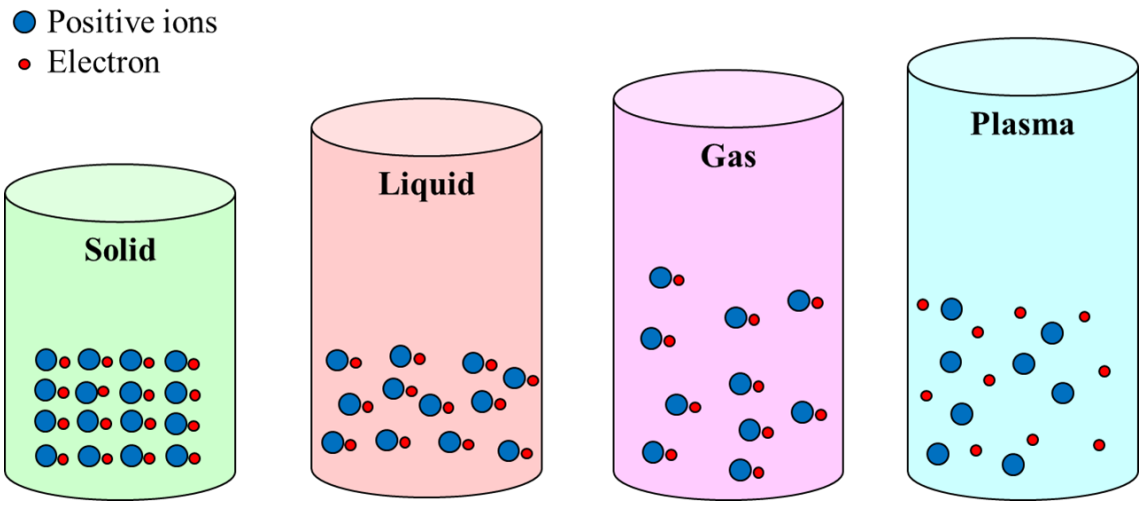

Figure 1.1. The fourth fundamental states of matter, solid, liquid, gas and plasma. Blue = positive ions, red = electrons.

Recently, the applications of plasma–liquid interactions have drawn much attention and are being developed rapidly with amounts of research being carried out due to the unique properties. In plasma–liquid interaction systems, the plasma discharges are placed in or over a liquid. When the plasma is in

or in contact with a liquid, a plasma-liquid interface appears. As shown in figure 1.2, in the gaseous plasma and the interface, many physical and chemical processes appear rapidly and produce a great amount of highly reactive species such as OH radical, H radical, solvated electron, O_3, H_2O_2, UV light, and so on [2]. Some of these ultra-reactive species like H radicals can hardly exist in normal reactive conditions. During the discharge, these highly reactive compositions can be transported from the gaseous plasma and the interface into the bulk liquid by diffusion and convection, leading to the further physical and chemical reactions in the liquid phase. Consequently, the plasma-liquid interface as well as bulk liquids can be reaction zones for many specific physical and chemical processes.

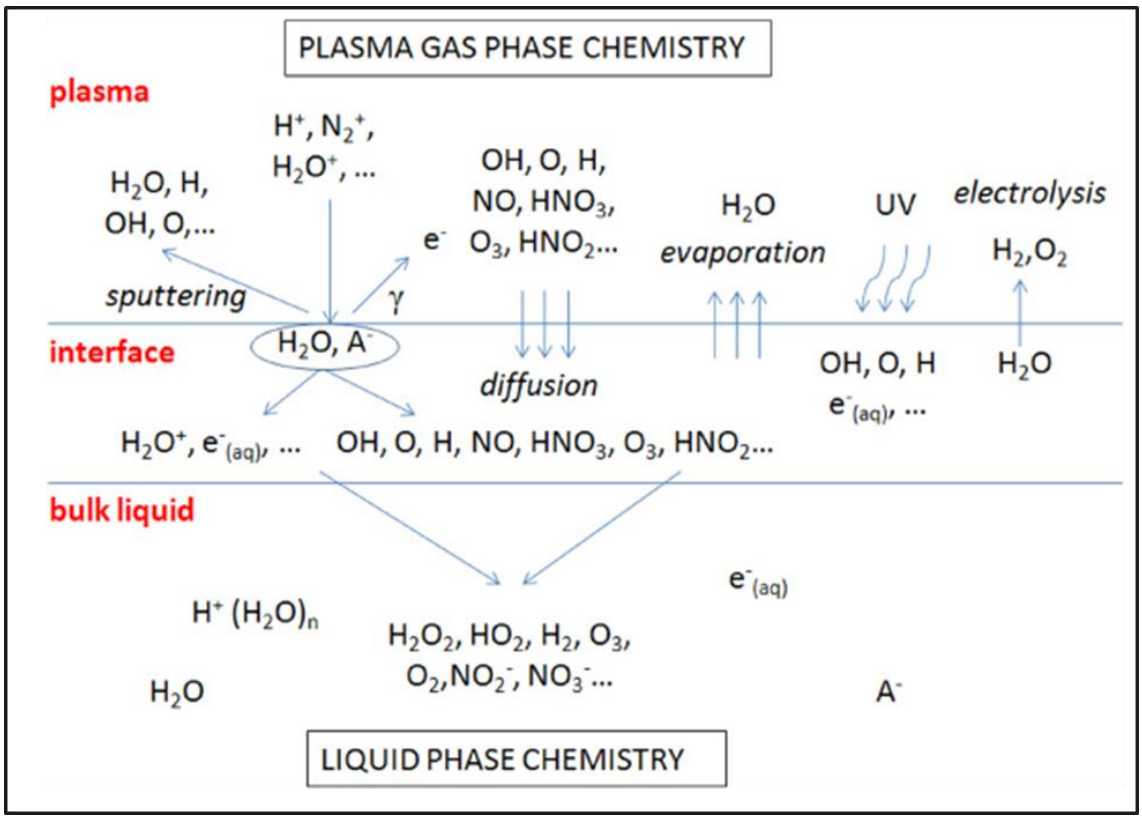

Figure 1.2. Schematic diagram of part of the highly reactive species produced via plasma in contact with a liquid. [2]

Due to the fact that plasma in and in contact with liquids are rich sources of highly reactive species, the plasma-liquid interactions have been applied to a variety of application areas including electrical

switching [3], analytical chemistry [4, 5], waste-water purification [6], nanomaterial synthesis [7], material processing [8, 9], chemical synthesis (such as H_2O_2, H_2) [10] and plasma medicines [11, 12]. These interesting applications have encouraged researchers to explore and broaden the field of plasma science.

1.2 Nanomaterial synthesis by the plasma-liquid interaction

Nanomaterial synthesis by the plasma–liquid interactions is a main focus among the amounts of applications of plasma–liquid interactions and has been well developed over the past several decades. In fact, using plasma-liquid interactions to synthesize nanomaterial is not unusual and it can be dated back to the late 1880s when Gubkin and coworkers [13], who used a discharge to reduce the silver ions in an aqueous solution of silver nitrate. However, in the next one hundred years, only a few alike researches were followed, for example, the production of iodine from aqueous solution of potassium iodide [14], the formation of hydrogen peroxide from dilute sulfuric acid solutions [15, 16] and the synthesis of amino acid from elemental carbon related materials [17-20]. One reason for the small number of researches may be the lack of the necessary equipment which makes it difficult to probe the formed materials during that period. Another one is that the researches on electrolysis induced by plasma-liquid interaction have attracted most of the attention.

Because of the rapidly developed plasma sources and the growing demands for large-scale synthesis of nanomaterials, the field of nanomaterial synthesis by plasma–liquid interactions has grown significantly in recent decades. It is well known that materials with nano-scale sizes perform quite different properties compared with bulk materials. The properties of nanoparticles are usually size-dependent and when the particle's size approaches the nanoscale, the number ratio of surface area to the number of bulk atoms increases rapidly, which usually affects the quantum confinement in semiconductor particles [21], localized surface plasmon resonance (LSPR) in metal particles [22], ferromagnetic and ferroelectric effects in magnetic materials [23] and the melting point [24] as well as the catalysis capability of materials [25]. Solution-based synthesis is one of the most common methods used for nanomaterial synthesis. It is based on the reduction of metal ions in solutions [26, 27]. This method has been proved to be a useful route for synthesizing nanomaterials with different sizes, shapes and compositions. Since the plasma-liquid interactions can produce various kinds of highly reactive

species, and the metal ions can dissolve into the liquid, it makes the unique plasma-liquid interactions system strongly attractive for nanomaterial synthesis.

Due to its unique properties, amounts of research have been carried out on the nanomaterial synthesis by the plasma-liquid interactions system, such as noble metals [28,29], magnetic materials [30-32], metal oxides [33-37], and carbon materials [36]. Kaneko and coworkers [38] have successfully synthesized gold nanoparticles by using plasma irradiation to ionic liquid and found that the hydrogen radicals in the ionic liquid generated by ion irradiation were effective for the synthesis. Chen et al. [39] synthesized Au nanoparticles from an $HAuCl_4$ aqueous solution with the capping agent deoxyribonucleic acid (DNA) by using a pulsed plasma at a pressure of 20 kPa. Zhong et al. [40] demonstrated a one-step microplasma-chemical method by which they successfully synthesized size controllable Au_xAg_{1-x} nanoparticle alloys in solution under ambient conditions. FeO_x nanoparticles can also be rapidly synthesized by atmospheric-pressure multi-microplasmas generated over a mixed aqueous solution of $FeCl_2$, dextrane and dimercaptosuccinic acid [41]. ZnO nanoparticles were synthesized by generating submerged plasma between Zn wire cathode and a Pt mesh anode in an aqueous solution of K_2CO_3 [42]. The power input resulted in the formation of flower-like ZnO nanoparticles or aggregated ZnO nanoparticles. C_{60} was synthesized by electrical discharges in liquid toluene [43]. Sano et al [44, 45] reported that carbon 'onion' was rapidly formed by using arc discharge in water with graphite.

The synthesis of metallic and metallic oxide nanoparticles has been the main focus among the research of the nanomaterial synthesis by plasma–liquid interactions. In principle, the electrons generated from the plasma cathode can reduce any metal ions in the liquid. Therefore, the prototype of using the plasma as the cathode and the liquid as the anode has been widely used in many subsequent instances for synthesizing nanomaterials. Compared with the conventional, solution-based synthesis methods, one of the key advantages of nanomaterial synthesis via plasma–liquid interactions is that the reducing agents can be automatically produced during the discharge. The plasma can not only produce free electrons and ions with certain energies, but also highly reactive radicals produced at the plasma-liquid interface. These highly reactive free electrons, ions and radicals can lead numerous physical and chemical reactions in the plasma-liquid interface as well as in the bulk liquid. The synthesis of nanomaterials can be attributed to the complicated physical and chemical processes in the plasma-liquid interactions, including reduction and oxidation. The synthesis process can be tuned by both the liquid

phase as in conventional, solution-based synthesis, and by the gaseous plasma such as applied voltage and current. Since the reducing species produced by the plasma-liquid interactions have different lifetimes and different reducing abilities [46], the process of nanomaterial synthesis can also be tuned by tailoring the relative yields of specific reducing species from the plasma phase. Although the diversity of reducing species in the plasma-liquid interactions increases the complexity of analyzing the synthesis mechanism, it also expands the routes available to tune the synthesis process. Moreover, the reactive radicals in the plasma-liquid interactions allow the possibility of controlling the shape and composition of nanomaterials by adjusting the plasma parameters.

1.3 Plasma electrolysis

The plasma-liquid interactions system can be classified based on the method for generating plasmas or the configurations. What's more, the type of interactions between plasma and liquid is particularly important because it highly influences the plasma properties. The type of plasma–liquid interaction system can be roughly classified into plasma in and in contact with liquid. As shown in figure 1.3, a typical classification scheme is as follows.

- Direct liquid phase discharges
- Gas phase discharges

  Without direct contact/electrical coupling with the liquid

  With direct contact/electrical coupling with the liquid (liquid electrode)

  At the plasma liquid interphase (surface discharges)
- Multiphase discharges including

  Gas phase plasmas with dispersed liquid phase (aerosols)

  Gas phase plasmas in dispersed gas phase (bubbles) in liquid

This classification scheme emphasizes the different kinds of interactions of plasmas as well as the differences in plasma generation and the transport of heat, mass and species [47].

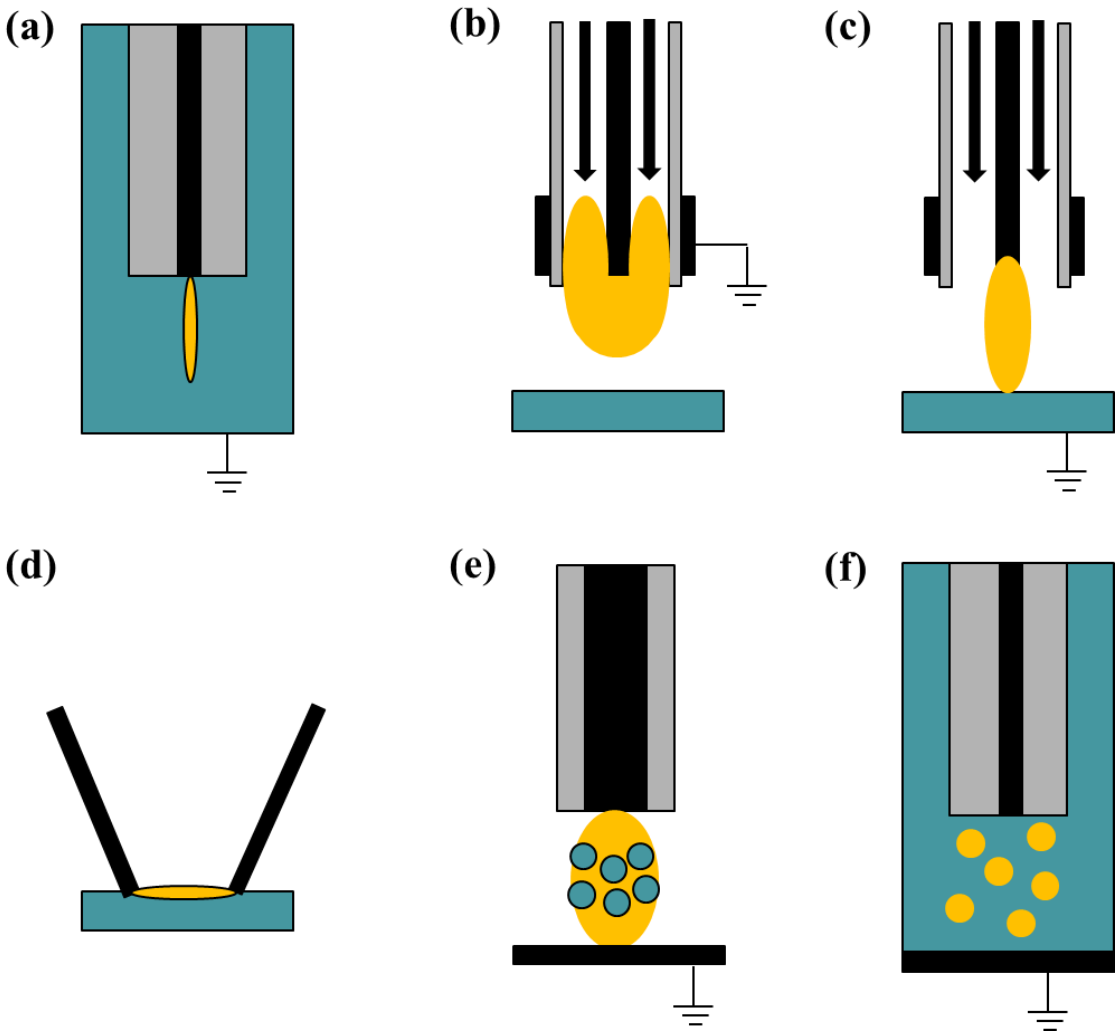

Figure 1.3. Schematic of different discharges used in plasma-liquid interactions system: (a) direct discharge in liquid, (b) plasma jet without direct contact with liquid, (c) gas phase plasma with liquid electrode, (d) surface discharge, (e) gas phase plasma with dispersed liquid phase (aerosols) and (f) discharges in bubbles. Green = liquid, yellow = plasma, grey = dielectric, black = metal electrodes. [47]

Among these types of plasma-liquid interaction systems, gaseous plasmas with direct contact/electrical coupling with the liquid, which is also referred to as plasma electrolysis, have attracted a lot of interests because of the similarity to the conventional electrolysis. In the conventional electrolysis system, both the electrodes are immersed in electrolyte. While in the plasma electrolysis system, one electrode is submerged and the other is placed over the solution instead of being submerged. By applying a high voltage between the electrode and the solution surface (~kV), the interstitial gas between the electrode and the liquid breaks down to generate a conductive plasma. Depending on the electrode polarity, the plasma electrolysis has two different modes as shown in figure 1.4.

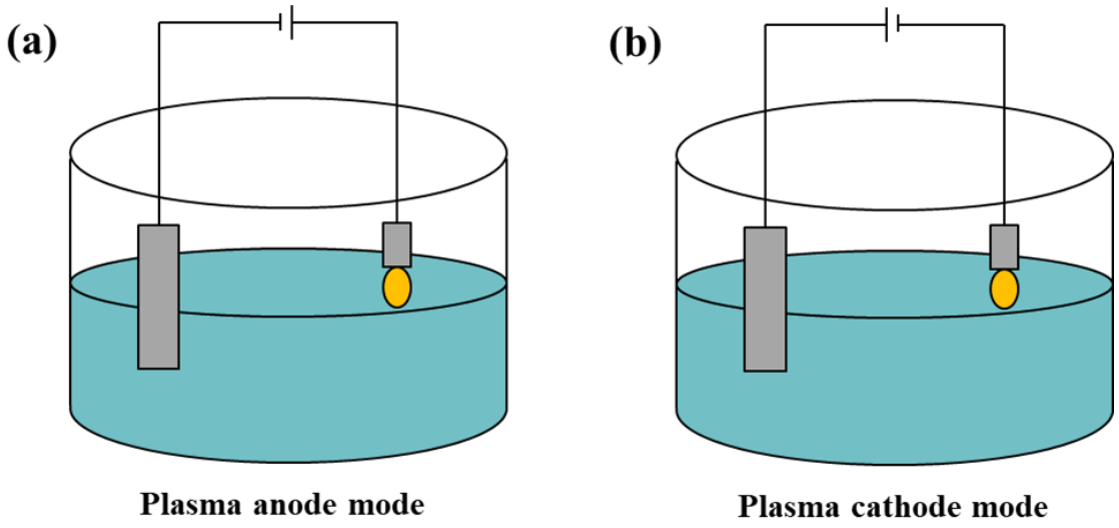

Figure 1.4. The schematic diagrams of two plasma modes: (a) plasma anode mode and (b) plasma cathode mode.

Figure 1.4(a) presents the plasma anode mode. The ions (depending on the working gas) in the gaseous plasma phase move toward the liquid surface. During the transport to the liquid surface, they possess an energy on the order of tens to hundreds of eV which depends on the gas pressure and the discharge voltage. Then the energetic ions attack the liquid surface, consequently generating secondary electrons and decompose the constituents in the liquid. When the liquid phase is aqueous solution, water molecules can be decomposed into atomic hydrogen and OH radical, which has been confirmed by

optical emission spectra detected near the liquid surface [46]. Atomic hydrogen can combine to form H_2. H_2O_2 can be formed in plasma-liquid interactions by many different pathways including the direct combination of OH radicals [48]. Atomic hydrogen and H_2, which have high reducing ability, are able to reduce metal ions in the solution. Even though H_2O_2 is usually a strong oxidizing species, it can present different reducing abilities for certain metal ions like Au (III) shown in equation (1.1) which depends on the pH value [49–51].

$$3H_2O_2 + 2Au(III) \rightarrow 2Au(0) + 6H^+ + 3O_2 \quad (1.1)$$

The hydride (H^-) which is a very strong reducing species can be formed by dissociative electron attachment and can also dissolve into the liquid.

$$H_2O + e \rightarrow H^- + OH \quad (1.2)$$

UV light is usually observed in plasma-liquid interactions systems [52, 53]. Therefore, the high energy of UV photons can be transferred to water, producing potential reducing/oxidizing species like atomic H and OH.

$$H_2O + hv \rightarrow H + OH \quad (1.3)$$

For the plasma cathode mode, as indicated in figure 1.4(b), electrons from the gaseous plasma phase directly bombard the liquid surface and then dissolve into the liquid to form solvated electrons. In addition, atomic H, H^-, OH, H_2 and H_2O_2 can also be generated in the gaseous plasma phase by decomposing water vapor and cascade reactions. UV light can also function as the energy source for producing atomic H and OH.

As discussed above, both the plasma anode mode and the cathode mode can generate the same reducing species. In addition to the reducing species, the oxidizing species including atomic O [54], O_3 [55] and OH radicals, can also be generated in plasma-liquid interactions. All the species can diffuse into the bulk liquid. The OH radicals are easily combined to form H_2O_2, then H_2O_2 passes through the interface and drift in the bulk liquid. H_2O_2 as well as dissolved oxygen can act as oxidizing species. As

a result, reactive metals such as iron, cobalt, might be oxidized again after the formation of metal nanoparticles by the reduction of metal ions. It is noted that these reducing and oxidizing species can be classified as two types considering their lifetimes: short-lived and long-lived species. The short-lived reactive species include free electrons, solvated electrons, atomic O, atomic hydrogen, OH radicals, H^- and UV light which quickly decay after the termination of plasma. Therefore, even though the reducing species such as solvated electrons have a very strong reducing ability and can reduce most metal ions in an aqueous solution. They can only penetrate into a certain depth of the liquid. Thus, the reduction of metal ions takes place mainly at the plasma-liquid interface and at a limited depth under the liquid surface. On the other hand, the long-lived reactive species such as H_2, dissolved oxygen and H_2O_2 can exist in the bulk part of the solution for a long time. Nanomaterials can be synthesized under the competition between the two types of reactive species.

Depending on the compositions of the aqueous solutions, the plasma electrolysis can also be divided into two types: one is using metallic ions containing solution as the electrolyte and the other is using conductive aqueous solution without specific metallic ions such as NaCl and KCl solution as electrolyte.

The type of using metallic ions containing solution as electrolyte has been widely studied in the synthesis of noble metal nanoparticles including Au and Ag nanoparticles (figures 1.5(a) and (b)). In this type, the metallic ions which are contained in solution can be directly reduced to zero valent metal as $M^{n+} + ne^- = M$, and then form metal nanoparticles. For example, in the case of the Ag nanoparticles synthesized by plasma-liquid interactions, the Ag^+ ions are directly reduced by solvated electrons or H radicals to Ag^0 and finally form Ag nanoparticles.

However, when using transition metal ions containing solution as the electrolyte, things have become different. It is well known that the standard Gibbs free energy (ΔG°) of a chemical reaction can be expressed as $\Delta G^\circ = -nFE^\circ$, where n is the electron number involved in the chemical reaction, F is the Faraday constant (9.65×10^4 C/mol) and E° is the standard reduction potential. The polarity of ΔG° determines whether a chemical reaction can be proceeded or not. Based on the data of E^0 shown in equation (1.4) to equation (1.7), we can know that it is easier for $AuCl_4^-$ and Ag^+ ions to be reduced.

$$AuCl_4^- + 3e \rightarrow Au + 4Cl^-, E^0 = +1.50V \quad (1.4)$$

$$Ag^{+} + e \rightarrow Ag, E^{0} = +1.00V \quad (1.5)$$

$$Cu^{2+} + 2e \rightarrow Cu, E^{0} = +0.40V \quad (1.6)$$

$$Fe^{2+} + 2e \rightarrow Fe, E^{0} = -0.44V \quad (1.7)$$

In addition, it is more complicated in the case of transition metals, since they have at least two different valence states such as Fe^{2+} and Fe^{3+} (figure 1.5(c)). The metallic ions are tending to be hydrated with OH^{-} to form metal hydroxide which makes it more difficult to synthesize pure transition metal nanoparticles by plasma electrolysis. As so far, the most work of synthesizing transition metal nanoparticles by plasma electrolysis resulted in transition metal oxide nanoparticles.

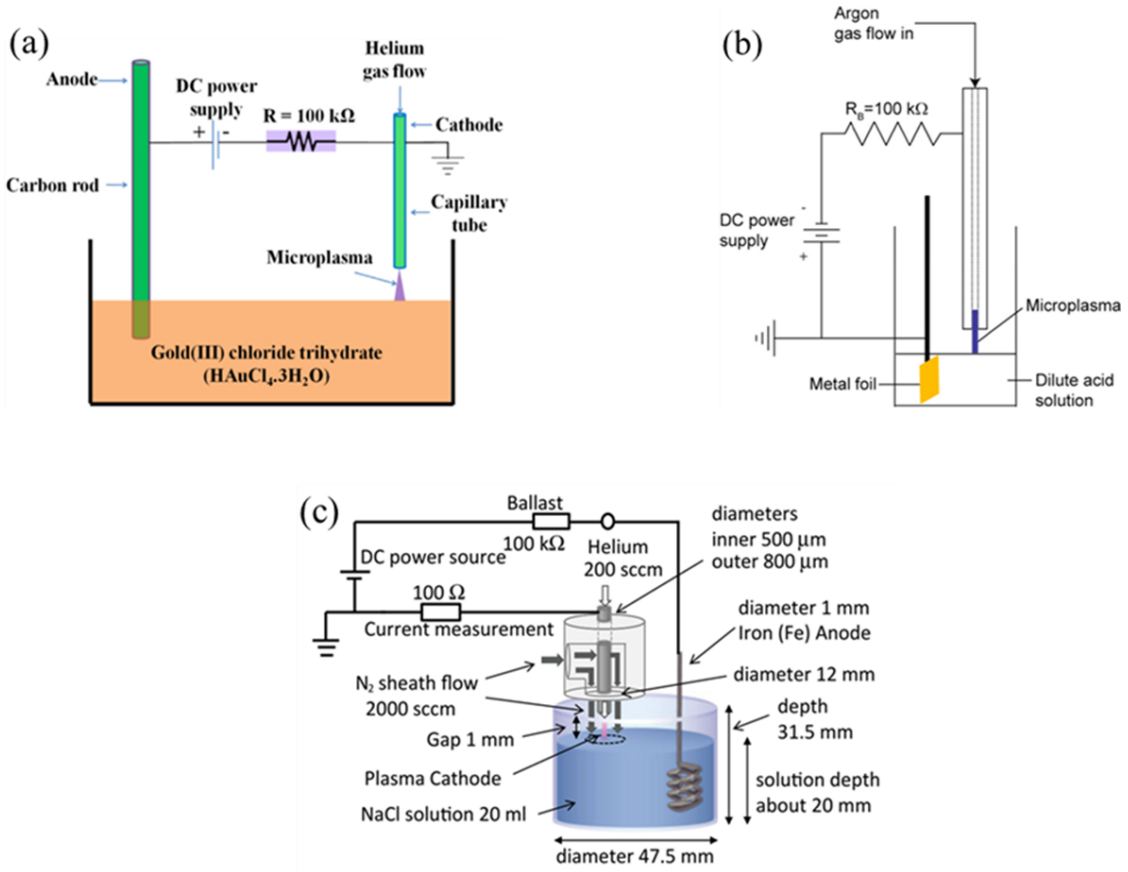

Figure 1.5. Schematic diagrams of the synthesis of (a) Au, (b) Ag and (c) Magnetite nanoparticles by plasma electrolysis. [56-58]

The other type without specific metallic ions contained in solution is commonly used to synthesize transition metal oxide nanoparticles such as magnetite [59]. In this case, plasma is usually used as the cathode while the counter electrode is a metal electrode composed of a target element. This metal electrode plays not only the role of anode, but also as the source of the metallic ions via anodic dissolution. It is noted that the anodic dissolution has an important effect on this type of nanomaterial synthesis. For example, Shirai and coworkers have reported that magnetite nanoparticles could be synthesized by using atmospheric-pressure DC glow-discharge electrolysis [59]. In his work, an iron electrode was immersed in the solution as the anode and NaCl aqueous solution was prepared as an electrolyte. Because the anodic dissolution took place at the iron anode, Fe^{2+} ions were liberated into the solution. After the plasma treatment, the magnetite nanoparticles were synthesized.

1.4 The synthesis of Cu_2O nanoparticles

Cuprous oxide (Cu_2O) is a typical p-type semiconductor which possesses a narrow bandgap energy of 2.2 eV [59]. It has unique optical, electronic, and magnetic properties due to its specific physical and chemical properties. Recently, due to their potential applications, such as in solar cells [60], gas sensing [61], magnetic storage devices [62], and catalysis [63-70], a lot of interests has been increasingly shown towards the synthesis of Cu_2O nanoparticles as well as the study of their properties. Various kinds of methods have been developed to synthesize Cu_2O nanoparticles with different sizes and shapes, including thermal relaxation [71], hydrothermal treatment [72], solution-phase synthesis [73], electrodeposition [74,75], the arc discharge process [76], sonochemical method [77], chemical precipitate [78], and irradiation process [79].

Among these methods, the chemical precipitation method is the typical solution-based method to synthesize Cu_2O nanoparticles with controlled sizes and shapes. The schematic representation of the synthesizing Cu_2O nanoparticles by chemical precipitation method [80] is shown in figure 1.6. At first, the Cu ions contained solution is prepared by dissolving copper acetate into aqueous solution. Then NaOH is added into the solution under magnetic stirring. Blue flocculent precipitate is formed rapidly and aqueous $Cu(OH)_2$ is produced. In the next step, a solution of reducing agent is added into the prepared $Cu(OH)_2$ solution. Within a few minutes, the deep blue solution gradually becomes colorless and then it turns burgundy color, which suggests the formation of Cu_2O colloid in presence of oxygen

atmosphere.

The reactions during the synthesis of Cu_2O can be described as follow:

$$Cu^{2+} + 2OH^- \rightarrow Cu(OH)_2 \quad (1.8)$$

$$2Cu(OH)_2 + Reducing\ agent \rightarrow Cu_2O \downarrow + H_2O + Product \quad (1.9)$$

According to these equations, it's obvious that the synthesis of Cu_2O is a two-step process: first is the formation of $Cu(OH)_2$ and the next is the reduction of $Cu(OH)_2$ to Cu_2O. Therefore, in the chemical precipitation method, the alkaline condition and reducing agent are necessary. As aforementioned, plasma electrolysis can produce lots of reducing species as well as OH^- ions. Therefore, it is possible to synthesize Cu_2O nanoparticles by using plasma electrolysis. In addition, the sizes and shapes of the particles can also be tuned by adjusting not only the liquid parameters, but also the plasma parameters.

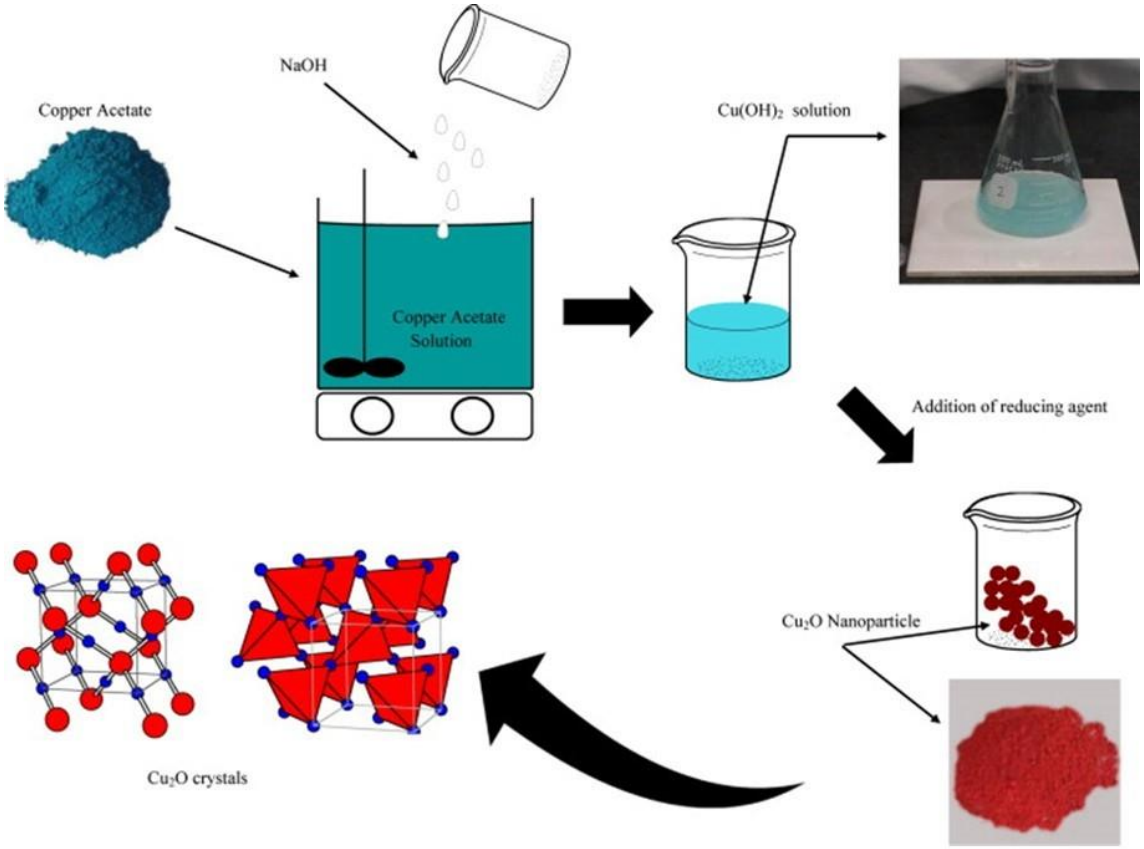

Figure 1.6. A schematic diagram of the representation of the Cu_2O nanoparticles synthesis. [80]

1.5 Objectives and importance of this study

Plasma-liquid interactions are rich sources of highly reactive species including solvated electron, atomic H, OH radical, O_3 and H_2O_2. These reactive species possess either highly reducing or oxidizing abilities. As aforementioned, magnetite (Fe_3O_4) nanoparticles were successfully synthesized by using plasma electrolysis. In this dissertation, we have chosen Cu as the raw material because it's cheap and widely used. Therefore, the objectives of this dissertation are synthesizing Cu_2O nanoparticles by using plasma electrolysis method, exploring the photocatalytic abilities of obtained samples and revealing the synthesis mechanism of Cu_2O nanoparticles.

During the study on the synthesis mechanism of Cu_2O nanoparticles, we have investigated various kinds of influence factors that affect the synthesis of Cu_2O nanoparticles and found out that the anodic dissolution of Cu and the OH^- ion (referred to as pH value) dominated the synthesis process. Based on our knowledge, the anodic dissolution and the production of OH^- ions are also existing in conventional electrolysis. We have compared plasma electrolysis and conventional electrolysis, and observed the production of Cu_2O nanoparticles via conventional electrolysis when the synthesis conditions were optimized. This result indicates that the synthesis mechanism in both plasma electrolysis and conventional electrolysis is the same even though we have found several differences between the obtained products synthesized by the two methods.

Revealing the synthesis mechanism is one of the most important research in the nanomaterial synthesis by plasma-liquid interactions. In this dissertation, we have proposed the synthesis mechanism of Cu_2O nanoparticles by using plasma electrolysis. The physical and chemical processes during the plasma discharge are very complicated. We must consider not only the functions of plasma, but also the other factors. The synthesis mechanism of Cu_2O nanoparticles via plasma electrolysis can be extended to other transition metals. Plasma electrolysis is a promising method to synthesize the metal oxide nanoparticles of Mn, Co and Ti.

1.6 Outline of this study

In this dissertation, we have used atmospheric-pressure plasma electrolysis to synthesize Cu_2O nanoparticles. Firstly, Cu_2O nanoparticles were successfully synthesized by a simple plasma electrolysis system in association with glucose. Then we investigated the effects of added surfactants on the shapes

and sizes of the products and their photocatalytic abilities. In order to clarify the synthesis mechanism of Cu_2O nanoparticles, we also conducted the experiments using NaCl solutions without any impurity and studied the influence factors which affect the synthesis of Cu_2O nanoparticles. Based on these results, we proposed the synthesis mechanism of Cu_2O nanoparticles by plasma electrolysis and made a comparison between plasma electrolysis and conventional electrolysis.

In Chapter 1, the general introduction of this thesis was presented. It outlined the plasma-liquid interactions, the nanomaterial synthesis by plasma-liquid interactions, plasma electrolysis as well as the synthesis of Cu_2O nanoparticles. Depending on the theory, it is possible to synthesize Cu_2O nanoparticles by using plasma electrolysis.

In Chapter 2, we described the successful synthesis of Cu_2O nanoparticles by using a simple atmospheric-pressure argon plasma electrolysis system in the presence of glucose. The results proved that it is possible to synthesize Cu_2O nanoparticles by using plasma electrolysis. And the influence of glucose concentrations on the crystallinity and shape of the final products was also experimentally investigated. In this stage, we believed that the formation of Cu_2O nanoparticles was based on the reduction of a coordination complex of $Cu_2(OH)_2^{2+}$ by the reducing species produced by plasma-liquid interactions.

In Chapter 3, we described the experiments for studying the effects of the surfactants including glucose, ascorbic acid and cetyltrimethylammonium bromide (CTAB), on the shapes and sizes of the obtained products. The photocatalytic abilities of the produced products were also tested by visible-light photocatalytic degradation of organic dye methyl orange (MO). The results showed that the surfactant of glucose (2.0 mM) was favorable for obtaining Cu_2O nanoparticles with high absorption efficiency of MO molecules, while the surfactant of ascorbic acid (2.0 mM) favored the formation of Cu_2O nanoparticles with strong visible-light photocatalytic activity on the MO degradation. And the synthesized Cu_2O nanospheres by using CTAB showed good photocatalytic activity on MO degradation.

In Chapter 4, we described the study on the influence factors affect the synthesis of Cu_2O nanoparticles. Different from chapters 2 and 3, the electrolyte in this work was NaCl solution without any impurity. The effects of the concentration of NaCl solution, the concentration of dissolved oxygen, the electrolyte temperature and the pH value of electrolyte, were experimentally investigated. Some of these parameters affected the synthesis process but some were not. Among these parameters, we found that the NaCl concentrations and the pH values of the electrolyte as well as the anodic dissolution of the

Cu anode, dominated the synthesis of Cu_2O nanoparticles.

In Chapter 5, we described the proposed possible synthesis mechanism of the Cu_2O nanoparticles on the basis of experimental results. In this stage, we found out that our expectation in chapter 2 was not correct. The reaction between $CuCl_2^-$ produced via the anodic dissolution of Cu and OH^- produced by plasma irradiation is responsible for the formation of Cu_2O nanoparticles rather than the reducing species produced by plasma-liquid interactions. Since the anodic dissolution of Cu and the production of OH^- occurred in conventional electrolysis, the formation of Cu_2O nanoparticles by conventional electrolysis is also possible in principle. The results showed Cu_2O nanoparticles could also be synthesized by conventional electrolysis if the synthesis parameters were adjusted. Then, the comparison between conventional electrolysis and plasma electrolysis was explored. We found the differences between the obtained products synthesized by conventional electrolysis and plasma electrolysis. There was the synthesis rate, the minimum NaCl concentration, and the size and the shape of synthesized nanoparticles.

In Chapter 6, we presented the general conclusions. It summarized this thesis and the experimental results. The future research and prospects were also outlined in this chapter.

In this dissertation, we proved the possibility of using plasma electrolysis to rapidly synthesize Cu_2O nanoparticles and investigated various kinds of parameters which affect the synthesis products. We proposed the synthesis mechanism of Cu_2O nanoparticles by plasma electrolysis on the basis of the experimental results and found it could also occur in the conventional electrolysis. As a result, this thesis gives a new opinion on the nanomaterial synthesis by plasma electrolysis especially in the case of transition metal nanoparticles.

References

[1] Lieberman M A and Lichtenberg A J, Principles of Plasma Discharges and Materials Processing (New Jersey: Wiley-Interscience) (2005).

[2] Samukawa S, Hori M, Rauf S, Tachibana K, Bruggeman P, Kroesen G, Whitehead J C, Murphy A B, Gutsol A F, Starikovskaia S, J. Phys. D: Appl. Phys. **45** 253001 (2012).

[3] Martin J C, J.C. Martin on Pulsed Power (New York: Plenum) (1996).

[4] Webb M R and Hieftje G M, Anal. Chem. **81** 862 (2009).

[5] Smoluch M, Mielczarek P and Silberring J, Mass Spectrom. Rev. **35** 22 (2016).

[6] Foster J E, Sommers B S, Gucker S N, Blankson I M and Adamovsky G, IEEE Trans. Plasma Sci. **40** 1311 (2012).

[7] Mariotti D, Patel J, Svrcek V and Maguire P, Plasma Proc. Polym. **9** 1074 (2012).

[8] Ishijima T, Nosaka K, Tanaka Y, Uesugi Y, Goto Y and Horibe H, Appl. Phys. Lett. **103** 142101 (2013).

[9] Friedrich J F, Mix N, Schulze R-D, Meyer-Plath A, Ranjit J R and Wettmarshausen S, Plasma Proc. Polym. **5** 407 (2008).

[10] Bruggeman P J and Locke B R, Low Temperature Plasma Technology ed P K Chu and X P Lu (London: Taylor and Francis) (2013).

[11] Sato M, Ohgiyama T and Clements J S, IEEE Trans. Ind. Appl. **32** 106 (1996).

[12] Fridman G, Friedman G, Gutsol A, Shekhter A B, Vasilets V N and Fridman A, Plasma Proc. Polym. **5** 503 (2008).

[13] Gubkin J, Ann. Phys., Lpz. **268** 114 (1887).

[14] Klüpfel K, Ann. Phys., Lpz. **321** 574 (1905).

[15] Makowetsky A, Z. Elektrochem. **17** 217 (1911).

[16] Hickling A and Ingram M, Trans. Faraday Soc. **60** 783 (1964).

[17] Harada K, Amino acid synthesis by glow discharge electrolysis: a possible route for prebiotic synthesis of amino acids The Origin of Life and Evolutionary Biochemistry K Dose et al ed (New York: Plenum) (1974).

[18] Harada K and Iwasaki T, Nature **250** 426 (1974).

[19] Harada K and Iwasaki T, Chem. Lett. **4** 185 (1975).

[20] Harada K and Suzuki S, Nature **266** 275 (1977).

[21] Cahay M, Proc. 6th Int. Symp. Quantum Confinement: Nanostructured Materials and Devices (San Francisco, CA: The Electrochemical Society) (2001).

[22] Zeng S, Yong K-T, Roy I, Dinh X-Q, Yu X and Luan F, Plasmonics **6** 491 (2011).

[23] Gittleman J, Abeles B and Bozowski S, Phys. Rev. B **9** 3891 (1974).

[24] Qi W and Wang M, Mater. Chem. Phys. **88** 280 (2004).

[25] Daniel M-C and Astruc D, Chem. Rev. **104** 293 (2004).

[26] Tao A R, Habas S and Yang P, Small **4** 310 (2008).

[27] Xia Y, Xiong Y, Lim B and Skrabalak S E, Angew. Chem. Int. Edn **48** 60 (2009).

[28] Shirafuji T, Ueda J, Nakamura A, Cho S P, Saito N, Takai O, Jpn. J. Appl. Phys. **52** 126202 (2013).

[29] Pootawang P, Saito N, Takai O, Mater. Lett. **65** 1037 (2011).

[30] Kelgenbaeva Z, Omurzak E, Takebe S, Abdullaeva Z, Sulaimankulova S, Iwamoto C, Mashimo T, Jpn. J. Appl. Phys. **52** 11NJ02 (2013).

[31] Abdullaeua Z, Omurzak E, Iwamoto C, Ganapathy H S, Sulaimankulova S, Chen L L, Mashimo T, Carbon **50** 1776 (2012).

[32] Kelgenbaeva Z, Omurzak E, Takebe S, Sulaimankulova S, Abdullaeva Z, Iwamoto C, Mashimo T, J. Nanopart. Res. **16** 2603 (2014).

[33] Saito G, Hosokai S, Tsubota M, Akiyama T, J. Appl. Phys. **110** 023302 (2011).

[34] Saito G, Hosokai S, Akiyama T, Mater. Chem. Phys. **130** 79 (2011).

[35] Du C M, Xiao M D, Sci. Rep. **4** 7339 (2014).

[36] Hagino T, Kondo H, Ishikawa K, Kano H, Sekine M, Hori M, Appl. Phys. Express **5** 035101 (2012).

[37] Liu J D, Chen Q, Li J S, Xiong Q, Yue G H, Zhang X H, Yang S Z, Liu Q H, J. Phys. D Appl. Phys. **49** 275201 (2016).

[38] Baba K, Kaneko T, Hatakeyama R, Appl. Phys. Express **2** 035006 (2009).

[39] Chen Q, Kaneko T and Hatakeyama R, Chem. Phys. Lett. **521** 113 (2012).

[40] Yan T, Zhong X, Rider A E, Lu Y, Furman S A, Ostrikov K, Chem. Commun. **50** 3144 (2014).

[41] Létourneau M, Sarra-Bournet C, Laprise-Pelletier M and Fortin M-A, Plasma–liquid electrochemistry: a fast method for synthesizing magnetic nanoparticles Int. Conf. Trends in Nanotechnology (Madrid, Spain) (2012).

[42] Saito G, Hosokai S and Akiyama T, Mater. Chem. Phys. **130** 79 (2011).

[43] Beck M T, Dinya Z, Kéki S and Papp L, Tetrahedron **49** 285 (1993).

[44] Sano N, Wang H, Chhowalla M, Alexandrou I and Amaratunga G, Nature **414** 506 (2001)

[45] Pech D, Brunet M, Durou H, Huang P, Mochalin V, Gogotsi Y, Taberna P-L and Simon P, Nat. Nanotechnol. **5** 651 (2010).

[46] Chen Q, Kaneko T and Hatakeyama R, Appl. Phys. Express **5** 6201 (2012).

[47] Bruggeman P J et al., Plasma Sources Sci. Technol. **25** 053002 (2016).

[48] Locke B R and Shih K-Y, Plasma Sources Sci. Technol. **20** 034006 (2011).

[49] Pourbaix M, Green J, Staehle R W and Kruger J, Lectures on Electrochemical Corrosion (New York: Springer) (1973).

[50] Rajeshwar K and Ibanez J G, Environmental Electrochemistry: Fundamentals and Applications in Pollution Sensors and Abatement (San Diego, CA: Academic) (1997).

[51] Haynes W M, Lide D R and Bruno T J, CRC Handbook of Chemistry and Physics 2012–2013 (Boca Raton, FL: CRC Press) (2012).

[52] Chen Q, Li J, Saito K and Shirai H, J. Phys. D: Appl. Phys. **41** 175212 (2008).

[53] Bruggeman P and Leys C, J. Phys. D: Appl. Phys. **42** 053001 (2009).

[54] Park Y S, Ku S H, Hong S H, Kim H J and Piepmeier E H, Spectrochim. Acta B **53** 1167 (1998).

[55] Lukes P, Clupek M, Babicky V, Janda V and Sunka P, J. Phys. D: Appl. Phys. **38** 409 (2005).

[56] J Patel1, L Nemcov ˇ a´2,3, P Maguire1, W G Graham2 and D Mariotti, Nanotechnology 24 245604 (2013).

[57] Huang X Z, Zhong X, Lu Y, Li Y S, Rider A E, Furman S A, Ostrikov K, Nanotechnol. **24** 095604 (2013).

[58] Yamazaki Y et al., Jpn. J. Appl. Phys. **57** 096203 (2018).

[59] Lu C, Qi L, Yang J, Wang X, Zhang D, Xie J and Ma J, Adv. Mater. **17** 2562 (2005).

[60] Cui J and Gibson U J, J. Phys. Chem. C **114** 6408 (2010).

[61] Zhang J, Liu J, Peng Q, Wang X and Li Y, Chem. Mater. **18** 867 (2006).

[62] Li X, Gao H, Murphy C J and Gou L, Nano Lett. **4** 1903 (2004).

[63] Kondo J, Chem. Commun. **357** (1998).

[64] de Jongh P and Kelly J, Chem. Commun. **1069** (1999).

[65] Barreca D, Fornasiero P, Gasparotto A, Gombac V, Maccato C, Montini T and Tondello E, ChemSusChem **2** 230 (2009).

[66] Huang L, Peng F, Yu H and Wang H, Solid State Sci. **11** 129 (2009).

[67] Zhang Y, Deng B, Zhang T, Gao D and Xu A-W, J. Phys. Chem. C **114** 5073 (2010).

[68] Xu H, Wang W and Zhu W, J. Phys. Chem. B **110** 13829 (2006).

[69] Shoeib M A, Abdelsalam O E, Khafagi M G and Hammam R E, Adv. Powder Technol. **23** 298 (2012).

[70] Ho J-Y and Huang M H, J. Phys. Chem. C **113** 14159 (2009).

[71] Deki S, Akamatsu K, Yano T, Mizuhata M and Kajinami A, J. Mater. Chem. **8** 1865 (1998)

[72] Yu H, Yu J, Liu S and Mann S, Chem. Mater. **19** 4327 (2007).

[73] Gou L and Murphy C J, Nano Lett. **3** 231 (2003).

[74] Huang L, Wang H, Wang Z, Mitra A, Zhao D and Yan Y, Chem. Mater. **14** 876 (2002).

[75] Zhang S, Zhang S, Peng F, Zhang H, Liu H and Zhao H, Electrochem. Commun. **13** 861 (2011).

[76] Yao W-T, Yu S-H, Zhou Y, Jiang J, Wu Q-S, Zhang L and Jiang J, J. Phys. Chem. B **109** 14011 (2005).

[77] Sun D D, Du Y, Tian X Y, Li Z F, Chen Z T, Zhu C F, Mater. Res. Bull. **60** 704 (2014).

[78] Gou L F, Murphy C J, Nano Lett. **3** 231 (2003).

[79] Liu W J, Chen G H, He G H, Zhang W, J. Nanopart. Res. **13** 2705 (2011).

[80] Rastabi A et al., J. Ind. Eng. Chem. **22** 34 (2015).

Chapter 2 Facile synthesis of cuprous oxide nanoparticles by atmospheric-pressure argon plasma electrolysis

Chapter 2 Facile synthesis of cuprous oxide nanoparticles by atmospheric-pressure argon plasma electrolysis

(This chapter of work is based on the following article: Jiandi Liu, Qiang Chen, Junshuai Li, Qing Xiong, Guanghui Yue, Xianhui Zhang, Size Yang and Qing Huo Liu, J. Phys. D: Appl. Phys. **49** 275201 (2016), which has been published at https://doi.org/10.1088/0022-3727/49/27/275201).

2.1 Introduction

Cuprous oxide (Cu_2O) is a typical p-type semiconductor which possesses a narrow bandgap energy of 2.2 eV [1]. It has unique optical, electronic, and magnetic properties due to its specific physical and chemical properties. Recently, because of their potential applications, such as in solar cells [2], gas sensing [3], magnetic storage devices [4], and catalysis [5-12], a lot of interests has been increasingly shown towards the synthesis of Cu_2O nanoparticles as well as the study of their properties. Various kinds of methods have been developed to synthesize Cu_2O nanoparticles with different sizes and shapes, including thermal relaxation [13], hydrothermal treatment [14], solution-phase synthesis [15], electrodeposition [16,17], the arc discharge process [18], and so on. However, it is still a big challenge to precisely control the size and shape of Cu_2O nanoparticles simultaneously, which is known to be closely related to the physical and chemical properties of the Cu_2O nanoparticles. For example, the (110) plane of Cu_2O has a better photocatalytic ability than the (111) plane [9]. Therefore, there is an urgent need to find a new method for synthesizing high-quality Cu_2O nanoparticles.

Recently, a modified electrolysis method [9], which is named plasma electrolysis [20,21], has been developed to synthesize nanomaterials. This method is quite similar to the conventional electrolysis. One solid electrode in the conventional electrolysis is replaced with a gaseous discharge of plasma, which favors the nanoparticles formation in the solution, and the counter electrode is a copper plate. Previously, similar devices have been used to form Au, Ag nanoparticles [22-26], perform surface engineering of nanomaterials [27,28], and produce even quite large-sized Cu_2O nanoparticles (from several hundred nm to several μm) with a complicated electrolyte system [29]. It's well known that plasma-liquid interactions can generate various kinds of reducing and oxidizing species [30-32], which

dissolve in the solution. Therefore, it's possible that these reactive species can react with the Cu ions released from the copper electrode by anodic dissolution. Compared with conventional electrolysis, the products should be directly formed in the electrolyte under the competition between the reducing and oxidizing reactions rather than the deposition on the solid electrode.

In this work, we used a simple atmospheric-pressure argon plasma electrolysis system to synthesize Cu_2O nanoparticles. NaCl aqueous solution accompanied with glucose was used as the electrolyte. It is noted that glucose is used as stabilizing agent which can prevent the aggregation of nanoparticles. We also studied the influence of glucose concentrations on the crystallinity and morphology of the final products. Based on the experiment results, we tried to explain the synthesis mechanism of the formation of Cu_2O nanoparticles.

2.2 Experimental Procedure

The schematic diagram of experimental devices of the plasma electrolysis is shown in figure 2.1(a). All the reagents used in experiments were purchased from Sinopharm Chemical Reagent Co., Ltd. 50 mL NaCl aqueous solution with the concentration of 0.25 M was kept in a beaker as the electrolyte. A polished copper plate (99.99%, 100mm × 20mm × 1mm) was immersed into the electrolyte as one electrode. The counter electrode was composed of the atmospheric-pressure argon plasma (in open air) which was generated from a stainless-steel tube (1.5mm and 3mm in inner and outside diameters, respectively) and placed 4 mm over the surface of the electrolyte. The pH of the solution was measured using a pH probe (Yesmylab SX620) before and after the plasma treatment. An AC voltage (CTP-2000A, Nanjing Suman Electronics Co., Ltd), with a frequency of 5kHz, was applied to the stainless-steel tube to generate the plasma. The voltage between the two electrodes was measured using a high voltage probe (Tektronix P6015A), and the current was achieved from dividing the voltage across a 10-Ω resistor. Figure 2-1(b) presents the typical waveforms of the applied voltage and current. The output voltage of the power source was a sine-waveform (measured when plasma is off without Argon supply), but it was largely distorted due to the plasma-induced charging on the solution surface. The actual voltage applied to the electrodes became a bipolar pulsed DC voltage. As a result, the Cu electrode alternated between acting as an anode and a cathode during the plasma discharge.

A photograph which was taken during the discharge is presented as an inset in figure 2.1(a). The

characteristics of plasmas which were in or in contact with a liquid were summarized in a review paper [33], which indicated that the electron density, the electron temperature, and the gas temperature were in the orders of 10^{18}-10^{19} m^{-3}, 0.3-1.35 eV, and 3500 K, respectively. Due to the high density and relative high electron temperature, this kind of plasma was a potential reactive source for many physical and chemical reactions.

In order to control the properties of the final products, various concentrations of glucose were added to the NaCl solution. To sustain a stable reaction, the peak-to-peak current was kept at 120 mA and the electrolyte was slightly stirred by using a polytetrafluoroethylene-coated magnetic stirrer during the whole synthesis process (30 min). After the plasma treatment, the samples were collected from the solutions by centrifugation (6500 rpm, 5 min) and washed with purified water and ethanol for three times. Then it was dried in an oven at 60 °C for 10 h for further characterization.

The final products were investigated using a powder x-ray diffractometer (XRD, Bruker D8with, Cu Ka radiation 40 kV, 40 mA), a scanning electron microscope (SEM, LEO 1530) as well as energy dispersive x-ray (EDX) analysis. X-ray photoelectron spectroscopy (XPS, ESCALAB 250) was also used to characterize the Cu states in the products.

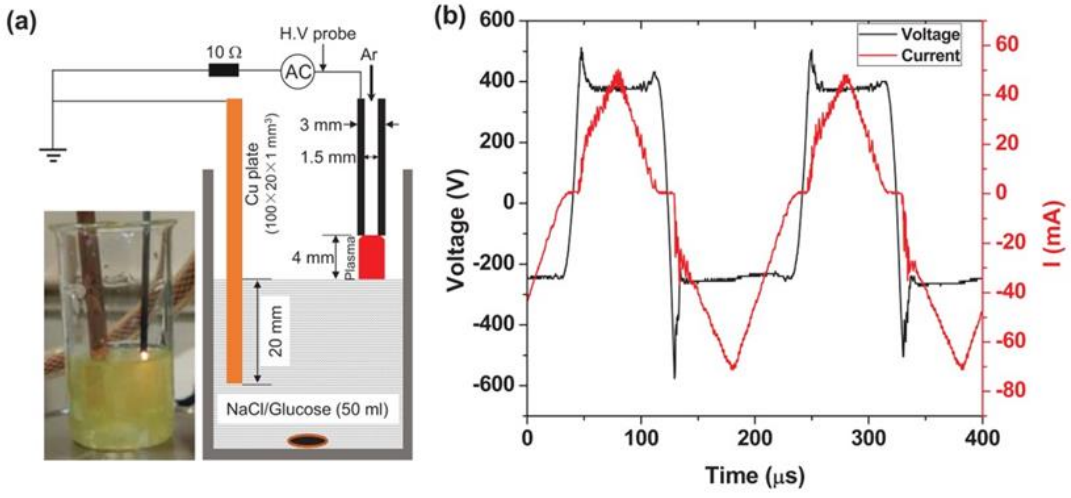

Figure 2.1. (a) A schematic of the experimental setup, and (b) typical waveforms of the applied voltage and current.

2.3 Results and Discussion

The XRD patterns of the obtained products synthesized in different glucose concentrations are shown in figure 2.2. According to the XRD patterns, the peaks of the sample formed at the glucose concentration of 0 mM coincided with the peaks of Cu_2O (No.65-3288) and $Cu_2Cl(OH)_3$ (No.50-1559) and all the left weak peaks not indexed were attributed to $Cu_2Cl(OH)_3$. In the case of pure NaCl solution, the products were a mixture of cubic Cu_2O and monoclinic $Cu_2Cl(OH)_3$ according to the XRD result. In the case of medium glucose concentrations, all the XRD peaks of the samples were attributed to Cu_2O which indicated that Cu_2O products were formed. In addition, amorphous products (confirmed by the broad XRD band) were formed in the case of the highest glucose concentration. These results implied that the glucose played an important role in controlling the crystallinity of synthesized products.

The changes of the pH value were also studied in this experiment. The pH value of the pure water was 7.1. After the plasma treatment, the pH values of the solutions were changed from 7.23 to 9.30, 7.25 to 6.57, 7.44 to 6.38, 7.60 to 6.31, and 7.55 to 6.12 corresponding to the aqueous solutions with the glucose concentrations of 0 mM, 4 mM, 8 mM, 10 mM and 16 mM, respectively. The pH values of the plasma-treated solution decreased except for the solution without glucose. The pH value of the solution could be increased by the water-electrolysis process [$2H_2O+2e^- \rightarrow 2OH^- + H_2$], and also could be decreased with the formation of HNO_2 and HNO_3 in the solution during discharge in an open air, N_2, or O_2 ambient [19]. In our case, the working gas was Ar in open air. Therefore, Ar, air, and the solution constituents, could influence the solution pH value. The Ar plasma which is in contact with the NaCl aqueous solution could increase the pH value, while the air participation in plasma could be partially leading to the solution acidification. When glucose wasn't added, the influence of Ar was stronger than that of air for the pH value change of the solution, and then the final pH value increased in the solution. However, when glucose was added in the solution, the glucose might be changed to gluconic acid by the plasma, which leads to the slight solution acidification. As a result, the basic $Cu_2Cl(OH)_3$ was not found in the cases with glucose.

We used more acidic or more basic initial solutions (by adding HCl or NaOH) to prove our assumption that the glucose-containing solution during plasma treatment could cause the solution acidification. The result showed the solutions after the plasma treatment were acidic (with glucose) or basic (without glucose). Cu_2O nanoparticles were always formed in solution with glucose, and a mixture

of Cu_2O and $Cu_2Cl(OH)_3$ was formed in solution without glucose.

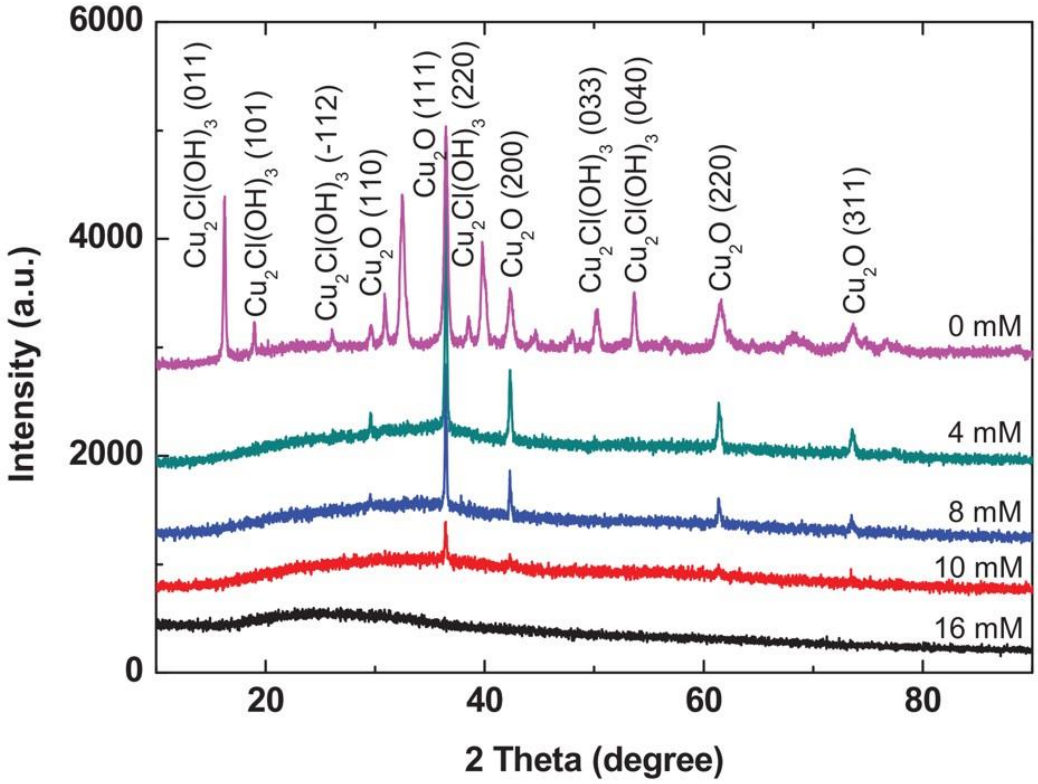

Figure 2.2. XRD patterns of products formed at different glucose concentrations.

The morphologies of the products are shown in figures 2.3((a)-(f)). In the case of the glucose concentration of 0 mM, the product was composed of polyhedral and star-like samples (>200nm) as shown in figures 2.3(a) and 2.3(b). In the case of the glucose concentrations of 4-16 mM, the products displayed similar morphologies although they had different crystallinities as indicated in figure 2.2. The sizes of Cu_2O nanoparticles estimated from the SEM images were 22 ± 6 nm for products formed at glucose concentrations of 4-10 mM (figures 2.3((c)–(e))). The size of amorphous products formed at the glucose concentration of 16 mM was 27 ± 9 nm. We also investigated the EDX spectrum of the product. Cu and O was detected in all cases, Cl was only found in the case of $Cu_2Cl(OH)_3$, and C was observed in the cases with glucose.

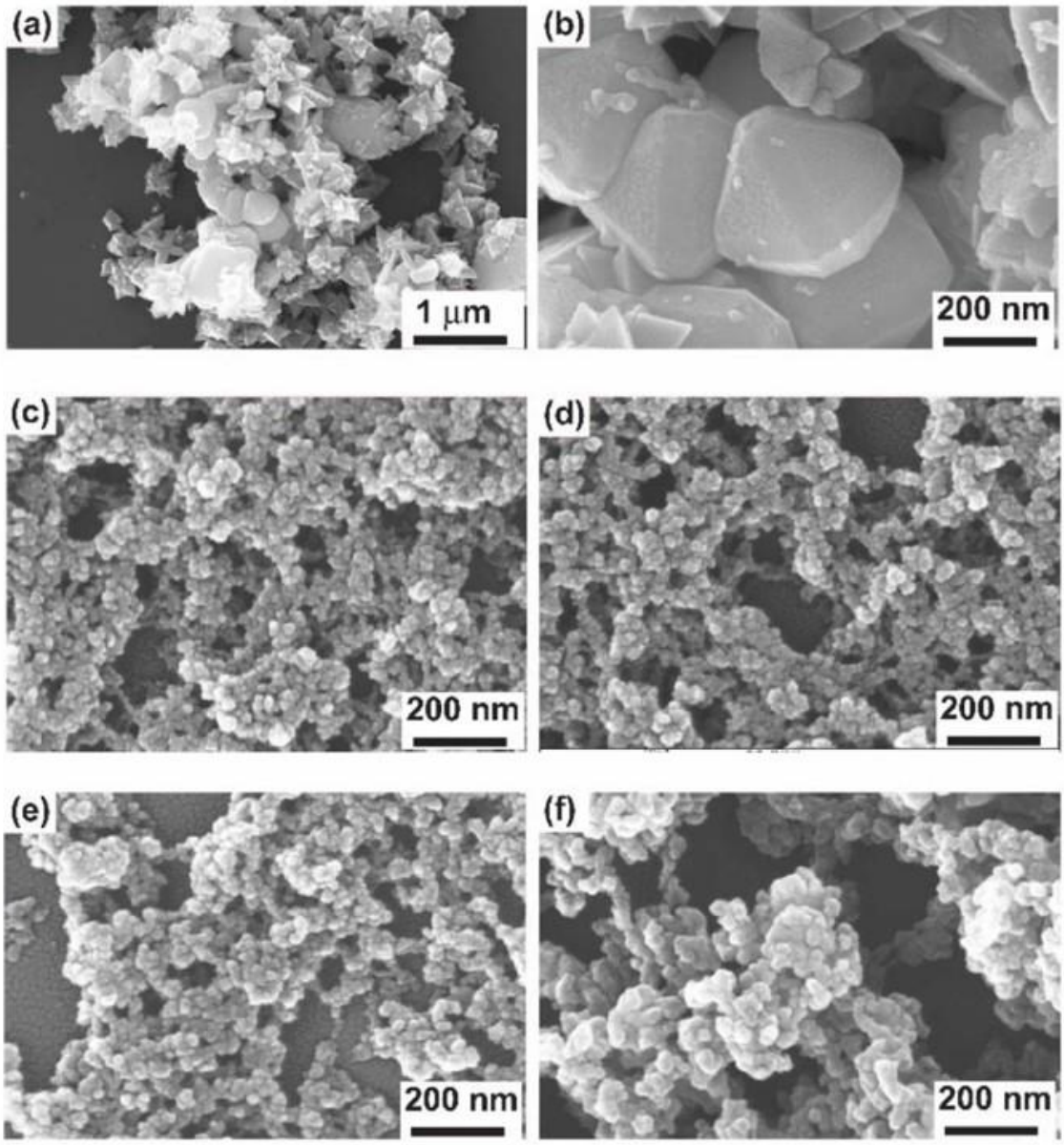

Figure 2.3. SEM images corresponding to the samples formed at glucose concentrations of (a)-(b) 0, (c)-(f) 4 mM, 8 mM, 10 mM, 16 mM, respectively.

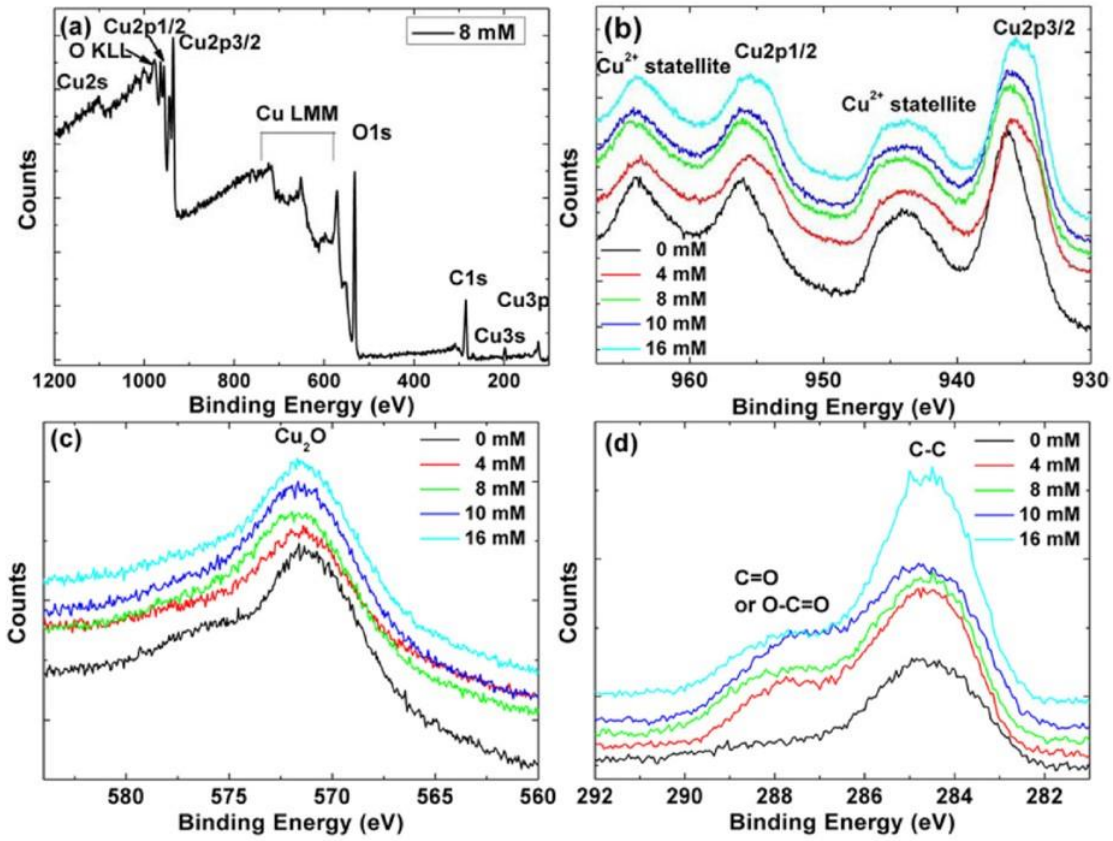

Figure 2.4. (a) A survey of x-ray photoelectron spectroscopy (XPS) datum for the product formed at glucose concentration of 8mM. (b) Cu 2p states, (c) Cu LMM, and (d) C states in the XPS results for products formed at glucose concentrations of 0 mM, 4 mM, 8 mM, 10 mM, and 16 mM, respectively.

In order to find the Cu states in the products, XPS analysis was performed and the results are presented in figure 2.4. Figure 2.4(a) shows a survey of the XPS datum of the product formed at the glucose concentration of 8 mM, and the other XPS data are similar. Cu 2p, Cu LMM, and C states are presented in figures 2.4((b)–(d)), respectively. The results indicated that Cu^{2+} states were present besides the Cu 2p states, although there was no CuO peak in the XRD data. It was difficult to distinguish Cu^{+} and Cu^{2+} from the Cu 2p because of the overlap of their binding energies. But from the Cu LMM, the Cu^{+} state could be distinguished from the Cu^{2+} state [34]. In figure 2.4(c), the Cu LMM peak at 571 eV could be attributed to the Cu^{+} state [34]. The C=O or O–C=O state [35] was present in the products when glucose was used as shown in figure 2.4(d). Based on the XPS data, we could find that Cu_2O and CuO were presented in all the products, although the CuO peak couldn't be observed in the XRD results. It was well-known that bulk Cu_2O was feasibly oxidized to CuO in air, and the specific surface of Cu_2O

increased with decreasing the particle size, by which one might expect that the synthesized Cu_2O nanoparticles were unstable. But in fact, the synthesized Cu_2O nanoparticles were very stable in air, which might be ascribed to a very thin coating of CuO on the small sized Cu_2O nanoparticles [36]. Balamurugan et al, [37] used XPS analysis and confirmed that the CuO coating was very thin, which might be the reason for the absence of CuO peaks in the XRD patterns. Therefore, we concluded that our products were also Cu_2O nanoparticles coated with a very thin CuO layer. Combining the XRD and XPS data, we assumed that the amorphous products might also be thin CuO-coated Cu_2O nanoparticles. In general, the charge transfer and material transport in a plasma-contacting liquid system were very complex [34,35,38], but a qualitative description of the main reaction path was possible if we considered the sufficient work made in the system driven by the DC power sources [22,23,39-41]. We also performed an experiment by using a DC power source. When the Cu electrode was the anode, the solution became turbid during the plasma discharge and nanoparticles could be formed, and when the Cu electrode was the cathode, many bubbles appeared on the Cu electrode, the solution remained apparent and no nanoparticles were formed.

Based on the above results, we propose here a synthesis mechanism of the Cu_2O nanoparticles by plasma electrolysis. When the Cu electrode acted as the anode, Cl^- and OH^- moved to the Cu electrode, Cu^{2+} was liberated from the electrode (rather than Cl_2 or O_2 formation on the electrode) because of the electron donating abilities of Cu, Cl^- and OH^- [42], and then Cu^{2+} ions became $Cu_2(OH)_2^{2+}$ by combining the ligand of OH^- in the solution [43],

$$Cu(solid) \rightarrow Cu^{2+}(liquid) + 2e \quad (2.1)$$

$$2Cu^{2+}(liquid) + 2OH^-(liquid) \rightarrow Cu_2(OH)_2^{2+}(liquid) \quad (2.2)$$

When the Cu electrode acts as the cathode, H_3O^+ and Na^+ move to the Cu electrode, H_2 was produced at the electrode by electrolysis, and the H_2 gas forms bubbles at the electrode which could partially clean the reacting Cu plate (bubbles had been observed at the Cu electrode during the experiment),

$$H_3O^+(liquid) + 2e \rightarrow H_2(gas) + OH^-(liquid) \quad (2.3)$$

On the other hand, many reactive species including reducing and oxidizing agents such as hydrated electrons, atomic H, atomic O, OH are produced by the plasma-liquid interactions. These gaseous species have been clearly indicated in the gas phase by optical emission spectra [34]. All these reactive species can dissolve in the solution and reacted with $Cu_2(OH)_2^{2+}$, for example, a hydrated electron,

$$Cu_2(OH)_2^{2+}(liquid) + 2e \rightarrow Cu_2O(solid) + H_2O \quad (2.4)$$

The properties of the final products are determined by the competition of a series of reducing and oxidizing reactions. Thereby, a possible method may be provided to control the properties of synthesized products, i.e. controlling the yields of reducing and oxidizing species by tuning the plasma conditions. The glucose may play two roles in the synthesis process. One is acting as a capping agent to tune the processes of particle nucleation and growth, by which the sizes of particles are limited. The other role of glucose may be as a reducing agent to reduce $Cu_2(OH)_2^{2+}$ to Cu_2O. However, we believe that the former is the main role of glucose since plasma-generated reducing species has very strong reducing abilities compared with glucose [30-32]. If there is not enough glucose, the small sized Cu_2O initially formed by plasma reducing $Cu_2(OH)_2^{2+}$ would experience a coalescence process to form large-sized particles as shown in figure 2.3(b) [44]. In addition, after plasma treatment, the solution turns out to be basic in the case without glucose, which favors the formation of $Cu_2Cl(OH)_3$ from the reaction of $2Cu^{2+} + 3OH^- + Cl^- \rightarrow Cu_2Cl(OH)_3$ in a basic solution [45]. When the glucose concentration is moderate, glucose on the Cu_2O nanoparticle surface prevents the coalescence, resulting in the formation of small-sized Cu_2O nanoparticles. However, excessive glucose might inhibit the reactions between $Cu_2(OH)_2^{2+}$ and the plasma-produced species, leading to the formation of the amorphous phase.

2.4 Conclusion

Cu_2O nanoparticles with a size distribution of 22 ± 6nm were synthesized by a simple plasma electrolysis system in association with glucose. Plasma-produced reactive species probably reacts with the $Cu_2(OH)_2^{2+}$ formed from Cu electrode, resulting in the final production of Cu_2O. The glucose plays an important role as the capping agent which can tune the crystallinity and the phase by changing the concentrations. Amorphous Cu_2O, Cu_2O nanoparticles and a mixture of Cu_2O nanoparticles and $Cu_2Cl(OH)_3$ were synthesized under the conditions corresponding to high, medium, and low concentrations of glucose, respectively. In terms of simplicity, the feasibility of scaling-up, and the low cost of the plasma electrolysis system, this work provide a novel method to synthesize small-sized Cu_2O nanoparticles, and we believe that it can also be used to synthesize nanoparticles of many other materials if suitable conditions are selected.

References

[1] Lu C, Qi L, Yang J, Wang X, Zhang D, Xie J and Ma J, Adv. Mater. **17** 2562 (2005).

[2] Cui J and Gibson U J, J. Phys. Chem. C **114** 6408 (2010).

[3] Zhang J, Liu J, Peng Q, Wang X and Li Y, Chem. Mater. **18** 867 (2006).

[4] Li X, Gao H, Murphy C J and Gou L, Nano Lett. **4** 1903 (2004).

[5] Kondo J, Chem. Commun. 357 (1998).

[6] de Jongh P and Kelly J, Chem. Commun. 1069 (1999).

[7] Barreca D, Fornasiero P, Gasparotto A, Gombac V, Maccato C, Montini T and Tondello E, ChemSusChem **2** 230 (2009).

[8] Huang L, Peng F, Yu H and Wang H, Solid State Sci. **11** 129 (2009).

[9] Zhang Y, Deng B, Zhang T, Gao D and Xu A-W, J. Phys. Chem. C **114** 5073 (2010).

[10] Xu H, Wang W and Zhu W, J. Phys. Chem. B **110** 13829 (2006).

[11] Shoeib M A, Abdelsalam O E, Khafagi M G and Hammam R E, Adv. Powder Technol. **23** 298 (2012).

[12] Ho J-Y and Huang M H, J. Phys. Chem. C **113** 14159 (2009).

[13] Deki S, Akamatsu K, Yano T, Mizuhata M and Kajinami A, J. Mater. Chem. **8** 1865 (1998).

[14] Yu H, Yu J, Liu S and Mann S, Chem. Mater. **19** 4327 (2007).

[15] Gou L and Murphy C J, Nano Lett. **3** 231 (2003).

[16] Huang L, Wang H, Wang Z, Mitra A, Zhao D and Yan Y, Chem. Mater. **14** 876 (2002).

[17] Zhang S, Zhang S, Peng F, Zhang H, Liu H and Zhao H, Electrochem. Commun. **13** 861 (2011).

[18] Yao W-T, Yu S-H, Zhou Y, Jiang J, Wu Q-S, Zhang L and Jiang J, J. Phys. Chem. B **109** 14011 (2005).

[19] Rumbach P, Witzke M, Sankaran R M and Go D B, J. Am. Chem. Soc. **135** 16264 (2013).

[20] Chiang W-H, Richmonds C and Sankaran R M, Plasma Sources Sci. Technol. **19** 034011 (2010).

[21] Mariotti D and Sankaran R M, J. Phys. D: Appl. Phys. **44** 174023 (2011).

[22] Mariotti D and Sankaran R M, J. Phys. D: Appl. Phys. **43** 323001 (2010).

[23] Shirai N, Uchida S and Tochikubo F, Japan. J. Appl. Phys. **53** 046202 (2014).

[24] Kaneko T, Baba K, Harada T and Hatakeyama R, Plasma Process Polym. **6** 713 (2009).

[25] Tsuyoshi M, Takaaki M, Hirofumi N, Tomoko Y and Shinya Y, Japan. J. Appl. Phys. **53** 11RA03

(2014).

[26] Shirafuji T, Ueda J, Nakamura A, Cho S-P, Saito N and Takai O, Japan. J. Appl. Phys. **52** 126202 (2013).

[27] McKenna J, Patel J, Mitra S, Soin N, Švrček V, Maguire P and Mariotti D, Eur. Phys. J: Appl. Phys. **56** 323001 (2011).

[28] Yang F, Li Y, Liu T, Xu K, Zhang L, Xu C and Gao J, Chem. Eng. J. **226** 52 (2013).

[29] Du C and Xiao M, Sci. Rep. **4** 7339 (2014).

[30] Chen Q, Kaneko T and Hatakeyama R, Appl. Phys. Express **5** 086201 (2012).

[31] Chen Q, Kaneko T and Hatakeyama R, Chem. Phys. Lett. **521** 113 (2012).

[32] Rumbach P, Bartels D M, Sankaran R M and Go D B, Nat. Commun. **6** 8248 (2015).

[33] Richmonds C and Sankaran R M, Appl. Phys. Lett. **93** 131501 (2008).

[34] Chen Q, Li J, Saito K and Shirai H, J. Phys. D: Appl. Phys. **41** 175212 (2008).

[35] Richmonds C, Witzke M, Bartling B, Lee S W, Wainright J, Liu C-C and Sankaran R M, J. Am. Chem. Soc. **133** 17582 (2011).

[36] Palkar V, Ayyub P, Chattopadhyay S and Multani M, Phys. Rev. B **53** 2167 (1996).

[37] Balamurugan B, Mehta B and Shivaprasad S, Appl. Phys. Lett. **79** 3176 (2001).

[38] Akolkara R and Sankarana R M, J. Vac. Sci. Technol. A **31** 050811 (2013).

[39] Harris D C, Quantitative Chemical Analysis (New York: Macmillan) (2010).

[40] Brettholle M, Höfft O, Klarhöfer L, Mathes S, Maus-Friedrichs W, El Abedin S Z, Krischok S, Janek J and Endres F, Phys. Chem. Chem. Phys. **12** 1750 (2010).

[41] Hadzifejzovic E, Stankovic J, Firth S, McMillan P F and Caruana D J, Phys. Chem. Chem. Phys. **9** 5335 (2007).

[42] Rumbach P, Bartels D M, Sankaran R M and Go D B, Nat. Commun. **6** 7248 (2015).

[43] Perrin D, J. Chem. Soc. 3189 (1960).

[44] Koch W and Friedlander S, J. Colloid Interface Sci. **140** 419 (1990).

[45] Jia W, Reitz E, Sun H, Li B, Zhang H and Lei Y, J. Appl. Phys. **105** 064917 (2009).

Chapter 3 The effect of the surfactants on the plasma electrolytic synthesis of cuprous oxide nanoparticles and their visible-light photocatalytic abilities

Chapter 3 The effect of the surfactants on the plasma electrolytic synthesis of cuprous oxide nanoparticles and their visible-light photocatalytic abilities

(This chapter of work is based on the following articles: (1) Jiandi Liu, Bangbang He, Qiang Chen, Hai Liu, Junshuai Li, Qing Xiong, Xianhui Zhang, Size Yang, Guanghui Yue, and Qing Huo Liu, Electrochemica Acta 222 1677 (2016), which has already been published in final form at http://dx.doi.org/10.1016/j.electacta.2016.11.158; (2) Jiandi Liu, Bangbang He, Xin Wang, Qiang Chen, and Guanghui Yue, Eur. Phys. J. D 73: 11 (2019), which has been published in final form at https://doi.org/10.1140/epjd/e2018-90100-5).

3.1 Introduction

Discharge plasma is an electrically neutral medium of unbound positive and negative particles, accompanied by many reactive radicals. Because plasma includes versatile reactive constituents, it has demonstrated powerful ability in modern industry such as applications in surface modification of materials and surface processing in the integrated circuits processing [1]. However, the application and research of discharge plasma is mostly reacted with solid or gas, rarely with liquid. Plasma reacts with liquid have been well developed in the past few decades. If plasma is in contact with a liquid, the plasma-liquid interactions can produce energetic species which initiate physical and/or chemical reactions that can take place only with difficulty or not at all in ordinary chemical reactions. Consequently, the plasma-liquid interface as well as the plasma affected liquid layer becomes a reaction zone for many specific physical and chemical processes. This reaction zone can be used to form numerous novel nanomaterials such as noble metals [2-14], magnetic materials [15,16], and alloy [17-19], if suitable solution and electrode materials are used. Kaneko and coworkers [20] have successfully synthesized gold nanoparticles by using plasma irradiation to ionic liquid in gas-liquid interfacial discharges and found that the ion irradiation generated hydrogen radicals in the ionic liquid, which were effective for the synthesis. Zhong and coworkers [21] demonstrated a single-step, microplasma-chemical green synthesis of crystalline Au_xAg_{1-x} nanoparticles alloys in solution under ambient conditions, with the effective control over the size and the composition by adjusting the reaction time. Saito and coworkers [22] and

Yang et al. [23] reported that noble metal nanoparticles-modified carbon materials could be synthesized by plasma in contact with liquid.

The formation process is similar but not the same to a common solution-based synthesis. It is worth noting that the processes in the plasma-liquid interface are not only simply an electrochemical process, but also involve complicated processes: charge transfer [24], materials transports [25], numerous physical and chemical reactions, and so on. Although a full detailed account of the plasma-liquid interactions has not yet been presented up to date, they demonstrate many advantages in nanomaterials synthesis [10, 26-29] such as simplicity in device design, low cost, and easiness in controlling the ion irradiation on the liquid surface (for instance, by applying a voltage bias to the liquid surface [30]), compared with the pure solution-phase synthesis.

Because the plasma-liquid interactions consist of both plasma and liquid, the properties of the final products can be tuned from two sorts of parameters: one is of the plasma, and the other is of the liquid. Previously, we have demonstrated that the Cu_2O nanoparticles synthesis by the plasma electrolysis method was possible [31]. In this chapter, we demonstrated the ability to tune the final products by varying the liquid parameters, and Cu_2O nanoparticles are used as the model synthesized material. We further explored the possibility of tuning the shapes and sizes of the products by using different surfactants including glucose, ascorbic acid and cetyltrimethyl ammonium bromide (CTAB). What's more, we have also investigated the visible-light photocatalytic activity of the synthesized Cu_2O nanoparticles by photocatalytic degradation of methyl orange.

3.2 Experimental Procedure

Sodium chloride (NaCl), methyl orange ($C_{14}H_{14}N_3NaO_3S$, MO), glucose and ascorbic acid (AA) were purchased from Sinopharm Chemical Reagent Co. Ltd. Cetyltrimethylammonium bromide (CTAB; 99%) was acquired from Aldrich. All chemicals were used as received without further purification.

The schematic diagram of the experiment device is shown in figure 3.1. The experimental device was very similar to that shown in chapter 2. A home-made DC power source was used to generate the atmospheric-pressure Ar plasma between a tapered tungsten steel tube and a liquid surface, and the gap between the tube and the liquid surface was 3 mm. The gaseous plasma acted as the cathode and a pre-polished copper plate (99.99%, 100 mm×20 mm×1 mm) was the anode immersed into the electrolyte

which was 50 mL of the mixture of 0.25 M NaCl and different concentrations of surfactants. Surfactants (glucose, ascorbic acid and CTAB) were added into the solution to tune the morphology of the final products. During the experiment, the solution was stirred by a magnetic stirrer. The voltage between the two electrodes was measured using a high voltage probe (Tektronix P6015A) and the current was achieved from dividing the voltage across a10-Ω resistor. The discharge current and the time were 50 mA and 30 min, respectively. After the discharge plasma exposure, the samples in the solutions were collected by centrifugation (6500 rpm, 5 min) and washed with pure water and ethanol for three times, and then dried in an oven at 60 °C for 10 h for further analysis.

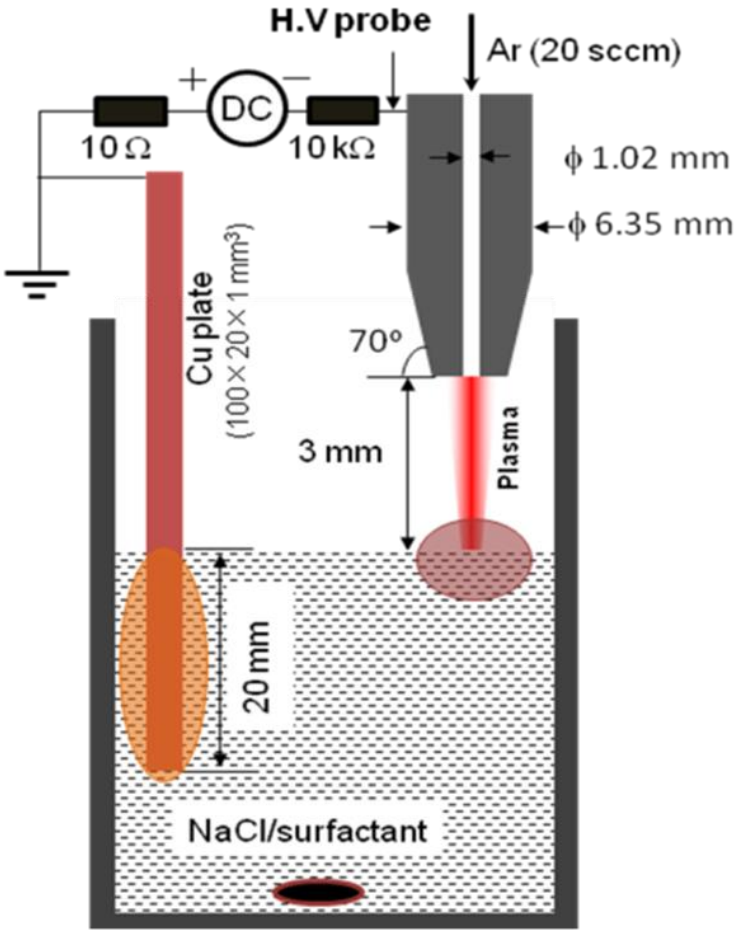

Figure 3.1. A schematic diagram of the experimental setup.

The X-ray diffraction (XRD) patterns of the dried samples were recorded by the Bruker AXS D8 Focus diffractometer with Ni-filtered Cu Kα radiation. To obtain the scanning electron microscopy (SEM) images of the synthesized products, the collected samples were re-dispersed in ethanol and a drop of the re-dispersed samples was dropped on a silicon substrate, and then the SEM images of the samples were obtained using LEO 1530 scanning electron microscope.

The photocatalytic activity of the products was measured based on the visible-light photocatalytic degradation of MO. Typically, a 30 mg as-prepared sample was dispersed into 300 mL MO solutions (with a concentration of 20 mg/L) in a Pyrex glass cell. A 300 W Xe-lamp with an UV cutoff filter was used as the visible-light source placed 12 cm above the solution. Before the irradiation, the suspension was magnetically stirred in the dark for 30 min for reaching the adsorption equilibrium between the catalyst molecule and MO molecule. At a given time interval of 10 min, 2 mL of suspension was sampled and centrifuged for 5 min to remove the catalyst. Then the resident supernatant was collected for the absorption analysis. The liquid absorbance was detected in quartz cell (1 cm in optical path length) by Ocean Optics USB2000+ spectroscopy with a light source (DH-2000). The light source continuously outputs from 200 to 2500 nm by using a combination of deuterium, tungsten, and halogen lamps.

The relative degradation of MO was estimated by the following equation: $(C_0 - C)/C_0 = (A_0 - A)/A_0$, where C_0 and C are the MO concentrations of the original and the extracted solutions, respectively, and A_0 and A are the absorbance of the original and the extracted solution at the characteristic absorption wavelength of 465 nm, respectively. The contrast experiments have also been conducted to reduce the experimental error for guaranteeing the reliability of the experiment.

3.3 Results and Discussion

3.3.1 Comparison of the effects between glucose and ascorbic acid

Figure 3.2 presented the XRD patterns of products synthesized by using glucose and ascorbic acid. In both the cases, the products consisted of Cu_2O and $Cu_2Cl(OH)_3$ at a low concentration, while Cu_2O was the only product in the case with high concentration surfactants.

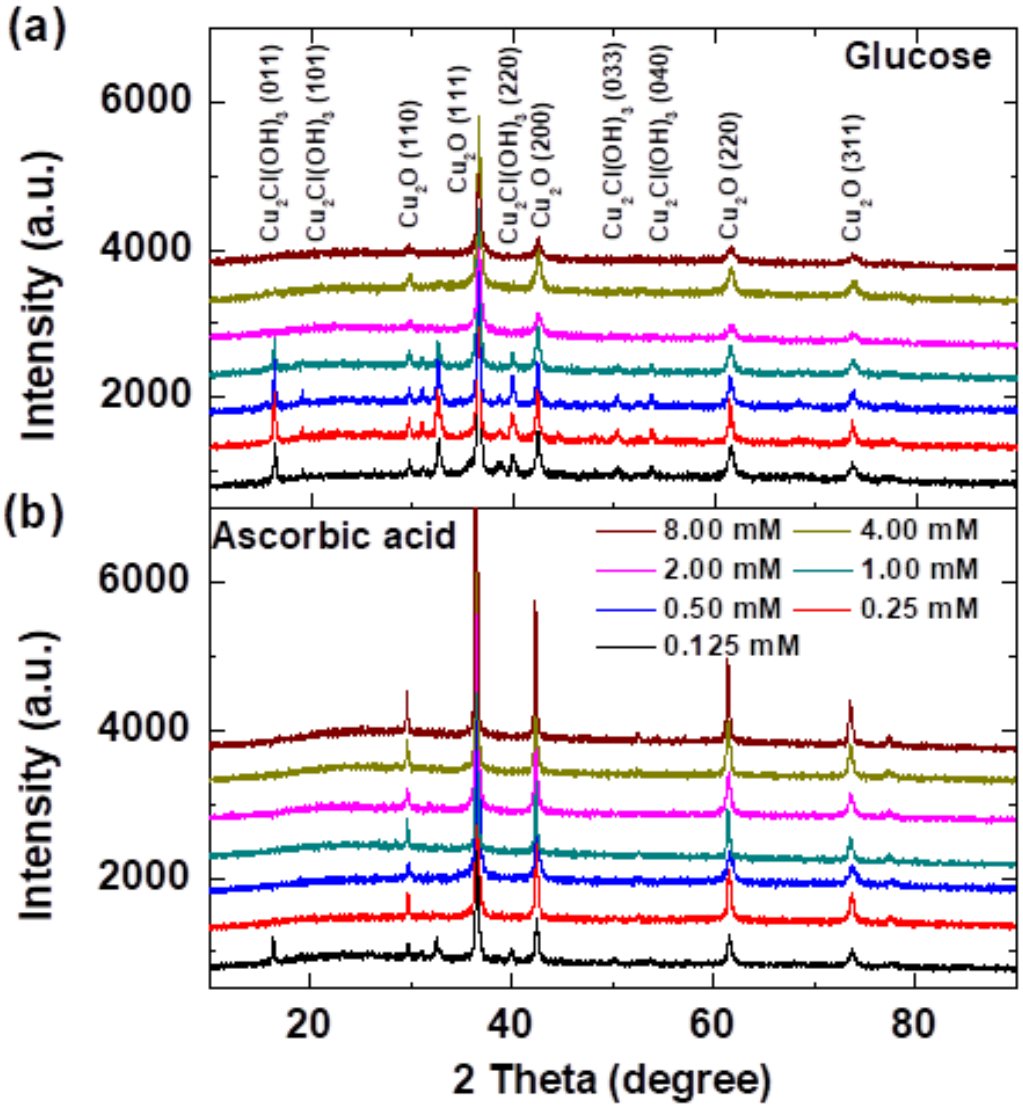

Figure 3.2. XRD patterns of products synthesized from liquids with (a) glucose, and (b) ascorbic acid at different concentrations.

The pH values of the solutions were changed by the plasma treatment. We observed that the pH values of the solution changed to basic range after the plasma treatment when there was no surfactants or low concentration of surfactants, and this condition favored the formation of $Cu_2Cl(OH)_3$ since $Cu_2Cl(OH)_3$ was soluble in acid medium yielding the corresponding copper salts. In addition, the samples free of $Cu_2Cl(OH)_3$ were all found formed from solutions with final pH values in the acidic range. These results suggested that the addition of glucose and ascorbic acid could acidify the solution,

which was unfavorable for the formation of $Cu_2Cl(OH)_3$, but benefited for the formation of Cu_2O. We also estimated the crystalline size from the Cu_2O (111) peak by the Scherrer equation

$$\tau = \frac{\lambda}{\beta \cos\theta} , \qquad (3.1)$$

where τ is the mean crystalline size of the ordered (crystalline) domains, λ is the X-ray wavelength, β is the line broadening at half the maximum intensity, and θ is the Bragg angle of the Cu_2O (111) peak. The estimated crystalline sizes of samples are summarized in Table 3.1.

Table 3.1. Crystalline size of products synthesized from liquids with surfactants of glucose and ascorbic acid.

Concentration of the	Crystalline size (nm)	
additives (mM)	Glucose	Ascorbic acid
0.125	22.5	26.4
0.25	30.9	31.0
0.50	25.1	21.3
1.00	20.9	37.5
2.00	17.1	23.9
4.00	20.7	31.6
8.00	18.8	37.7

In general, the crystalline size of products using ascorbic acid was larger than those using glucose. Usually, the surfactant would attach to the growing facets of the forming nanoparticles by coulombic forces in the solution, and then the growth rate of nanoparticles could be tuned by the property of surfactant. Large numbers of surfactants on the forming nanoparticles would decrease the growth rate of the nanoparticles. The number of surfactants attached on a facet of the nanoparticles depends on both the surface energy and the property of the surfactant. Therefore, the estimated crystalline sizes of the nanoparticles seem to show that the glucose has a stronger affinity on the formed nanoparticles than that

of the ascorbic acid. The size of nanoparticles obtained in solution without surfactant was also estimated, and it was about 42 nm, larger than nanoparticles formed with surfactants. In addition, the surfactant of ascorbic acid was better than glucose on suppressing the formation of $Cu_2Cl(OH)_3$ if we compared XRD peak at 16.25 degrees [attributing to $Cu_2Cl(OH)_3$] in figure 3.2. This result might be due to the acid nature of ascorbic acid, and therefore the ascorbic acid is more unfavorable for the $Cu_2Cl(OH)_3$ formation compared with glucose.

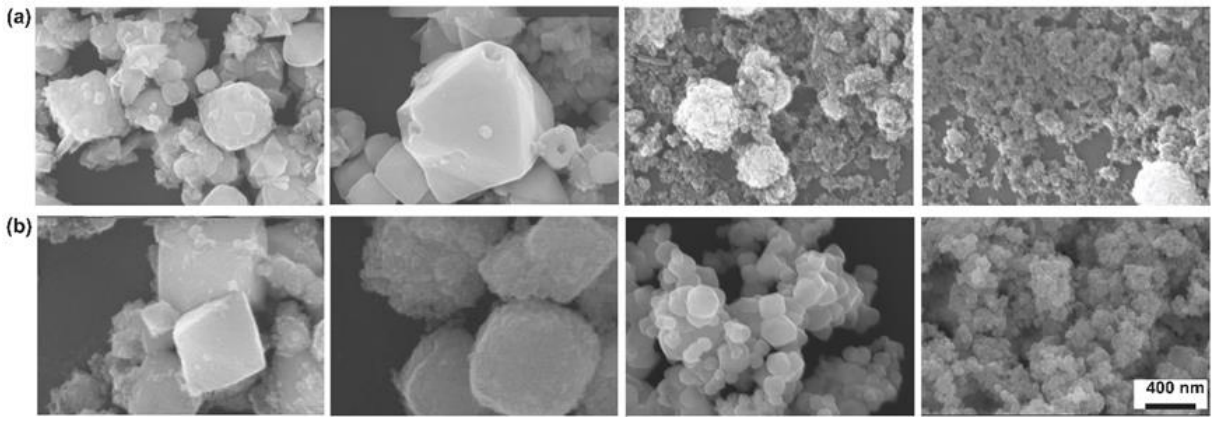

Figure 3.3. SEM images of products synthesized at different concentrations of (a) glucose, and (b) ascorbic acid. Concentration from left to right: 0.125 mM, 0.5 mM, 2.0 mM and 8.0 mM.

As shown in figure 3.3, the morphologies of typical products were tuned by the type and concentration of surfactants. In the case of glucose, similar to our previous work where an AC power source was used to generate the plasma [31], the product formed without surfactant or with low glucose concentration was made of polyhedral and star-like samples. The products formed at high glucose concentration consisted of small-sized nanoparticles and a few sphere-like structures formed by small-sized nanoparticles. In the case of ascorbic acid, as the ascorbic acid concentration increased, the morphologies of products evolved from polyhedral with surfaces littered with small-size nanoparticles, polyhedra with coarse surfaces, polyhedra with smooth surfaces, to small-sized nanoparticles. In a similar setup, Cu_2O with size of several hundred nm was formed in a microplasma-NaCl-NaOH-$NaNO_3$ electrolytic system [32]. As shown in figure 3.3 and our previous paper [31], it was possible to form

Cu_2O nanoparticles of ~22 nm by adding surfactant in the solution since the surfactant could limit the nanoparticles' size by combining on the surfaces. We also expected that the size of Cu_2O nanoparticles could be further decreased if we increased the concentration of surfactant, considering the trend shown in figure 3.3.

Figure 3.4(a) demonstrates the photocatalytic degradation of MO by the formed Cu_2O nanoparticles (the sample formed using 2.0 mM ascorbic acid). The photocatalytic activity curves are shown in figure 3.4(b) for several typical samples as well as the bank curve for comparison. The whole photocatalytic degradation was composed of two part: light off and light on. During the light off for 30 min, the as-prepared nanoparticles were combined with MO molecules to reach the adsorption equilibrium which leading to the decrease of absorbance. When the light turned on, the degradation of MO started.

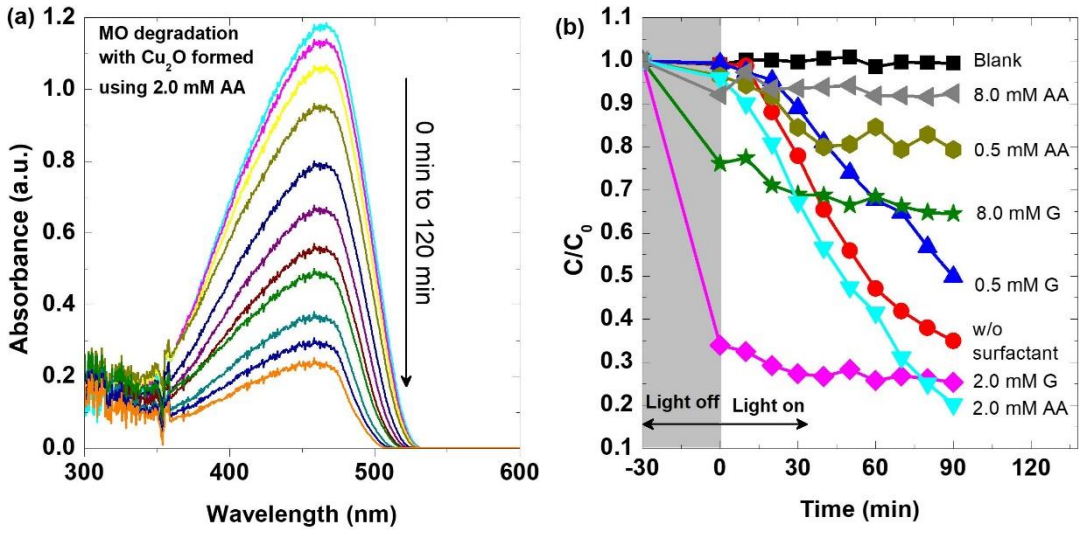

Figure 3.4. (a) Typical time-dependent absorption spectra of methyl orange under visible-light irradiation, and (b) the relative concentration change of methyl orange (C/C_0) as a function of the irradiation time for glucose and ascorbic acid with several concentrations.

The best photocatalytic performance was obtained in the product formed with 2.0 mM ascorbic acid, and the products formed without the surfactant and with 0.5 mM glucose also showed strong photocatalytic activity compared to other products. These results might be attributed to the fact: there

was polyhedral Cu_2O nanoparticles with smooth surfaces in those samples as shown in figure 3.3, and the photocatalytic performance depended on the content and quality of polyhedral Cu_2O nanoparticles. We could find that the relative MO concentration (C/C_0) decreased from 1 to ~ 0.33 after the pure MO solution was mixed with the Cu_2O nanoparticles synthesized with 2.0 mM glucose when light was off, and the C/C_0 decreased very slowly during 90 min light irradiation (0.33 to 0.25). These results indicated that the MO molecules were largely absorbed by the formed sample which was due to the large specific surface area of the small-sized nanoparticles. However, the same sample possessed a weak photocatalytic ability, which was probably owing to the lack of high-quality surfaces for the small-sized nanoparticles. The product formed with 8.0 mM ascorbic acid was also composed of small-sized nanoparticles, and it showed weak photocatalytic ability similar to the sample formed with 2.0 mM glucose, while it demonstrated insignificant MO adsorptive effect, and at present the reason remained unclear. It has been proposed that OH radicals were generated at the Cu_2O surface under visible-light irradiation and MO was decomposed by these OH radicals [33, 34], perhaps the combining manner of the surfactant at the particles' surface affected its photocatalytic property. An oscillation of C/C_0 with increasing time was observed in some samples, which was due to the desorption-adsorption process of MO molecules at the samples' surfaces. The sample formed with 0.5 mM ascorbic acid showed a weak photocatalytic ability because of its coarse surfaces.

3.3.2 The effects of the surfactant of CTAB

It is noted that the compositions of the aqueous solution were different with the solution described in section 3.3.1. The aqueous solution was composed of NaCl, ascorbic acid (a stabilizer promoting the crystallization of particles), and the surfactant of CTAB. The concentration of NaCl and ascorbic acid was adjusted to 0.25 M and 2×10^{-3} M, respectively. The concentrations of the added surfactant of CTAB ranged from 0 mM to 0.50 mM.

The XRD patterns of the obtained products synthesized with different concentrations of CTAB (0, 0.125, 0.25, 0.375, and 0.50 mM) are shown in figure 3.5. Obviously, all the diffraction peaks of these samples can be matched with the standard cubic crystal structure of Cu_2O (JCPDS No. 05-0667) without any impurities. Evidently, the XRD results indicated that the crystallization quality of samples formed in solution with CTAB of 0, 0.375, and 0.5 mM is better than samples formed in solutions with CTAB

of 0.125 and 0.25 mM.

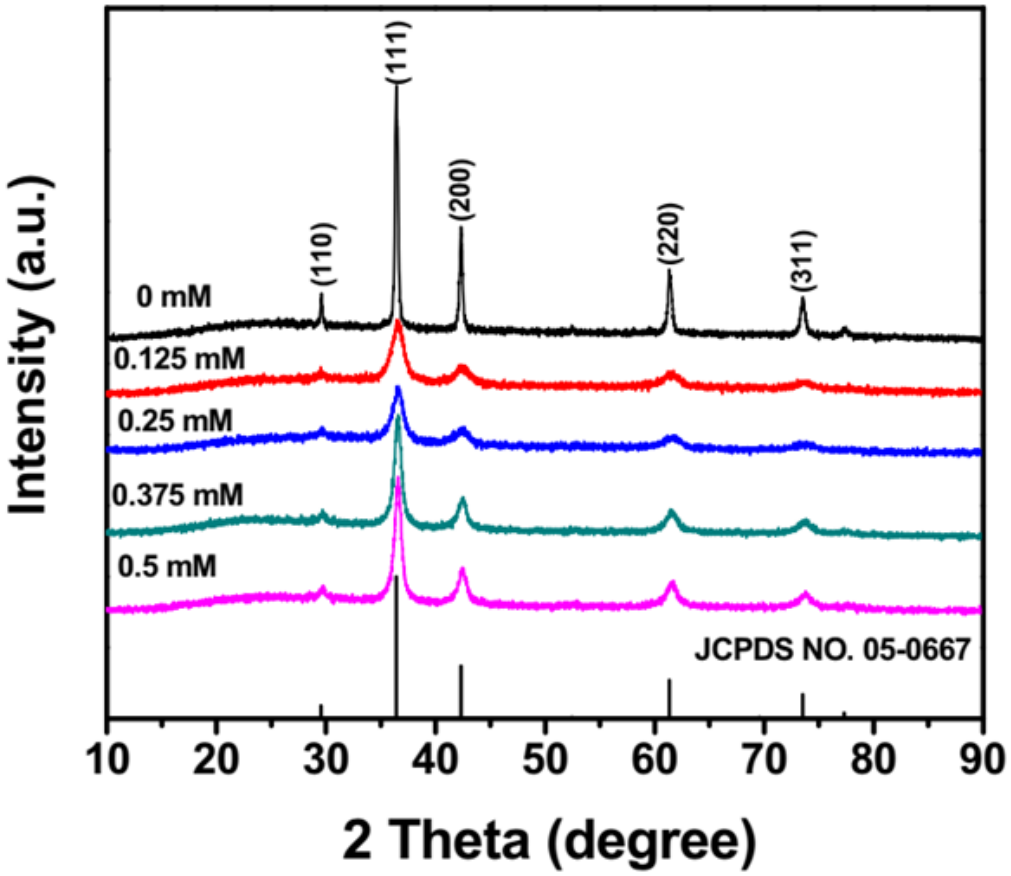

Figure 3.5. XRD patterns of products formed at different CTAB concentrations.

The morphology of the obtained products was analyzed by SEM. It was found that the concentration of CTAB had a strong influence on the final morphology of the samples. First, without CTAB, the product presented a polyhedron shape with mean particles diameter of 300 nm as shown in figure 3.6(a). After increasing the concentration of CTAB to 0.125 mM, the morphology of the prepared products changed to irregular shape as shown in figure 3.6(b). This might be ascribed to the low concentration of surfactant which does not reach the critical micelle concentration (CMC) of CTAB, leading to the irregular shape. When the concentration increased to 0.25 mM, the products showed a core-shell sphere shape, which could be referred to by the broken sphere as shown in the inset of figure 3.6(c). With the concentration increasing to 0.375 and 0.50 mM, the final morphology of the samples

was nearly the same spherical shape with mean particles diameters of 700 and 500 nm, respectively (Figures 3.6(d) and 3.6(e)). More close observation shows that the particles in figures 3.6(c) and 3.6(d) might be composed of small nanoparticles.

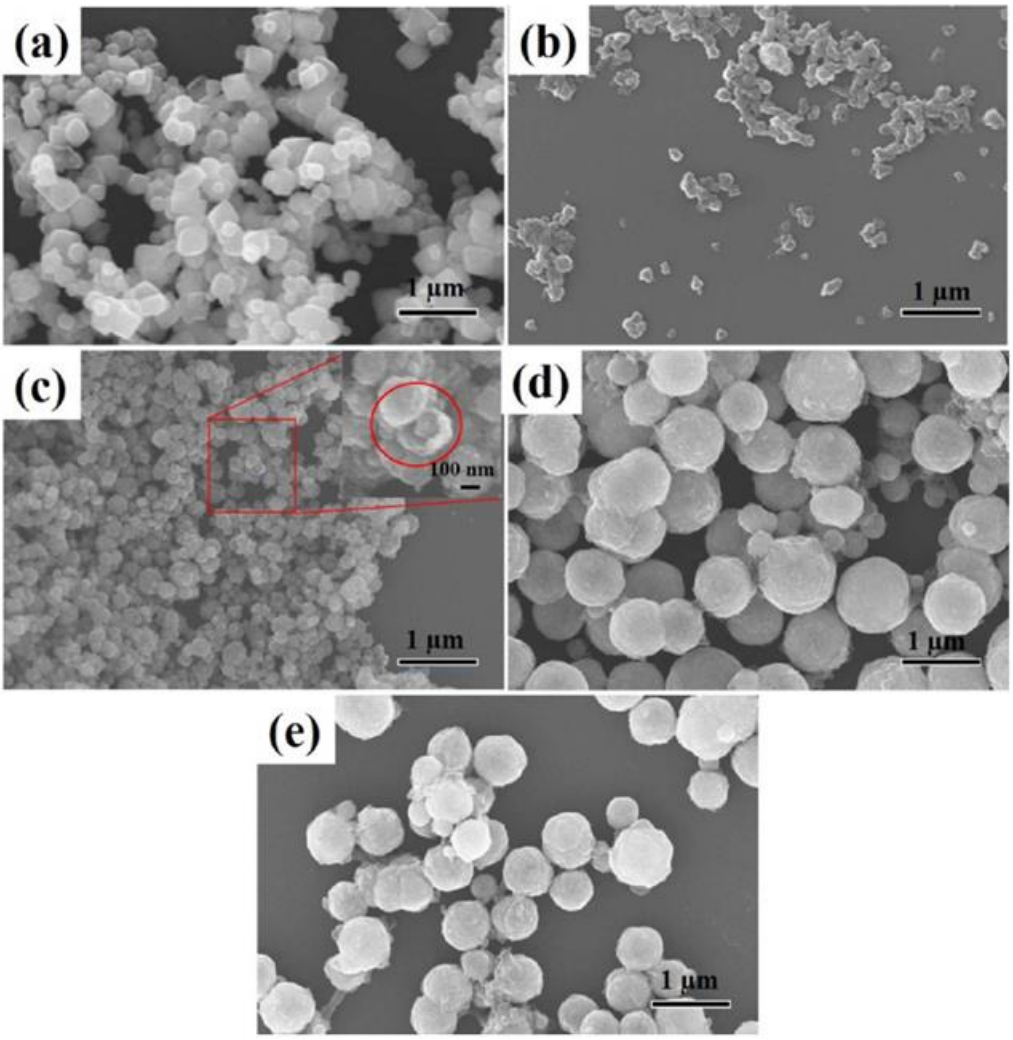

Figure 3.6. SEM images of the products synthesized with different concentrations of CTAB: (a) 0 mM; (b) 0.125 mM; (c) 0.25 mM; (d) 0.375 mM, and (e) 0.50 mM. Inset in part (c) shows the selected part with larger magnification of the corresponding image.

The formed Cu_2O nanoparticles are stable in air, which can be attributed to a very thin layer coating of CuO. To investigate the photocatalytic activity of the products, the photocatalytic decomposition of MO was performed as a probe reaction under the irradiation of visible light. Figure 3.7(a) shows the evolution of MO absorption spectra in the presence of the sample e, in which the characteristic absorption peak of MO (465 nm) diminished gradually as the illumination time increased. The sample e was able to degrade over 71% of the original MO concentration. For comparison, a blank experiment has also been conducted under the same conditions in the absence of the photocatalyst. The result shown in figure 3.7(b) demonstrated that photocatalysts indeed played a dominant role in the decomposition of MO molecules.

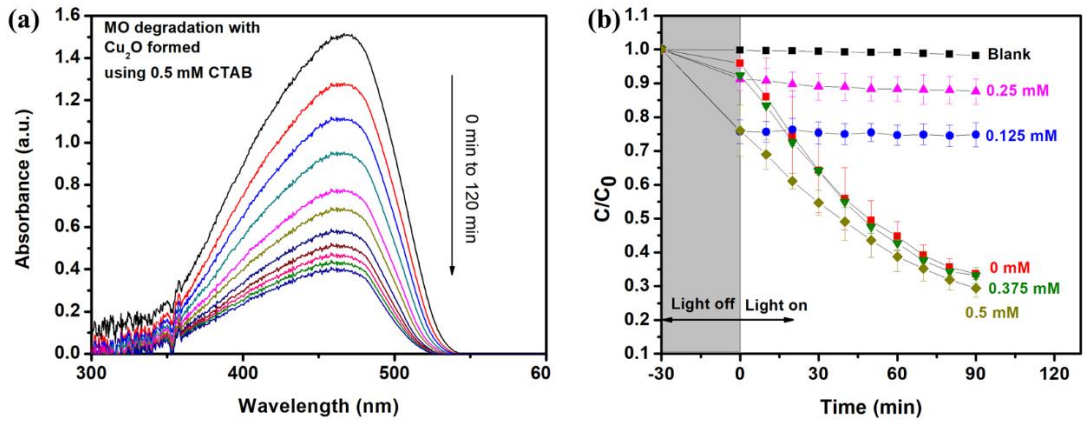

Figure 3.7. (a) Typical temporal absorption spectra of MO under visible-light irradiation (the sample formed with the CTAB concentration of 0.50 mM). (b) The relative concentration change of methyl orange (C/C_0) as a function of the irradiation time for CTAB with several concentrations (CTAB: 0, 0.125, 0.25, 0.375, and 0.50 mM).

Figure 3.7(b) presents the results of the MO degradation by the visible-light irradiation in Cu_2O nanoparticles solutions. From the data in the dark period, it could be found that the Cu_2O nanoparticles formed with the CTAB of 0.125 and 0.50 mM showed the most efficient adsorption effect of the MO molecules. Although the Cu_2O nanoparticles formed with the CTAB of 0.125 mM have higher adsorption of the MO, they present little photocatalytic ability for the MO degradation similar to the

Cu_2O nanoparticles formed with the CTAB of 0.25 mM. It has been proposed that the photocatalytic ability of Cu_2O is due to the MO decomposition by the OH radicals generated at the Cu_2O surface under visible-light irradiation [35,36]. Therefore, the surface properties of the Cu_2O nanoparticles such as crystallinity and coating can affect their photocatalytic ability. Naturally, as shown in figures 3.7(b) and 3.5, the well-crystallized samples (with CTAB of 0, 0.375, and 0.5 mM) show better photocatalytic ability on the MO degradation than that of the low-quality crystallized samples (with CTAB of 0.125 and 0.25 mM).

3.3 The effect of surfactant on the synthesis of Cu_2O nanoparticles

The synthesis process of Cu_2O nanoparticles is proposed as follows. When plasma phase is in contact with liquid phase, the plasma-liquid interactions lead to the decomposition and ionization of water molecules, producing various kinds of highly reactive species such as hydrogen atom, OH radical, and hydrated electron. Due to their high activity, these reactive species quickly change to other long-lived species such as H_2, H_2O_2, O_3, OH^-, and so on. In the works presented here, argon plasma was used as the cathode while the copper plate as the anode. During the process of interactions between the plasma and liquid, the copper electrode released Cu^{2+} ions into the aqueous solution by anodic dissolution and quickly coordinated with OH^- to form $Cu_2(OH)_2^{2+}$. On the other hand, the formed $Cu_2(OH)_2^{2+}$ is forced to move toward the plasma cathode zone by electric field where it is reduced, and the Cu_2O nanoparticles are formed finally.

In the presence of surfactant, the molecules or ions produced by surfactant attach to the growing facets of the forming nanoparticles by coulombic forces in the solution. Thus, the growth rate of nanoparticles can be tuned by the property of surfactant. A large number of surfactant molecules or ions attached to the forming nanoparticles decrease the growth rate. The number of surfactant molecules or ions attached on a facet of the nanoparticles depends on both the surface energy and the property of the surfactant. Based on the results, the glucose has a stronger affinity on the formed nanoparticles than that of the ascorbic acid. As for the surfactant CTAB, it has the characteristic of a critical micelle concentration (CMC) when dissolved in the solution [37]. When the CTAB concentration is equal to or larger than the CMC, the aqueous medium is populated heavily with the surfactant micelles. The surface of the spherical micelle is approached by the Cu^{2+} ions, forming a Cu^{2+} added spherical surface. Thus,

the reduction of Cu^{2+} ions to Cu_2O takes place at the surface of micelle, leading to the formation of sphere-like nanostructures [38-40].

3.4 Conclusion

An atmospheric pressure plasma was used as a gaseous cathode to replace the solid cathode in the conventional electrochemical device, and the reducing species generated from the plasma-liquid interactions reacted with the Cu^{2+} ions released from the copper anode by anodic dissolution, resulting in the formation of Cu_2O nanoparticles in the liquid. By altering the components of the aqueous solutions (adding surfactants of glucose, ascorbic acid and CTAB), the sizes, the shapes and the Cu valence of the obtained Cu_2O nanoparticles was tuned. The results showed that the surfactant of glucose (2.0 mM) was favorable for obtaining Cu_2O nanoparticles with high absorption efficiency of MO molecules, while the surfactant of ascorbic acid (2.0 mM) favored the formation of Cu_2O nanoparticles with strong visible-light photocatalytic activity on the MO degradation. In the case of the surfactant of CTAB, the well-crystallized samples (with high CTAB concentrations) showed better photocatalytic ability on the MO degradation.

References

[1] Lieberman M A, Lichtenberg A J, Principles of Plasma Discharges and Materials Processing (New Jersey: Wiley-Interscience) (2005).

[2] Chen Q, Li J, Li Y, J. Phys. D: Appl. Phys. **48** 424005 (2015).

[3] Saito G, Akiyama T, J. Nanomater. **2015** 123696 (2015).

[4] Huang X, Li Y, Zhong X, Nanoscale Res. Lett. **9** 1 (2014).

[5] Huang X Z, Zhong X, Lu Y, Li Y S, Rider A E, Furman S A, Ostrikov K, Nanotechnol. **24** 095604 (2013).

[6] Wang R, Zuo S, Wu D, Zhang J, Zhu W, Becker K H, Fang J, Plasma Process. Polym. **12** 380 (2015).

[7] Meiss S A, Rohnke M, Kienle L, Zein El Abedin S, Endres F, J. Janek, ChemPhysChem **8** 50 (2007).

[8] Höfft O, Endres F, Phys. Chem. Chem. Phys. **13** 13472 (2011).

[9] Richmonds C, Sankaran R M, Appl. Phys. Lett. **93** 131501 (2008).

[10] Kaneko T, Baba K, Harada T, Hatakeyama R, Plasma Process Polym. **6** 713 (2009).

[11] Baba K, Kaneko T, Hatakeyama R, Appl. Phys. Express **2** 035006i (2009).

[12] Hu X, Cho S P, Takai O, Saito N, Cryst. Growth Des. **12** 119 (2011).

[13] Saito N, Hieda J, Takai O, Thin Solid Films **518** 912 (2009).

[14] Hieda J, Saito N, Takai O, J. Vac. Sci. Technol. A **26** 854 (2008).

[15] Toriyabe Y, Watanabe S, Yatsu S, Shibayama T, Mizuno T, Appl. Phys. Lett. **91** 041501 (2007).

[16] Saito G, Hosokai S, Tsubota M, Akiyama T, Plasma Chem. Plasma Process. **31** 719 (2011).

[17] Tokushige M, Yamanaka T, Matsuura A, Nishikiori T, Ito Y, IEEE Tran. Plasma Sci. **37** 1156 (2009).

[18] Tokushige M, Nishikiori T, Lafouresse M, Michioka C, Yoshimura K, Fukunaka Y, Ito Y, Electrochim. Acta **55** 8154 (2010).

[19] Pootawang P, Saito N, Takai O, Lee S Y, Nanotechnol. **23** 395602 (2012).

[20] Baba K, Kaneko T, Hatakeyama R, Appl. Phys. Express **2** 035006 (2009).

[21] Yan T, Zhong X, Rider A E, Lu Y, Furman S A, Ostrikov K, Chem. Commun. **50** 3144 (2014).

[22] Kang J, Li O L, Saito N, Nanoscale **5** 6874 (2013).

[23] Yang F, Li Y, Liu T, Xu K, Zhang L, Xu C, Gao J, Chem. Eng. J. **226** 52 (2013).

[24] Akolkara R, Sankarana R M, J. Vac. Sci. Technol. A **31** 050811 (2013).

[25] Chen Q, Li J, Saito K, Shirai H, J. Phys. D: Appl. Phys. **41** 175212 (2008).

[26] Mariotti D, Sankaran R M, J. Phys. D: Appl. Phys. **43** 323001 (2010).

[27] N. Shirai, S. Uchida, F. Tochikubo, Jpn. J. Appl. Phys. **53** 046202 (2014).

[28] Tsuyoshi M, Takaaki M, Hirofumi N, Tomoko Y, Shinya Y, Jpn. J. Appl. Phys. **53** 11RA03 (2014).

[29] Shirafuji T, Ueda J, Nakamura A, Cho S P, Saito N, Takai O, Jpn. J. Appl. Phys. **52** 126202 (2013).

[30] Chen Q, Kaneko T, Hatakeyama R, Curr. Appl. Phys. **11** S63 (2011).

[31] Liu J, Chen Q, Li J, Xiong Q, Yue G, Zhang X, Yang S, Liu Q H, J. Phys. D: Appl. Phys. **49** 275201 (2016).

[32] Du C, Xiao M, Sci. Rep. **4** 07339 (2014).

[33] Zheng Z, Huang B, Wang Z, Guo M, Qin X, Zhang X, Wang P, Dai Y, J. Phys. Chem. C **113** 14448 (2009).

[34] Huang L, Peng F, Yu H, Wang H, Solid State Sci. **11** 129 (2009).

[35] Zheng Z, Huang B, Wang Z, Guo M, Qin X, Zhang X, Wang P, Dai Y, J. Phys. Chem. C **113** 14448 (2009).

[36] L. Huang, F. Peng, H. Yu, H. Wang, Solid State Sci. **11** 129 (2009).

[37] De S, Mandal S, Colloids Surf. A Physicochem. Eng. Asp. **421** 72 (2013).

[38] Wang W, Tu Y, Zhang P, Zhang G, Cryst. Eng. Comm. **13** 1838 (2011).

[39] Zhang H, Shen C, Chen S, Xu Z, Liu F, Li J, Gao H, Nanotechnology **16** 267 (2005).

[40] Xu H, Wang W, Angew. Chem., Int. Ed. **46** 1489 (2007).

Chapter 4 Study on the influence factors affects the synthesis of Cu_2O nanoparticles by plasma electrolysis

Chapter 4 Study on the influence factors affects the synthesis of Cu_2O nanoparticles by plasma electrolysis

(This chapter of work is partially based on the following article: Jiandi Liu, Naoki Shirai and Koichi Sasaki, which has been accepted by J. Phys. D: Appl. Phys., and the details of paper can be seen at https://doi.org/10.1088/1361-6463/abca2a).

4.1 Introduction

Electrochemistry has a long history and plays an important role in electrolytic processing and energy production [1-3]. Commonly, the conventional electrochemical system is simply composed of two solid electrodes and electrolyte. The reduction and oxidation (redox) reactions occur at the interface between the solid electrodes and the electrolyte. When one or both the solid electrodes are replaced with a plasma, the conventional electrochemical system becomes a plasma electrochemical system. In this case, one or both the reduction and oxidation reactions occur at the interface between the plasma and the electrolyte. Plasmas are sources of various kinds of highly reactive species including ions, free electrons, excited molecules and radicals [4-14]. These species themselves, as well as secondary species produced at the interface and in the liquid phase, can lead many reactions. The plasma electrolysis is a novel technology based on the plasma-liquid interaction [15]. The system of the plasma electrolysis is similar to the conventional electrolysis except that a solid electrode is replaced with a gaseous plasma. The use of the gaseous plasma instead of the solid electrode benefits from the plasma-liquid interactions and turns the conventional electrolysis into the plasma electrolysis. Because the plasma electrolysis is composed of a plasma and a liquid, both the plasma and liquid parameters can influence the properties of final products.

In previous works, we have already used atmospheric-pressure argon plasma electrolysis for synthesizing Cu_2O nanoparticles and investigated the effects of additive surfactants such as glucose, ascorbic acid, and cetyltrimethylammonium bromide (CTAB) [16-18]. However, these works focused on the influence of the surfactants, and the synthesis route of Cu_2O is still unknown. Further works need to be done to reveal the synthesis mechanism.

In chapters 4 and 5, we have used atmospheric-pressure helium plasma electrolysis to synthesize

Cu_2O nanoparticles. It is noted that the difference between argon and helium glow discharge is the gas temperature. The gas temperature in argon glow discharge is higher than in helium glow discharge [19]. However, we believe that the ability for producing highly reactive species is same.

In order to clarify the synthesis mechanism of Cu_2O, we have investigated the effects of numerous parameters in the plasma electrolysis. These tuned parameters include the concentration of NaCl solution, the concentration of dissolved oxygen, the electrolyte temperature and the concentration of NaCl solution. The results indicate that some of them have effects, but some don't. A higher concentration of NaCl solution is more suitable for the formation of Cu_2O. The concentration of dissolved oxygen does not affect the synthesis of Cu_2O. The higher electrolyte temperature can improve the crystallinity of the final products. A high concentration of OH^- around the anode Cu plate is an important factor for the synthesis of Cu_2O nanoparticles. Consequently, the most important influence factors are the concentration of NaCl solution and the pH values of electrolyte. In addition, we originally expected that the reduction of $Cu_2(OH)_2^{2+}$ which should be driven by solvated electrons and/or atomic hydrogen at the plasma-liquid interface is the key for the synthesis of Cu_2O. However, we observed that the production of Cu_2O occurred in the vicinity of the anode plate even though the plasma was used as the cathode in the electrolysis system. This phenomenon makes us reconsider the synthesis mechanism of Cu_2O.

4.2 Experimental Procedure

Figure 4.1 shows the schematic diagram of the experimental apparatus for the sample preparation. Sodium chloride (NaCl) was dissolved into pure water to prepare the electrolyte with concentrations of 0.25, 0.5 and 1.0 M. The volume of the electrolyte was 50 mL. These concentrations resulted in the electrical conductivities of 24, 46 and 87 mS/m. A pre-polished copper plate (99.8%), which was partly immersed into the electrolyte, was used as the anode. The cathode was an atmospheric-pressure helium plasma which was generated between a brass tube (0.5 and 0.8 mm in inner and outer diameters, respectively) and the electrolyte surface. During the discharge, a plasma spot with a ring-like shape was observed on the electrolyte surface at all the experimental conditions. The tip of the brass tube was placed at a distance of 3 mm from the electrolyte surface. This distance was kept during discharge when the electrolyte was 50 mL. Helium was fed toward the electrolyte surface from the tube in air. The gas flow rate was maintained at 200 sccm which was controlled using a mass flow controller. A direct-

current power supply (Matsusada HAR-5P120) was used for producing a glow discharge along the helium flow. The voltage between the brass tube and the electrolyte was measured using a high voltage probe (Tektronix P6015A). In order to keep a stable discharge, the discharge current was kept at 20 mA. The duration of the discharge or the electrolysis reaction was 20 min. It is noted that the changes in the voltage and the current were negligible during the electrolysis experiment.

After the discharge, the suspension which included synthesized nanoparticles was concentrated by the centrifugation (5500 rpm, 5min), and nanoparticles were washed with purified water and ethyl alcohol for three times. After that, the sample was dried in an oven at 50 ◦C for 10 h for the characterization. We employed powder X-ray diffraction (XRD, Rigaku SmartLab 9 kW), field emission scanning electron microscopy (FESEM, JEOL JSM-7001FA), and transmission electron microscopy (TEM, JEOL JEM-2010 operated at 200 kV) for characterizing synthesized nanoparticles.

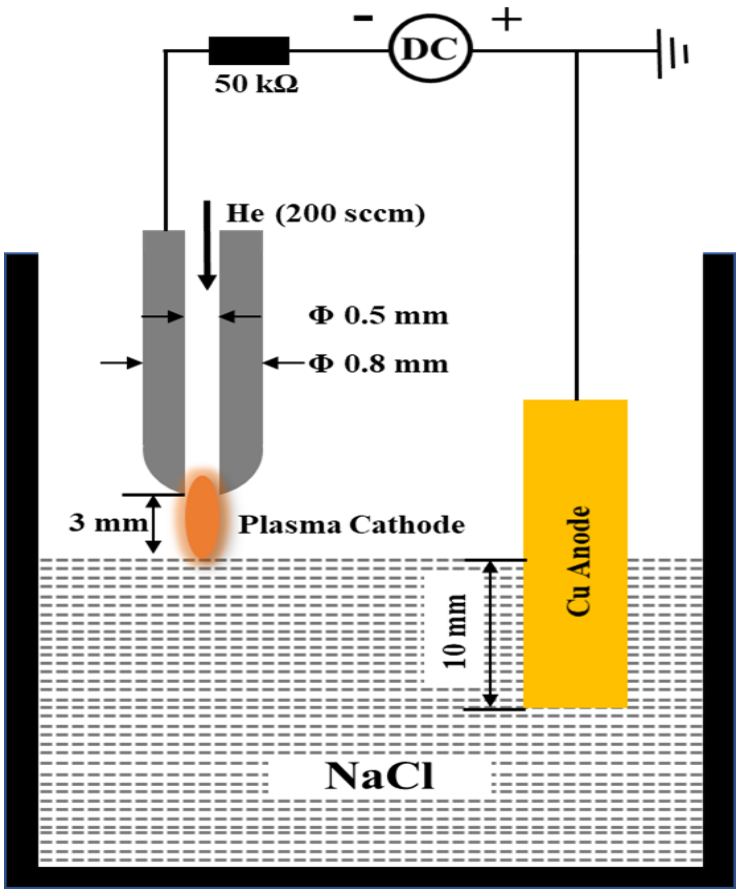

Figure 4.1. Schematic diagram of the experimental apparatus.

4.3 Results and Discussion

4.3.1 Effect of NaCl concentration

Several concentrations of NaCl, ranging between 0.25 and 1.0 M, were used for examining the effect of the Cl^- concentration on the synthesis of Cu_2O nanoparticles. Figure 4.2 shows the XRD patterns of the products synthesized at three NaCl concentrations. It is obvious that the major diffraction peaks of these samples coincide with the peaks of Cu_2O listed in the JCPDS database (No. 05-0667). On the other hand, the peaks corresponding to $Cu_2(OH)_3Cl$ were also found in all the samples synthesized at different NaCl concentrations. In addition, the peaks of by-product CuO were observed for the sample synthesized at an NaCl concentration of 0.25 M. This result indicates that the formations of Cu_2O and by-product CuO are related with the NaCl concentration. A higher concentration of NaCl solution is more suitable for the formation of Cu_2O.

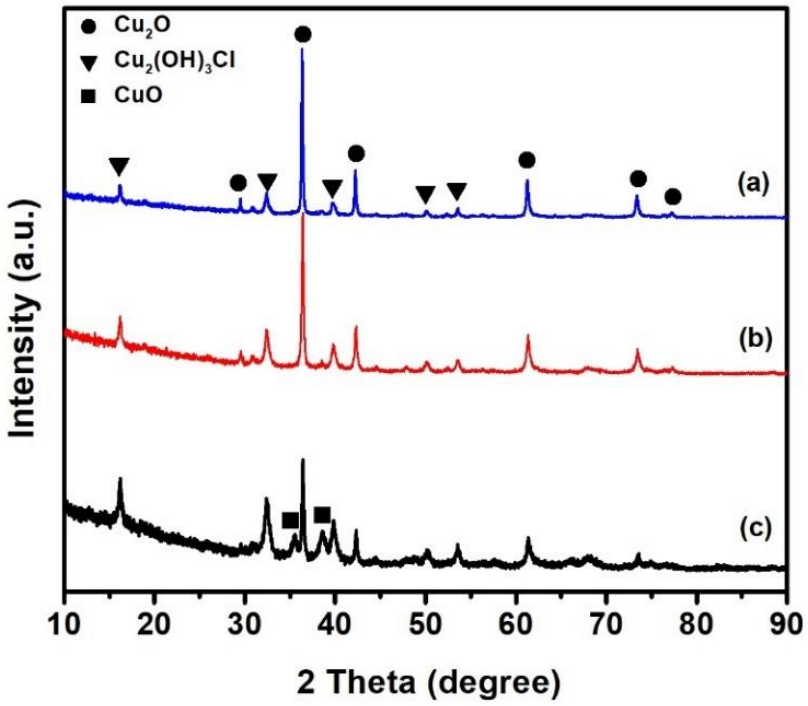

Figure 4.2. XRD patterns of nanoparticles synthesized at NaCl concentrations of (a) 1.0, (b) 0.5, and (c) 0.25 M.

Figure 4.3 shows FESEM pictures of nanoparticles synthesized at three NaCl concentrations. It is easy to understand that the NaCl concentration had a strong effect on the size of nanoparticles. The nanoparticles were composed of octahedrons, fibers, and small flakes with irregular sizes in all the cases. In the case of the 1.0 M NaCl solution, the sizes of octahedrons were larger than 1 μm, and the apexes of octahedrons were corroded as shown in figure 4.3(a). In the case of the 0.5 M NaCl solution, octahedrons with the size of ~ 500 nm were observed, and they had relatively sharp apexes. In the case of the 0.25 M NaCl solution, large-size octahedrons disappeared and the relative abundance of fiber structures increased, as shown in figure 4.3(c).

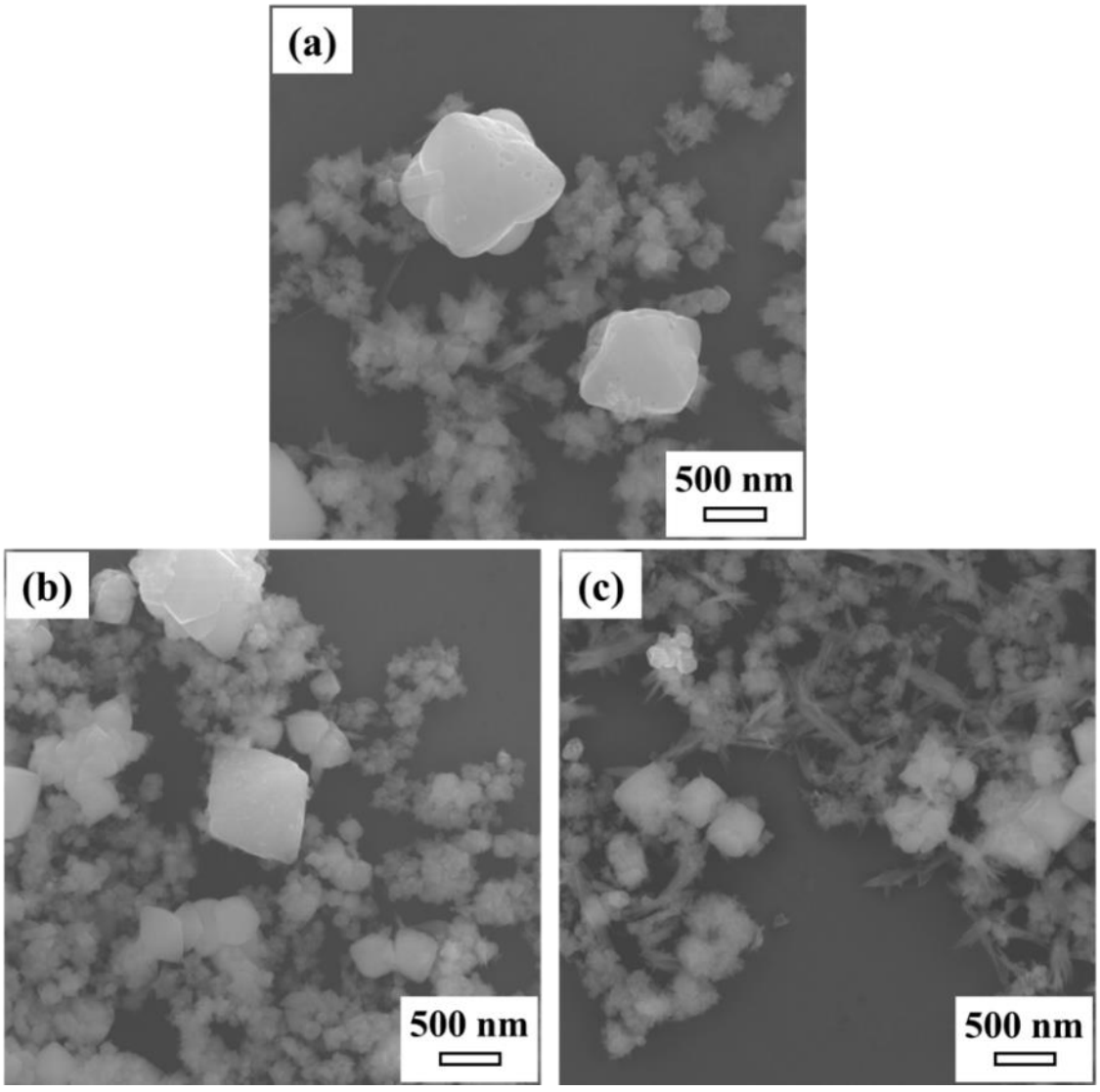

Figure 4.3. FESEM images of nanoparticles synthesized at NaCl concentrations of (a) 1.0, (b) 0.5, and (c) 0.25 M.

The details of the microstructure of nanoparticles synthesized at an NaCl concentration of 1.0 M were further investigated by TEM. Figure 4.4(a) demonstrates that the sample was composed of octahedrons and fiber structures, which is the same result as the FESEM pictures shown in figure 4.3(a). Figures 4.4(b) and 4.4(c) show the selected-area electron diffraction (SAED) patterns. The selected areas are indicated in figure 4.4(a). Figure 4.4(b) shows the SAED pattern which is taken from the edge of an octahedron structure. According to the SAED pattern, the lattice fringes with interlayer spacings of 0.246 and 0.135 nm can be attributed to the (111) and (310) facets of Cu_2O, respectively. The SAED pattern which was taken from the fiber structure is shown in figure 4.4(c). The SAED pattern shows the interlayer spacings of 0.303, 0.193, and 0.252 nm, which can be attributed to the (200), (222) and (103) facets of $Cu_2(OH)_3Cl$, respectively.

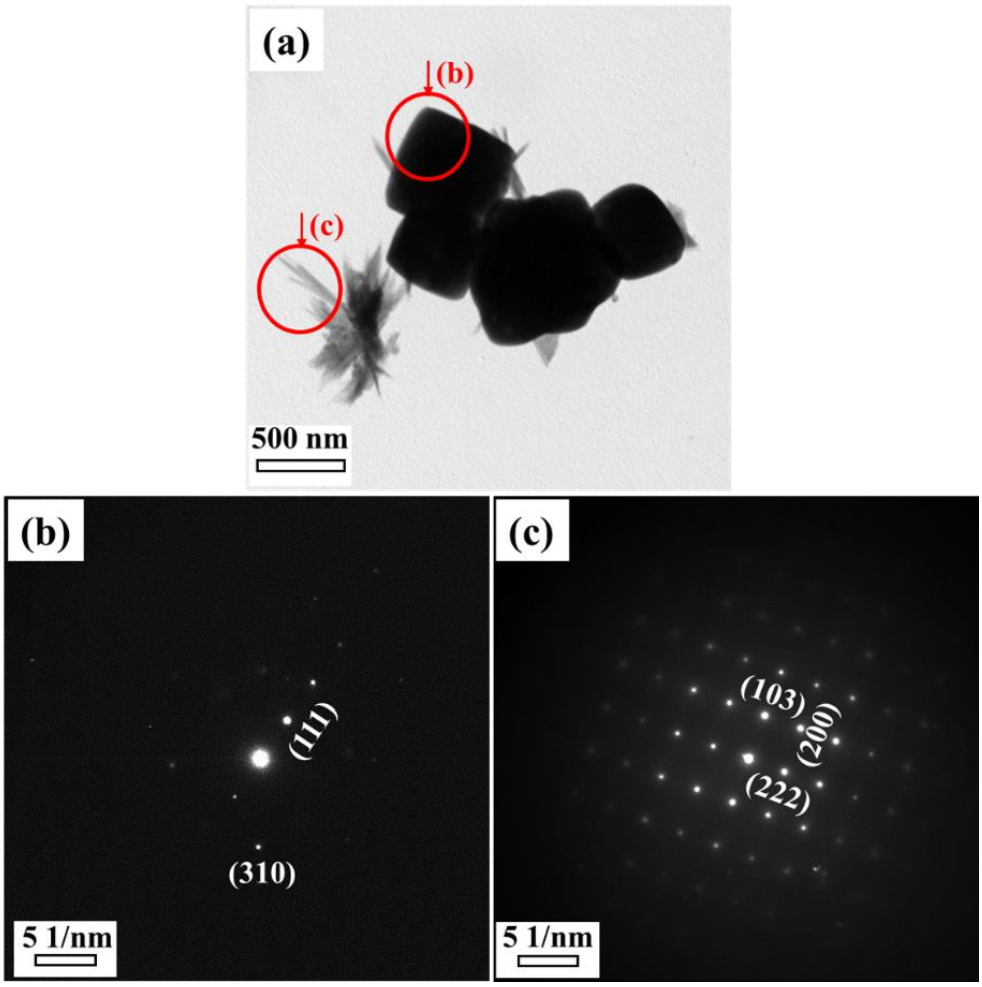

Figure 4.4. (a) TEM image of nanoparticles synthesized at an NaCl concentration of 1.0 M. (b) and (c) are SAED patterns of the regions indicated in (a) by circles.

4.3.2 Effect of dissolved oxygen

It is well known that oxygen can dissolve into solutions. In general, dissolved oxygen (DO) affects chemical reactions in the solution. For example, Yamazaki and coworkers have reported that the DO concentration is a key parameter in the synthesis of magnetite nanoparticles by glow-discharge electrolysis [20]. The concentration of DO significantly determines the kind of the final product, nonmagnetic hematite (Fe_2O_3) nanoparticles or ferromagnetic magnetite (Fe_3O_4) nanoparticles.

As described in Section 4.3.1, the peaks corresponding to CuO were found in the XRD pattern only for the sample synthesized at an NaCl concentration of 0.25 M. It is noted here that the DO concentration is affected by the salinity (Table 4.1). The concentrations of NaCl solution of 1.0 M and 0.25 M are referred to the salinity of 60 and 15 g/kg, respectively. According to the relationship between DO and the salinity, the difference of DO concentration should be higher than 1.8 mg/L. This suggests the possibility that the NaCl concentration works as an indirect parameter to control the DO concentration, and the direct parameter which dominates the synthesis of Cu_2O is the DO concentration. Hence, we examined the effect of the DO concentration on the synthesis characteristics with keeping the NaCl concentration at 0.5M and 0.25 M.

Table 4.1. Relationship between dissolved oxygen with temperature and salinity (DO/ mg/L).

Temperature	Salinity (g/kg)						
(°C)	0	5	10	15	20	25	30
20	9.1	8.8	8.7	8.3	8.1	7.9	7.7
22	8.7	8.5	8.2	8.0	7.8	7.6	7.3
24	8.4	8.1	7.9	7.7	7.5	7.3	7.1
26	8.1	7.8	7.6	7.4	7.2	7	6.8
28	7.8	7.6	7.6	7.2	7.0	6.8	6.6
30	7.5	7.3	7.1	6.9	6.7	6.5	6.3
32	7.3	7.3	6.8	6.7	6.5	6.3	6.1

The DO concentration was varied by changing the duration of the nitrogen bubbling. The DO concentration was measured using a commercial DO meter. The DO concentration of the 0.5 M and 0.25 M NaCl solutions were 8.4 and 7.9 mg/L, respectively, when the nitrogen bubbling was not adopted. The DO concentrations after the nitrogen bubbling for 30 min were 1.1 and 1.0 mg/L. It was shown that the DO concentrations were significantly decreased by nitrogen bubbling. It is noted that the recovery of the DO concentration was slow and it changed from 1.0 to 3.1 mg/L after the one-night aging.

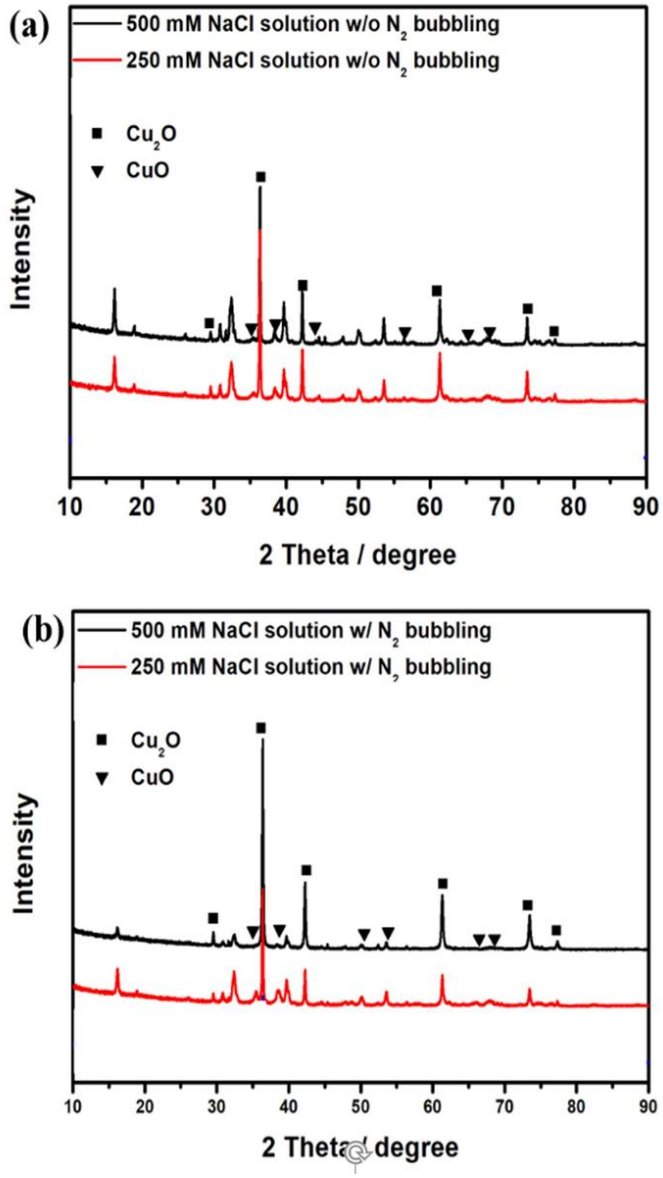

Figure 4.5. XRD patterns of nanoparticles synthesized (a) without nitrogen bubbling and (b) with nitrogen bubbling. The NaCl concentration was 0.5 M and 0.25 M.

The XRD patterns of the samples synthesized without and with nitrogen bubbling are shown in figure 4.5. In the case of without nitrogen bubbling, as shown in figure 4.5(a), we observed the strong peaks corresponding to Cu_2O and the weak peaks corresponding to CuO in both the NaCl concentrations. In the case with nitrogen bubbling, as shown in figure 4.5(b), it was difficult to find the difference in the products synthesized without and with nitrogen bubbling.

We also checked the relationship between the changes of DO concentrations and the duration of nitrogen bubbling. In the case of 0.25 M NaCl solution, the initial DO concentration was 7.9 mg/L as mentioned previously. The DO concentrations after the nitrogen bubbling for 1, 2.5, 5, and 10 min were 6.4, 5.2, 3.7 and 1.9 mg/L, respectively. The XRD patterns of the samples synthesized at several DO concentrations are shown in figure 4.6. As shown in the XRD patterns, the strong peaks corresponding to Cu_2O and the weak peaks corresponding to CuO were observed in all the samples, and it was difficult to find the difference in the products synthesized at different DO concentrations. Therefore, it is suggested that the DO concentration has negligible effect on the synthesis of Cu_2O nanoparticles.

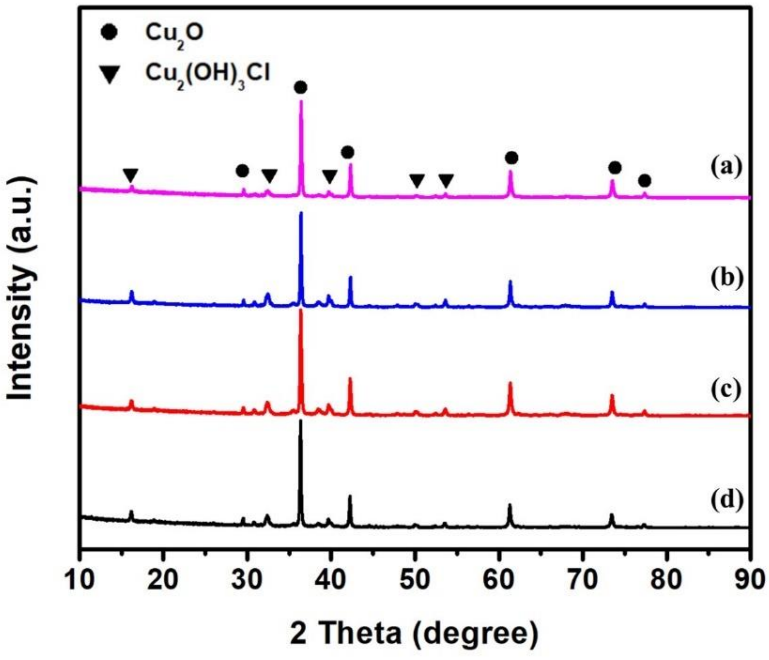

Figure 4.6. XRD patterns of nanoparticles synthesized at DO concentrations of (a) 6.4, (b) 5.2, (c) 3.7, and (d) 1.9 mg/L. The NaCl concentration was 0.25 M.

4.3.3 Effect of electrolyte temperature

In solution-based nanomaterial synthesis, the temperature of the electrolyte plays an important role on the formation of nanoparticles as well as the microstructure. The growth rate of nanoparticles can be tuned by the appropriate temperature of the solution as well as sufficient duration time of the maintained temperature. In the plasma electrolysis system, it is also a key parameter on the nanoparticles synthesis. In order to investigate the effect of the electrolyte temperature, a heater is used to heat the solution to specified temperature including 20, 50 and 80 ºC, then the heated solution is used as the electrolyte.

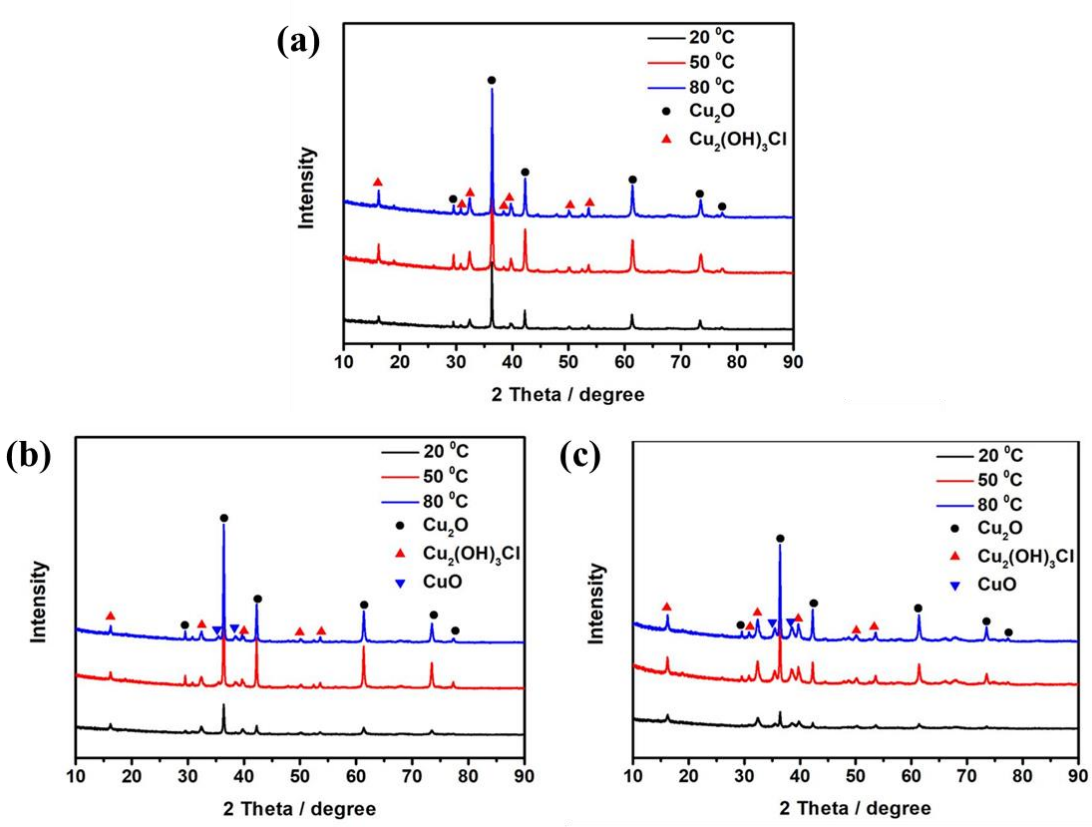

Figure 4.7. XRD patterns of products formed at different electrolyte temperatures: (a) 1.0 M NaCl solution, (b) 0.5 M NaCl solution and (c) 0.25 M NaCl solution.

Several concentrations of NaCl, ranging between 0.25 and 1.0 M, were used for examining the effect of the electrolyte temperature on the synthesis of Cu_2O nanoparticles. Figure 4.7 shows the XRD patterns of the synthesized products at different solution temperatures. In the case of 1.0 M NaCl solution, we observed that the major diffraction peaks of the obtained samples were nearly the same as and coincided with the peaks of Cu_2O listed in the JCPDS database (No. 05-0667). On the other hand, the peaks corresponding to $Cu_2(OH)_3Cl$ were also found in all the samples synthesized at different electrolyte temperatures. In the case of 0.5 M NaCl solution, it is obvious that the compositions of the obtained samples were nearly the same. In addition, the sharpness of the major diffraction peaks corresponding to Cu_2O increases as the increase in electrolyte temperature, which means the higher electrolyte temperature can improve the crystallinity of the final products. In the case of 0.25 M NaCl solution, the same results were obtained.

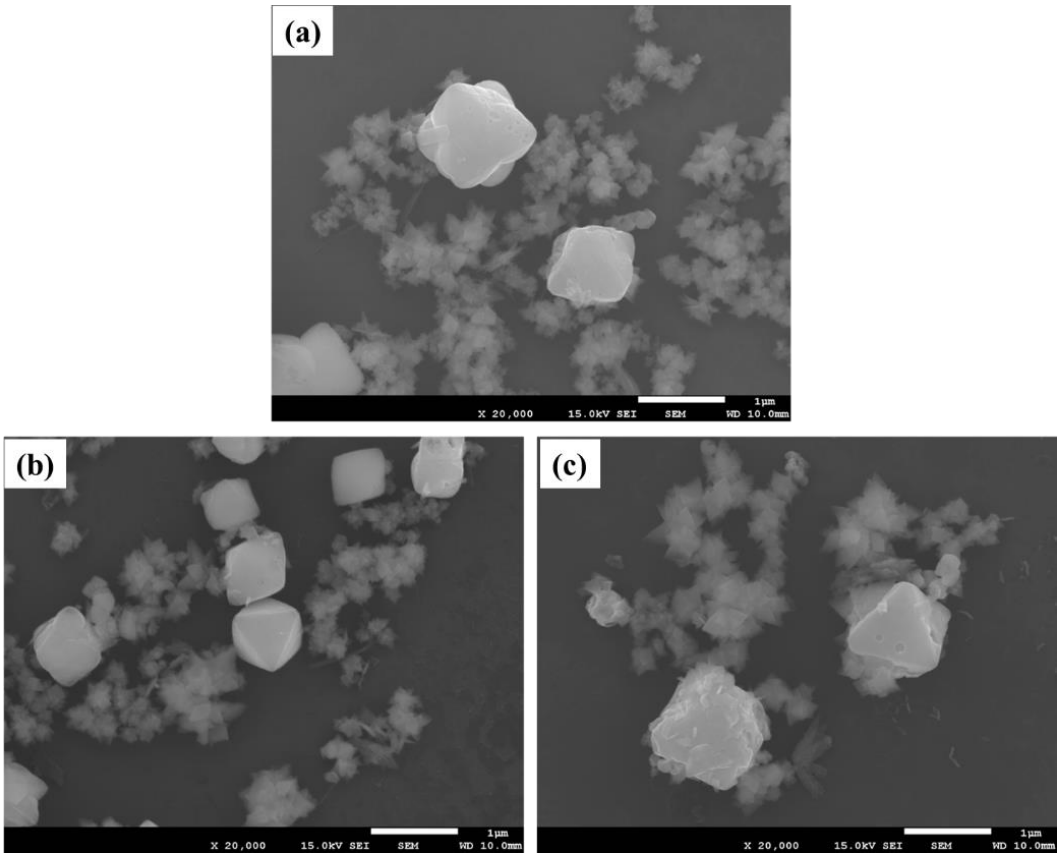

Figure 4.8. FESEM images of nanoparticles synthesized at temperatures of (a) 20 ºC, (b) 50 ºC and (c) 80 ºC, respectively. The NaCl concentration was 1.0 M.

Figure 4.8 shows FESEM pictures of nanoparticles synthesized at three temperatures: 20 ºC, 50 ºC and 80 ºC. According to figure 4.8, in all the cases, the nanoparticles were mainly composed of octahedrons and small flakes with irregular sizes. At the temperatures of 20 ºC, the sizes of octahedrons were larger than 1 µm, and the apexes of octahedrons were corroded as shown in figure 4.8(a). At the temperatures of 50 ºC, octahedrons with the size ranging from ~ 400 nm to ~ 800 nm were observed, and they had relatively sharp apexes. At the temperatures of 50 ºC, the sizes of octahedrons became larger and the surfaces of octahedrons were rough, as shown in figure 4.8(c). It suggested that the electrolyte temperature of 50 ºC is the best parameter to obtain Cu_2O nanoparticles with fine morphology.

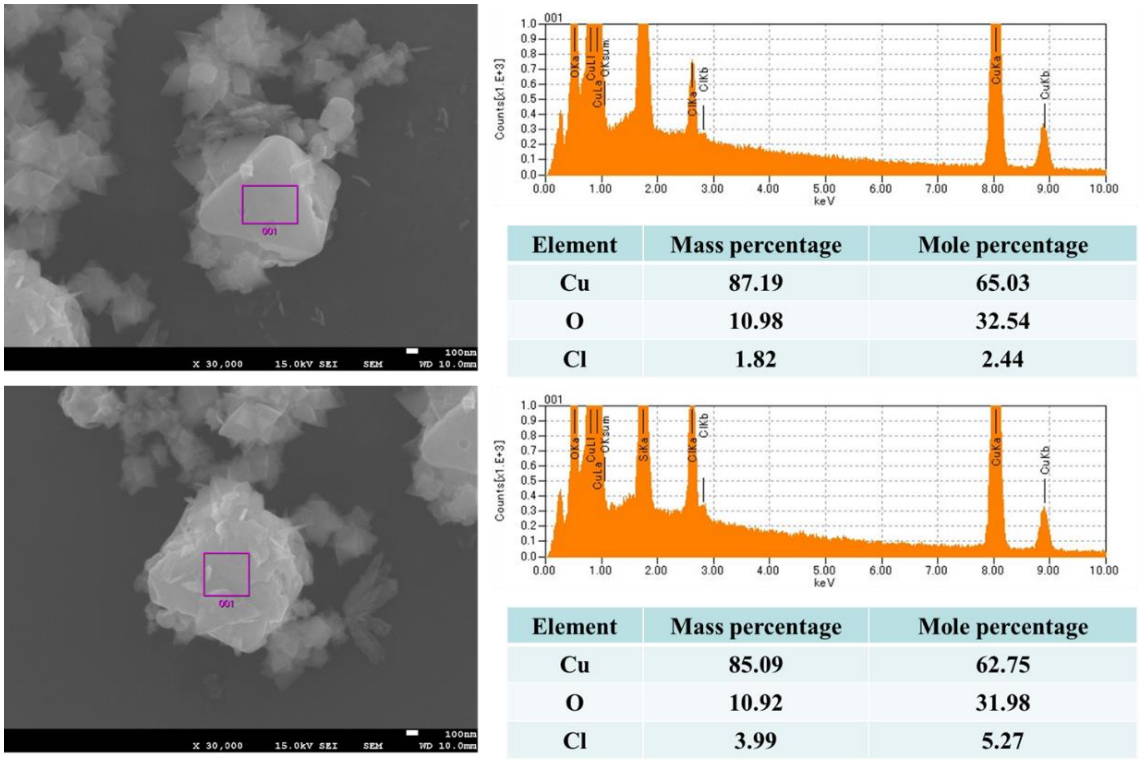

Element	Mass percentage	Mole percentage
Cu	87.19	65.03
O	10.98	32.54
Cl	1.82	2.44

Element	Mass percentage	Mole percentage
Cu	85.09	62.75
O	10.92	31.98
Cl	3.99	5.27

Figure 4.9. EDS spectrums of the obtained products synthesized at the electrolyte temperature of 80 ºC. The NaCl concentration was 1.0 M.

Energy dispersive X-ray spectroscopy (EDS) is a chemical microanalysis technique used in conjunction with SEM. The EDS technique detects x-rays emitted from the sample during bombardment by an electron beam to characterize the elemental composition of the analyzed volume. In order to clarify the elemental composition of the samples, we also did the EDS testing in the case of the temperatures of 80 ºC. As shown in figure 4.9, two areas of the octahedrons were selected for the EDS test. According to the EDS spectrum, we could observe the peaks corresponding to the elements of Cu, O and Cl. The mass and mole percentages of the elements of Cu, O and Cl, are also listed in figure 4.9. It is easy to find that the molar mass ratio between Cu and O is nearly 2:1 which suggests that the octahedrons are composed of Cu_2O. This result is similar to the result shown in figure 4.4.

4.3.4 Effect of pH value

In general, the pH value of the solution is a non-negligible factor in most researches using aqueous solutions as well as the plasma electrolysis. The pH value of the 0.5 M NaCl solution with no additives was 5.8. The pH values of the 0.5 M NaCl solutions before starting the electrolysis were controlled between 10.5 and 3.2 by adding various amounts of hydrochloric acid (HCl) or sodium carbonate (Na_2CO_3). The XRD patterns of the products synthesized at several pH values are shown in figure 4.10. We observed that the XRD pattern of the sample synthesized at a pH value of 3.2 was significantly different from those synthesized at other pH values. In the cases of the alkaline conditions with pH values of 10.5 and 8.0, the products are the mixture of Cu_2O and $Cu_2(OH)_3Cl$. The sample synthesized at a weak acid condition with a pH value of 5.8 was similar to those synthesized at alkaline conditions. In contrast, in the sample synthesized at a strong acid condition with a pH value of 3.2, only the peaks of $Cu_2(OH)_3Cl$ were observed and the peaks of Cu_2O disappeared. This result demonstrates that the pH value of the electrolyte has significant influence on the synthesis of Cu_2O nanoparticles.

Even though the pH value before starting the electrolysis was controlled, it was varied during the electrolysis by the production of OH^- from the region of the electrolyte in contact with the plasma cathode [21]. The pH values after the electrolysis were 10.7, 10.3, 10.0 and 5.7 when the original values were 10.5, 8.0, 5.8 and 3.2, respectively. The pH value was still lower than 6 after the electrolysis only when the original pH value was 3.2, and as shown in figure 4.10, Cu_2O nanoparticles were not synthesized only in this case. Note that these pH values were volume-averaged ones in the reactor.

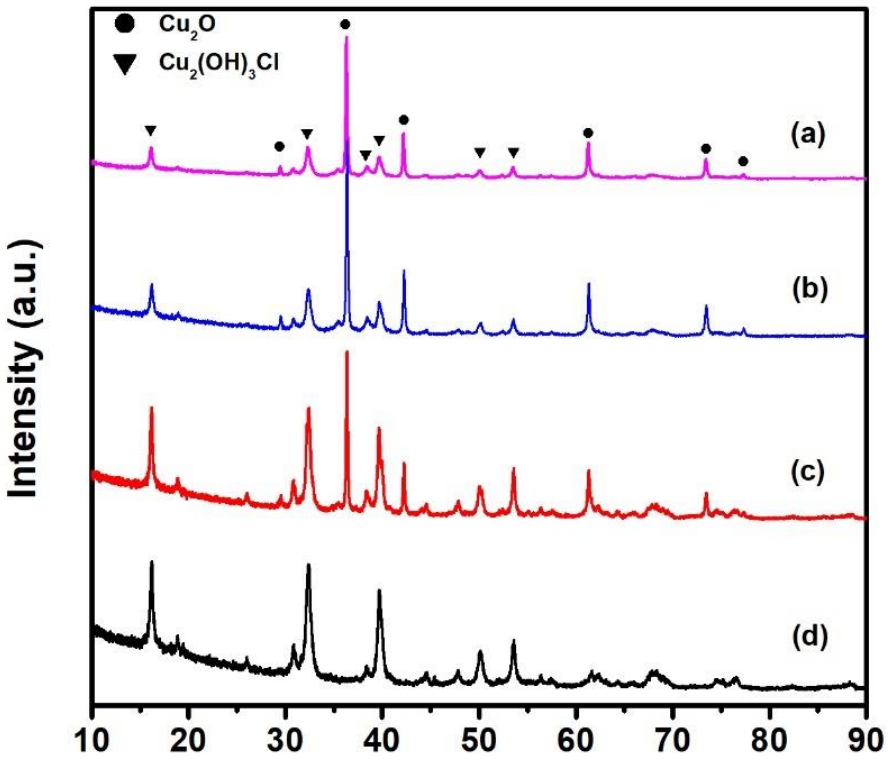

Figure 4.10. XRD patterns of nanoparticles synthesized in 0.5 M NaCl solutions with pH values of (a) 10.5, (b) 8.0, (c) 5.8, and (d) 3.2. The NaCl concentration was 0.5 M.

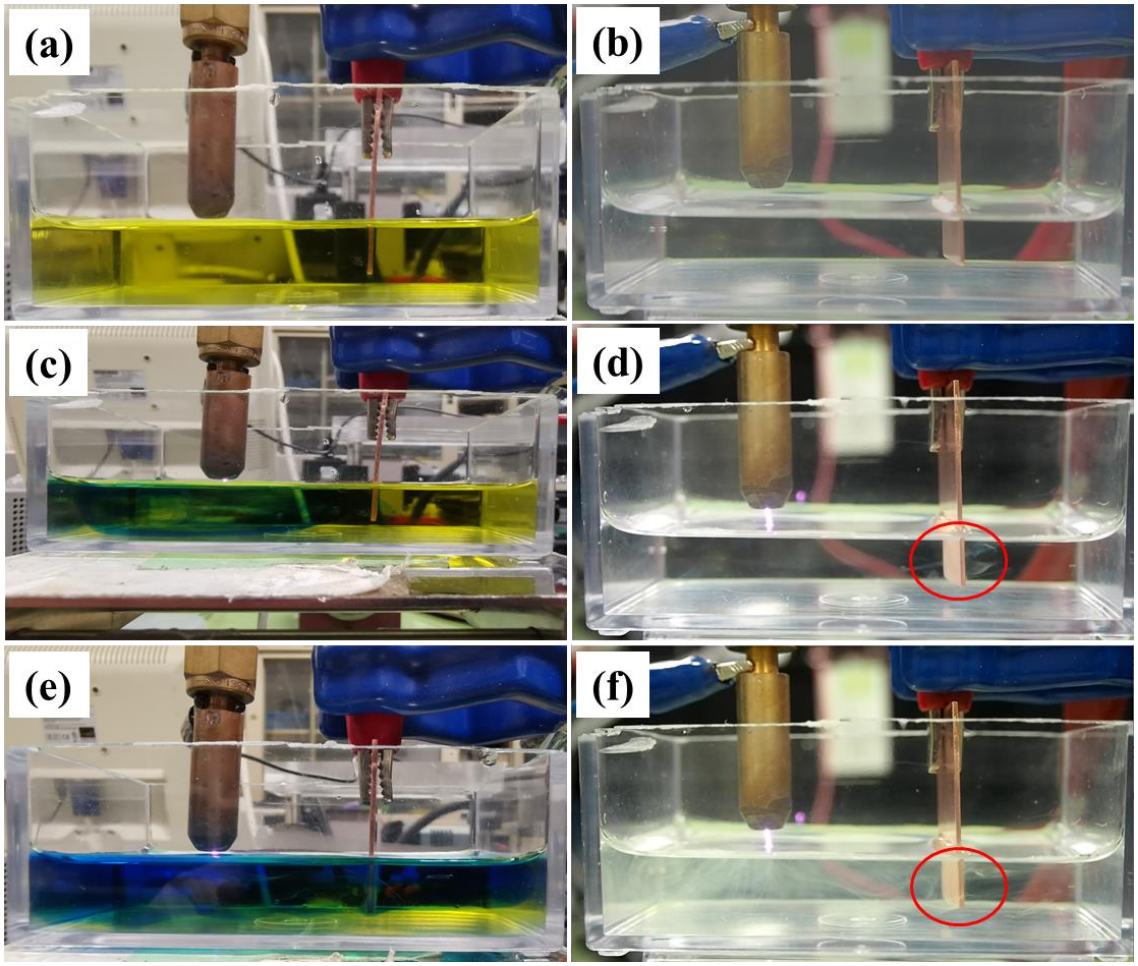

Figure 4.11. Photographs of reactors with ((a), (c), and (e)) and without ((b), (d), and (f)) the admixture of BTB. (a) and (b): before the discharge, (c) and (d): 30 s after the initiation of the discharge, and (e) and (f): at 2 min after the initiation of the discharge.

In order to observe the variation of the pH value visually during the discharge, a pH indicator named bromothymol blue (BTB) was admixed into the electrolyte. The BTB-admixed electrolyte is yellow in the acid condition ($pH \leq 6$), but the color is blue when the pH value is higher than 7.6. Figure 4.11 shows the temporal variation of the color of the BTB-admixed electrolyte, together with the pictures of the reactor with no BTB admixture at the same delay times after the initiation of the discharge. The pH value before the initiation of the discharge was 5.8 and the color of the electrolyte was yellow as shown in figure 4.11(a). At 30 s after the initiation of the discharge, we observed that the electrolyte just below the plasma cathode became alkaline, as shown in figure 4.11(c). This is due to the production of OH^-. The blue area expanded toward the Cu anode area. At the same time, we observed the production of yellow insoluble precipitates from the anode, as shown in figure 4.11(d). These insoluble precipitates were Cu_2O nanoparticles. The blue or alkaline area expanded to the most region of electrolyte at 2 min after the initiation of the discharge, as shown in figure 4.11(e). Meanwhile, the insoluble yellow precipitates diffused to the entire region of the electrolyte as shown in figure 4.11(f). This result indicates that an alkaline condition or a high concentration of OH^- around the anode Cu plate is an important factor for the synthesis of Cu_2O nanoparticles.

4.4 Conclusions

In order to clarify the synthesis mechanism of Cu_2O, we have investigated the effects of numerous parameters including the concentration of NaCl solution, the concentration of dissolved oxygen, the electrolyte temperature and the concentration of NaCl solution. The results indicate that some of them have effects, but some don't. A higher concentration of NaCl solution is more suitable for the formation of Cu_2O. The concentration of dissolved oxygen does not affect the synthesis of Cu_2O. The higher electrolyte temperature can improve the crystallinity of the final products. A high concentration of OH^- around the anode Cu plate is an important factor for the synthesis of Cu_2O nanoparticles. In addition, we observed that the production of Cu_2O occurred in the vicinity of the anode plate even though the plasma was used as the cathode in the electrolysis system which exceeded our expectation. We originally expected that the reduction of $Cu_2(OH)_2^{2+}$ which should be driven by solvated electrons and/or atomic hydrogen at the plasma-liquid interface is the key for the synthesis of Cu_2O. This phenomenon makes us reconsider the synthesis mechanism of Cu_2O.

References

[1] Qiao J, Liu Y, Hong F, Zhang J, Chem Soc Rev **43**:631(2014).

[2] Ni M, MKH Leung, DYC Leung, Sumathy K, Renew Sustain Energy Rev **11**:401 (2007).

[3] Liu H, Song C, Zhang L, Zhang J, Wang H, Wilkinson D P, J Power Sources **155**:95 (2006).

[4] Samukawa S, Hori M, Rauf S, Tachibana K, Bruggeman P, Kroesen G, Whitehead J C, Murphy A B, Gutsol A F, Starikovskaia S, J. Phys. D: Appl. Phys. **45** 253001 (2012).

[5] Martin J C, J.C. Martin on Pulsed Power (New York: Plenum) (1996).

[6] Webb M R and Hieftje G M, Anal. Chem. **81** 862 (2009).

[7] Smoluch M, Mielczarek P and Silberring J, Mass Spectrom. Rev. **35** 22 (2016).

[8] Foster J E, Sommers B S, Gucker S N, Blankson I M and Adamovsky G, IEEE Trans. Plasma Sci. **40** 1311 (2012).

[9] Mariotti D, Patel J, Svrcek V and Maguire P, Plasma Proc. Polym. **9** 1074 (2012).

[10] Ishijima T, Nosaka K, Tanaka Y, Uesugi Y, Goto Y and Horibe H, Appl. Phys. Lett. **103** 142101 (2013).

[11] Friedrich J F, Mix N, Schulze R-D, Meyer-Plath A, Ranjit J R and Wettmarshausen S, Plasma Proc. Polym. **5** 407 (2008).

[12] Bruggeman P J and Locke B R, Low Temperature Plasma Technology ed P K Chu and X P Lu (London: Taylor and Francis) (2013).

[13] Sato M, Ohgiyama T and Clements J S, IEEE Trans. Ind. Appl. **32** 106 (1996).

[14] Fridman G, Friedman G, Gutsol A, Shekhter A B, Vasilets V N and Fridman A, Plasma Proc. Polym. **5** 503 (2008).

[15] Bruggeman P J et al., Plasma Sources Sci. Technol. **25** 053002 (2016).

[16] Liu J D, Chen Q, Li J S, Xiong Q, Yue G H, Zhang X H, Yang S Z, Liu Q H, J. Phys. D Appl. Phys. **49** 275201 (2016).

[17] Liu J D, He B B, Chen Q, Liu H, Li J S, Xiong Q, Zhang X H, Yang S Z, Yue G H, and Liu Q H, Electrochemica Acta **222** 1677 (2016).

[18] Liu J D, He B B, Wang X, Chen Q, and Yue G H, Eur. Phys. J. D **73**: 11 (2019).

[19] David S, Bakhtier F, Alexander G and Alexander F, Plasma Sources Sci. Technol. **17** 025013 (2008).

[20] Yamazaki Y, Shirai N, Nakagawa Y, Uchida S, and Tochikubo F, Jpn. J. Appl. Phys. **57** 096201

(2018).

[21] Shirai N, Uchida S, and Tochikubo F, Jpn. J. Appl. Phys. **53** 046202 (2014).

Chapter 5 Study on the synthesis mechanism of Cu_2O nanoparticles synthesis and the comparison between plasma electrolysis and conventional electrolysis

Chapter 5 Study on the synthesis mechanism of Cu_2O nanoparticles synthesis and the comparison between plasma electrolysis and conventional electrolysis

(This chapter of work is partially based on the following article: Jiandi Liu, Naoki Shirai and Koichi Sasaki, which has been accepted by J. Phys. D: Appl. Phys., and the details of paper can be found at https://doi.org/10.1088/1361-6463/abca2a.

5.1 Introduction

Recently, nanomaterials synthesis by plasma-liquid interactions have developed rapidly due to the unique properties. Amounts of research have been carried out including noble metal [1,2], magnetic materials [3-5], metal oxide [6-9], and carbon materials [10]. Since plasma-liquid interactions can produce various kinds of high reactive species which then diffuse into liquid phase from gaseous plasma phase, the plasma-liquid interface and bulk liquid become reaction zones for the synthesis of nanomaterials. Therefore, it is very complicated to clarify which kinds of reactive species dominant the synthesis process.

In order to find out the synthesis mechanism of nanomaterials by plasma-liquid interactions, various kinds of research have been carried out especially on the novel metal nanoparticles. Shirai et al. [11] have synthesized Ag nanoparticles in a Hofmann electrolysis apparatus with two glow discharges acting as electrodes. They found that Ag nanoparticles were only produced at the anode and attribute the reduction of Ag^+ to electron injection. Sankaran et al. [12] have applied gravimetric analysis to quantify the charge transfer (faradaic) efficiency of the reduction of $AgNO_3$ aqueous solution in an electrolytic cell with a plasma cathode. The trends observed for the faradaic efficiency confirmed the importance of solvated electrons in the reduction of Ag^+ to Ag^0. Bruggeman et al. [13] presented a study of the chemical mechanism of Ag nanoparticles formation by a RF atmospheric pressure plasma jet and found that H radicals play an important role in the reduction of silver ions. Mariotti et al. [14] have successfully synthesized Au nanoparticles with various sizes by plasma-induced non-equilibrium liquid chemistry

and found that H_2O_2 played an important role of reducing Au^{3+} ions to Au^0 atoms, leading to nucleation growth of the Au nanoparticles. However, the synthesis mechanism of transition metal nanomaterials by plasma-liquid interactions is still unclear since the case of transition metal is more complicated compared with novel metal.

The plasma electrolysis is a novel technology based on the plasma-liquid interaction [15]. The system of the plasma electrolysis is like the conventional electrolysis except that a solid electrode is replaced with a gaseous plasma. The use of the gaseous plasma instead of the solid electrode benefits from the plasma-liquid interactions and turns the conventional electrolysis into the plasma electrolysis. Because the plasma electrolysis is composed of a plasma and a liquid, both the plasma and liquid parameters can influence the properties of final products.

In previous works, we have already synthesized Cu_2O nanoparticles by atmospheric-pressure plasma electrolysis and investigated the effect of additive surfactants [9,16,17]. These works focused on the influence of the surfactants, and the synthesis route of Cu_2O is still unknown. Then, we have investigated the effects of several parameters in the plasma electrolysis using NaCl aqueous solution without additives to understand the synthesis mechanism of the Cu_2O nanoparticles [18]. In this chapter, we propose an appropriate synthesis mechanism of Cu_2O nanoparticles according to the experiment results. During the synthesis, the reaction between $CuCl_2^-$ produced via the anodic dissolution of Cu and OH^- produced by plasma irradiation is responsible for the formation of Cu_2O. Considering the anodic dissolution of the Cu plate and the production of OH^- are also available in the conventional electrolysis, the comparison between the plasma and conventional electrolysis has also been carried out. The observation of the Cu_2O nanoparticles synthesized by the conventional electrolysis indicated that the plasma electrolysis was not a unique method to synthesize Cu_2O nanoparticles. In addition, we compared the plasma and conventional electrolysis and found out their differences in the synthesis rate, the minimum NaCl concentration, and the size and the shape of synthesized nanoparticles.

5.2 Synthesis mechanism of Cu_2O nanoparticles by plasma electrolysis

In chapter 4, section 4.3.6, we have investigated the effect of pH value on the synthesis process. A pH indicator, bromothymol blue (BTB), was admixed into the electrolyte to make sure the visual observation of the variation of the pH value during the discharge. The BTB-admixed electrolyte is

yellow in the acid condition (pH ≤ 6), but the color is blue when the pH value is higher than 7.6. Figure 5.1 shows the temporal variation of the color of the BTB-admixed electrolyte. The pH value before the initiation of the discharge was 5.8 and the color of the electrolyte was yellow as shown in figure 5.1(a). At 30 s after the initiation of the discharge, it was obvious that the electrolyte near the plasma cathode became alkaline, as shown in figure 5.1(b). This is due to the production of OH^-. The blue area or alkaline area expanded toward the Cu anode area and the most region of electrolyte became blue at 2 min after the initiation of the discharge, as shown in figure 5.1(c). At the same time, we could observe the production of insoluble precipitates from the anode and diffuse in solution as the region marked by red circles shown in figure 5.1(c). These insoluble precipitates were Cu_2O nanoparticles. After the discharge, we could clearly observe the insoluble precipitates diffused to the entire region of the electrolyte as shown in figure 5.1(d). This result indicates that an alkaline condition or a high concentration of OH^- around the anode Cu plate is an important factor for the synthesis of Cu_2O nanoparticles. In addition, the phenomenon of the Cu_2O nanoparticles synthesis from Cu anode was quite amazing. We expected that the production of reactive species such as solvated electrons and H radicals in the plasma-liquid interface would react with the Cu^{2+} released by the anodic dissolution of Cu and the Cu_2O nanoparticles were finally formed near the interface. However, this phenomenon showed our expectation was incorrect and the synthesis of Cu_2O nanoparticles was more complicated than the Au and Ag nanoparticles.

A comparison between the cases with and without the BTB-admixed has also been carried out under the same condition as shown in figure 5.2. Before the initiation of the discharge, the color of the BTB-admixed electrolyte was yellow while the BTB-unadmixed electrolyte was transparent as shown in figures 5.2(a) and 5.2(b). At 30 s after the initiation of the discharge, we observed that the electrolyte below the plasma cathode became alkaline and the blue area or alkaline area reached the surface of Cu anode, as shown in figure 5.2(c). At the same time, as shown in figure 5.2(d), the generation of yellow insoluble precipitates from the anode could clearly be observed by naked eyes. This phenomenon was so interesting that the formation of Cu_2O nanoparticles should be attributed to the reaction between OH^- and something on the Cu surface.

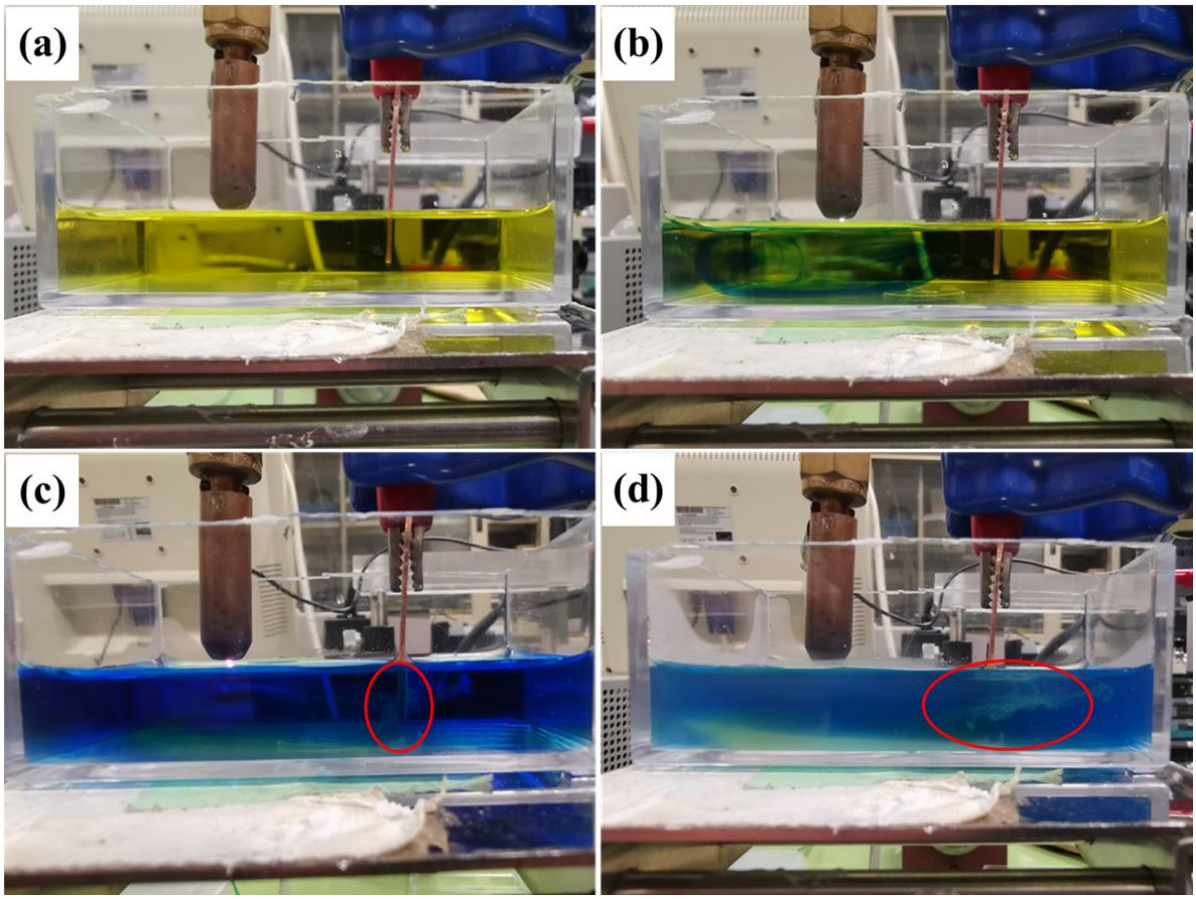

Figure 5.1. Photographs of reactors with the admixture of BTB. (a): before the discharge, (b): 30 s after the initiation of the discharge, (c): 2 min after the initiation of the discharge and (d): after the discharge.

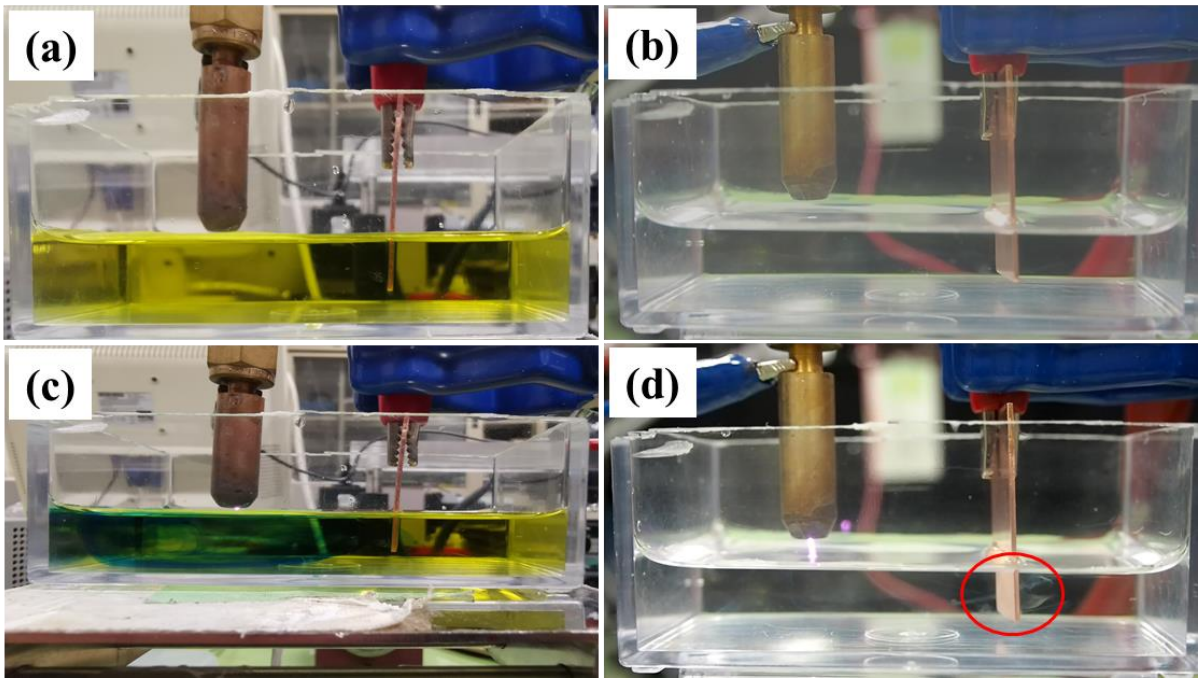

Figure 5.2. Photographs of reactors with ((a) and (c)) and without ((b) and (d)) the admixture of BTB. (a) and (b): before the discharge, and (c) and (d): at 30 s after the initiation of the discharge.

In our expectation, the Cu plate is not only severed as anode, but also the source of Cu^{2+} ions in the solution. The Cu^{2+} released by the anodic dissolution of Cu transports to the plasma-liquid interface and reacts with solvated electrons or other species to form Cu_2O. However, the anodic dissolution of Cu in chlorine solution is a complicated process and has been extensively studied by corrosion scientists and applied electrochemists [19]. In the copper metal/chloride corrosion system, the chloride ion has a strong influence on the copper corrosion mechanism [19-25]. The copper anodic dissolution reaction is usually carried out at chloride ion concentrations roughly equivalent to that of seawater (the concentration of $Cl^- \approx 0.5$-0.6 mol/L or 3.0-3.6% w/v NaCl). The anodic reaction is dominated by complex reactions between the cuprous ion and the chloride ion. While the cathodic reaction is dominated by oxygen reduction.

There were three possible models demonstrating the initial, anodic dissolution reactions of copper. The first model, which was developed by Bacarella and Griess [22], demonstrated that copper directly dissolves as the $CuCl_2^-$ ion in NaCl solution at the first step,

$$Cu^0 + 2Cl^- \rightarrow CuCl_2^- + e \quad (5.1)$$

Comparatively, Lee and Nobe assumed that the anodic reaction could be represented by a two-step process [20,21]:

$$Cu^0 + Cl^- \rightarrow CuCl + e \quad (5.2)$$

followed by

$$CuCl + Cl^- \rightarrow CuCl_2^- \quad (5.3)$$

According to the work by Smyrl [23], copper anodically dissolved in acidic chloride by the one electron reaction and then cuprous species participated in a complexation reaction:

$$Cu^0 \rightarrow Cu^+ + e \quad (5.4)$$

followed by

$$Cu^{+} + 2Cl^{-} \rightarrow CuCl_2^{-} \quad (5.5)$$

Bianchi et al. [26] demonstrated that $CuCl_2^-$ was the main cuprous chloride complex in seawater and NaCl solutions with the concentration of Cl^- approximating 0.55 mol/L. As a result, the formation of the copper complex $CuCl_2^-$ is common in the initial stage of anodic dissolution of Cu. What's more, the reaction between $CuCl_2^-$ complex and OH^- is responsible for the formation of Cu_2O.

$$2CuCl_2^{-} + 2OH^{-} \rightarrow Cu_2O + H_2O + 4Cl^{-} \quad (5.6)$$

Equation (5.6) is shifted to the right as the local concentration of $CuCl_2^-$ complex increases and cuprous oxide is deposited in response. The equilibrium constant, K_2, for the equation (5.6) at 25 °C is as follows,

$$K_2 = \frac{[Cl^{-}]^4}{[CuCl_2^{-}]^2[OH^{-}]^2} = 10^{20} \quad (5.7)$$

The stability of Cu_2O is inversely dependent on the concentration of chloride ions [26].

As described in figure 5.2(d), we observed the generation of yellow insoluble precipitates (Cu_2O) from the Cu anode at 30 s after the initiation of the discharge. This phenomenon makes us reconsider the synthesis mechanism of Cu_2O nanoparticles. According to the equation (5.6), we consider that the reaction between $CuCl_2^-$ and OH^- should be responsible for the synthesis of Cu_2O.

In order to confirm this speculation, we used a H-shape vessel as the reaction vessel so that the distance between cathode and anode zone becomes larger. Figure 5.3 shows the temporal variation of the color of the BTB-admixed electrolyte by using a reactor of H-shape vessel. The pH value before the initiation of the discharge was 5.8, thus the color of the electrolyte was yellow as shown in figure 5.3(a). After plasma treatment for 7 min, the part of the plasma cathode zone was completely filled with blue colored solution which meant the plasma treatment produced the OH^- ions and these ions were slowly diffused in the solution. As shown in figure 5.3(c), it was clear to see that the whole solution was

separated into blue and yellow parts after the plasma treatment for 19 min. This result showed that the blue liquid could not reach the Cu anode which might be the reason for gravity. After the collection of the products obtained at Cu anode area and XRD measurement, the result indicated that the products were composed of $Cu_2(OH)_3Cl$ which demonstrated the importance of OH^- ions.

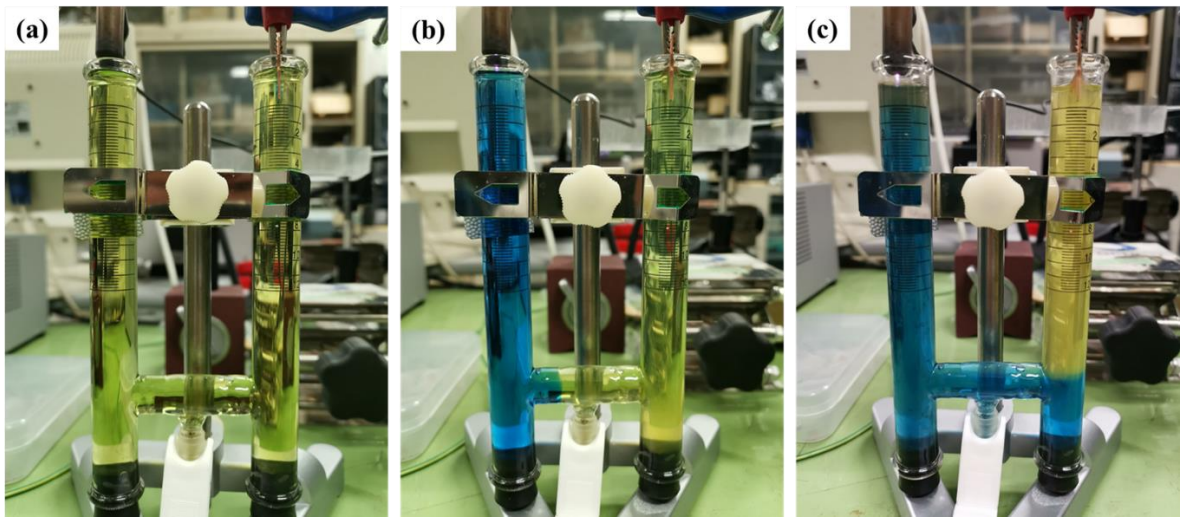

Figures 5.3. Photographs of H-shape reactors with the admixture of BTB. (a): before the discharge, (b): at 7 min after the initiation of the discharge and (c): at 19 min after the initiation of the discharge.

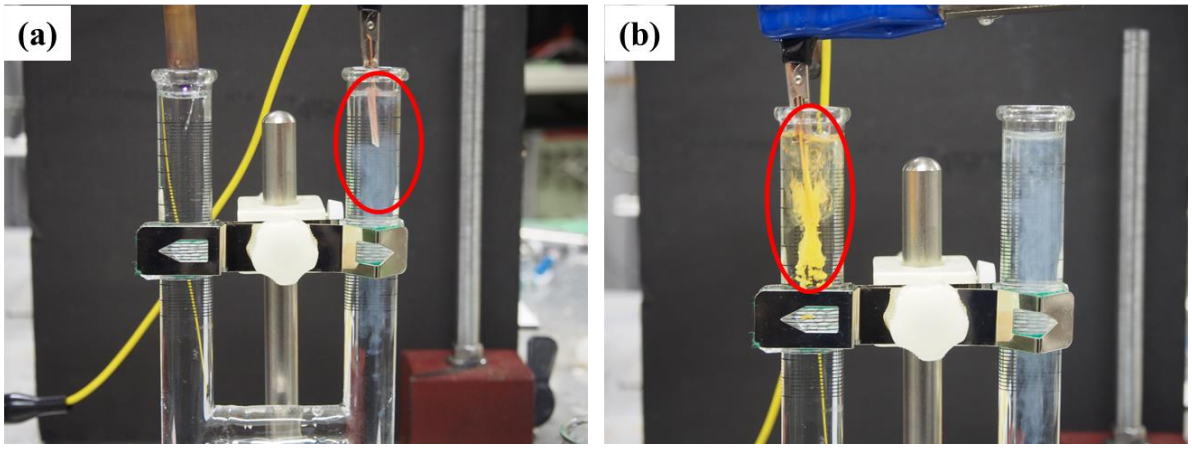

Figures 5.4. Photographs of H-shape reactors. (a): at 10 min after the initiation of the discharge, (b): the Cu anode after plasma treatment for 10 min was directly inserted into the cathode solution.

One more experiment was carried out and the result provided the direct evidence for our speculation. As shown in figure 5.4(a), after plasma treatment for 10 min, some insoluble precipitates were generated at the Cu anode area, while the solution at plasma cathode area was transparent. The plasma treatment ended at 10 min, and then the Cu plate was directly inserted into the solution of plasma cathode area as shown in figure 5.4(b). Immediately, amounts of yellow precipitates were generated from Cu plate. According to figure 5.3, we knew that the solution of the plasma cathode area was fulfilled with OH^- ions. As we speculated, when the Cu plate inserted into the solution, OH^- ions reacted with $CuCl_2^-$ complex at the Cu surface and finally Cu_2O was generated as the equation (5.6).

Therefore, based on the experimental results and our understanding on the anodic dissolution of Cu, we propose the possible synthesis mechanism of Cu_2O nanoparticles illustrated in figure 5.5. The synthesis mechanism has two steps. The first step is the production of $CuCl_2^-$ complex. When the electrolysis is started, $CuCl_2^-$ complex begins to form via the approaches described in the equation (5.1) – equation (5.6). It is noted that the equation (5.6) are reversible which means the higher concentration of Cl^- can contribute to the formation of $CuCl_2^-$ complex.

The second step is the reaction between $CuCl_2^-$ and OH^-. OH^- is generated under the irradiation point of the plasma, as shown in figure 5.1(b). The production of OH^- could be owing to the reaction between OH radicals and solvated electrons at the plasma-liquid interface. OH^- ions are transported toward the Cu anode. When OH^- reaches the anode, Cu_2O is formed via the equation (5.6). The importance of this reaction is confirmed by the experimental results shown in figures 5.2(c) and 5.2(d), where we observed the production of Cu_2O nanoparticles when OH^- (or the blue region) arrived at the anode.

The oxidizing of Cu^+ to Cu^{2+} also occurs via the reaction below.

$$CuCl_2^- \rightarrow Cu^{2+} + 2Cl^- + e \quad (5.8)$$

The formation of Cu^{2+} results in the productions of $Cu_2(OH)_3Cl$ and CuO via

$$2Cu^{2+} + 3OH^- + Cl^- \rightarrow Cu_2(OH)_3Cl \quad (5.9)$$

and

$$Cu^{2+} + 2OH^- \rightarrow CuO + H_2O \quad , (5.10).$$

respectively. These are the mechanism for the enhancement of the productions of $Cu_2(OH)_3Cl$ and CuO at a low pH value.

As described above, there are three important factors for the efficient synthesis of Cu_2O nanoparticles: (1) the high concentration of Cl^-, (2) the production of a large amount of OH^-, and (3) the efficient transport of OH^- toward the anode. We tested the synthesis of Cu_2O nanoparticles by using $NaNO_3$ solutions with concentrations of 0.25, 0.5 and 1.0 M. As a result, we did not observe Cu_2O nanoparticles and the products were occupied by CuO. This result suggests that $CuCl_2^-$ is the particular intermediate for the synthesis of Cu_2O.

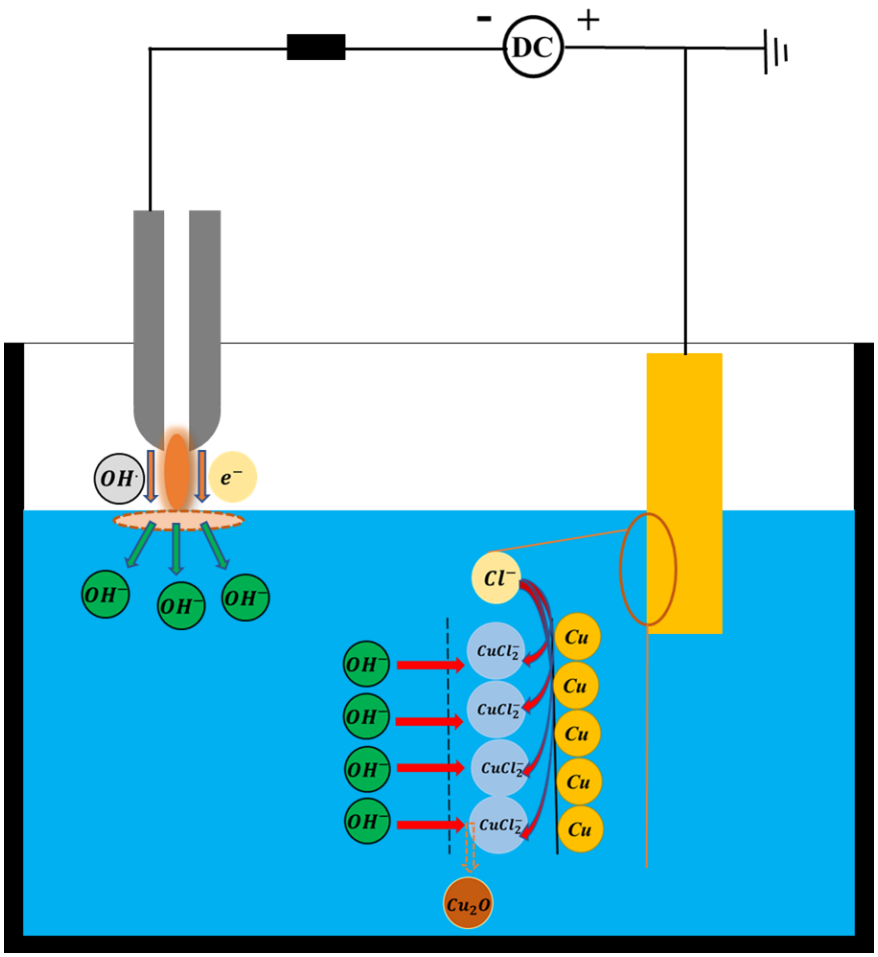

Figure 5.5. Schematic of possible synthesis mechanism of Cu_2O nanoparticles.

5.3 Cu_2O nanoparticles synthesized by conventional electrolysis

It is well known that OH^- is produced on the cathode via

$$2H_2O + 2e \rightarrow H_2 + 2OH^- \quad (5.11)$$

in the conventional electrolysis. Therefore, according to the mechanism proposed in section 5.2, the plasma electrolysis is not the unique method for the synthesis of Cu_2O nanoparticles.

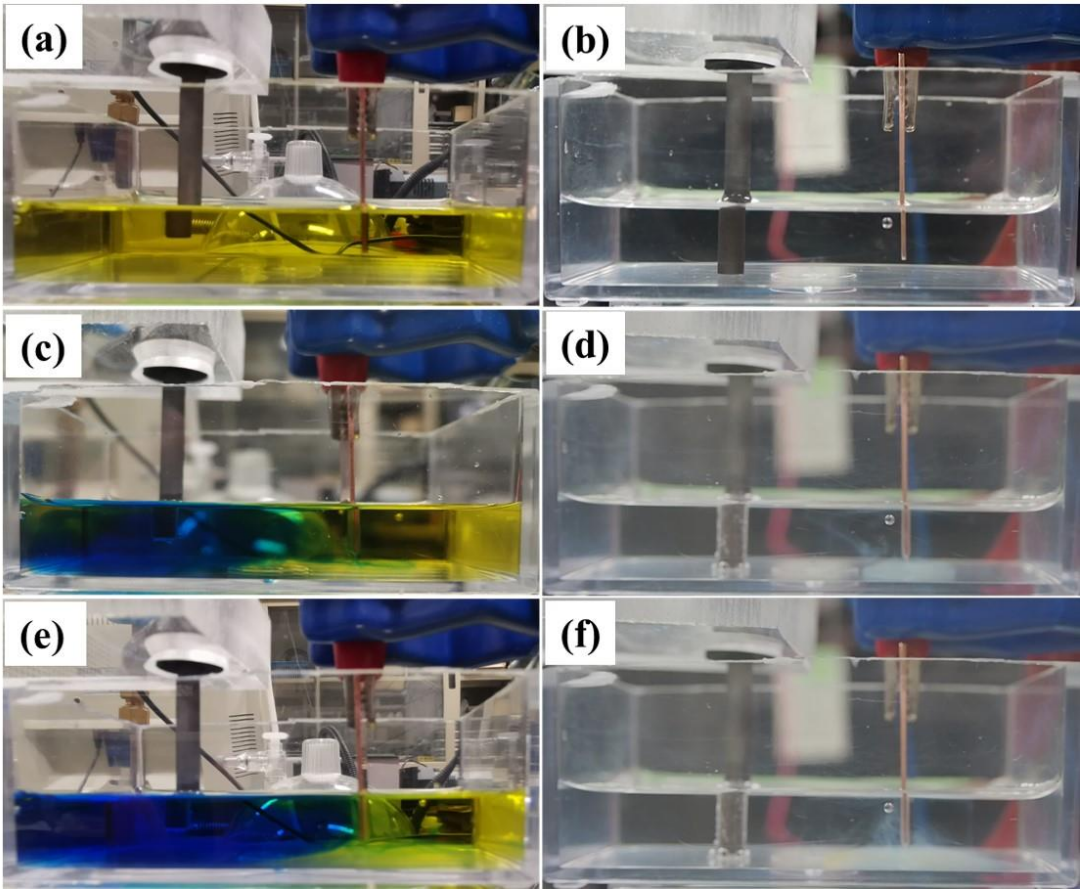

Figure 5.6. Photographs of reactors in conventional electrolysis with ((a), (c), and (e)) and without ((b), (d), and (f)) the admixture of BTB. (a) and (b): before the discharge, (c) and (d): 3 min after the initiation of the discharge, and (e) and (f) at 7 min after the initiation of the discharge.

Figure 5.6 shows the pictures of the reactor when the plasma cathode was replaced with a carbon rod which was immersed into the NaCl solution with the admixture of BTB. The NaCl concentration was 0.5 M. As shown in the figure 5.6(c), at 3 min after the initiation of the discharge, the region of the electrolyte below the carbon rod cathode became blue color which meant this area of solution was alkaline. Compared with plasma electrolysis shown in figure 5.1(c), the transport of OH^- was quite slow. Since the most region of electrolyte became blue at 2 min after the initiation of the discharge in plasma electrolysis. At 7 min after the initiation of the discharge, we observed that the blue area or alkaline area reached the Cu anode as shown in figure 5.6(e). At the same time, insoluble precipitates could be clearly found in the electrolyte.

As a result, we observed the synthesis of Cu_2O nanoparticles from the Cu anode. However, we needed a much longer time to observe the production of Cu_2O. This may be due to the less efficient production and transport of OH^- toward the anode.

Figure 5.7 shows the XRD patterns of the products synthesized by conventional electrolysis at three NaCl concentrations between 0.25 and 1.0 M. In the case of the 1.0 M NaCl solution, we observed only the peaks corresponding to Cu_2O. The peaks corresponding to $Cu_2(OH)_3Cl$ and CuO appeared in the case of the 0.5 M NaCl solution. In addition, at an NaCl concentration of 0.25 M, the peaks corresponding to Cu_2O disappeared, and the product was occupied by $Cu_2(OH)_3Cl$ and CuO which was different with the case of plasma electrolysis under the same condition as shown in figure 4.2.

The FESEM images of nanoparticles synthesized by the conventional electrolysis at three NaCl concentrations are shown in figure 5.8. It is obvious that the NaCl concentration affects the size and the shape of synthesized nanoparticles. In the case of the 1.0 M NaCl solution, nanoparticles were composed of octahedrons, fibers, and small flakes. The size of octahedrons was smaller than 1 μm, and octahedrons had sharp apexes, as shown in figure 5.8(a). The morphologies of nanoparticles synthesized at NaCl concentrations of 0.5 and 0.25 M were similar. Octahedrons were not observed, and the products were occupied by flakes and fibers. The flower shape structures, which were probably aggregated fibers, were also observed.

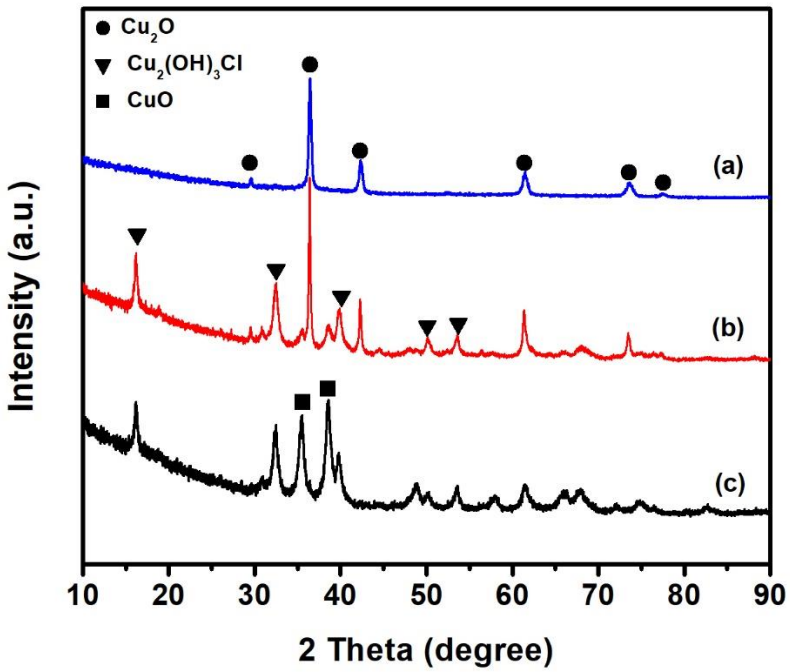

Figure 5.7. XRD patterns of nanoparticles synthesized by conventional electrolysis at NaCl concentrations of (a)1.0, (b) 0.5, and (c) 0.25 M.

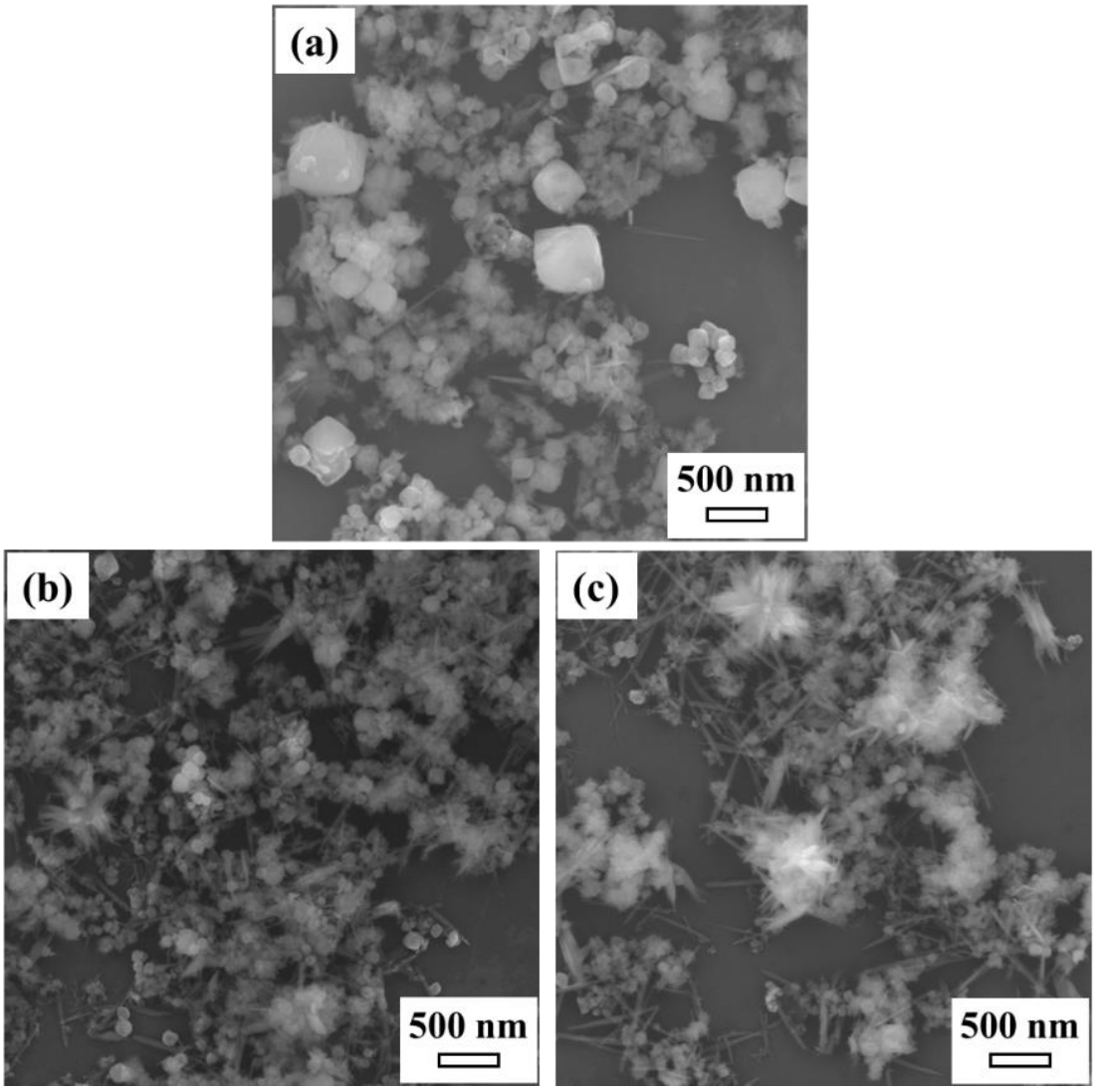

Figure 5.8. FESEM images of nanoparticles synthesized by conventional electrolysis at NaCl solutions of (a) 1.0, (b) 0.5, and (c) 0.25 M.

The samples synthesized at NaCl concentrations of 1.0 and 0.5 M were analyzed by TEM. Figure 5.9(a) demonstrates that the sample synthesized in the 1.0 M NaCl solution was composed of octahedrons and fiber structures. Figure 5.9(b) shows the SAED pattern which was taken from the edge of an octahedron. The SAED pattern shows that the octahedron is Cu_2O having the (110), (111), and (211) facets with interlayer spacings of 0.302, 0.246, and 0.174 nm, respectively. Figure 5.9(c) shows the detailed image of the fiber structure synthesized at an NaCl concentration of 0.5 M. The SAED pattern of the fiber structure is shown in figure 5.9(d). The diffraction rings centered at the transmission spot can be indexed as (113) and (411) with interlayer spacings of 0.237 and 0.142 nm, respectively, indicating that the fiber structure is the polycrystal of $Cu_2(OH)_3Cl$.

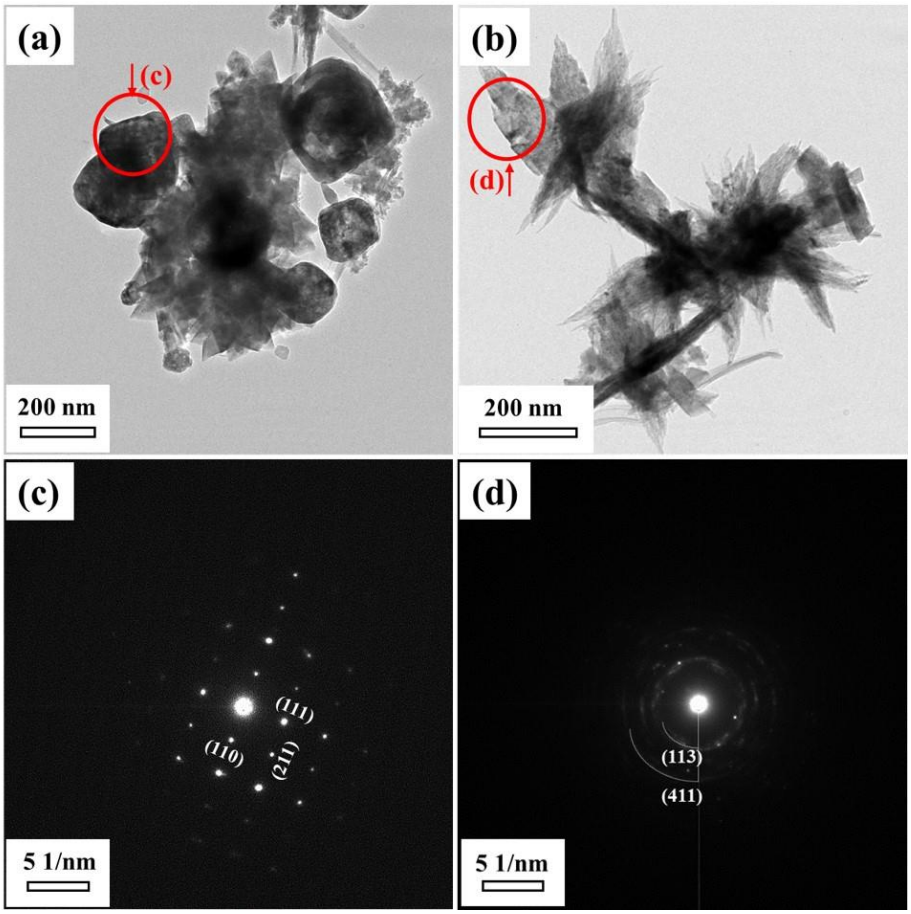

Figure 5.9. (a) and (c) show TEM images of nanoparticles synthesized by conventional electrolysis at NaCl concentrations of (a) 1.0 and (b) 0.5 M. (b) and (d) are SAED patterns of the regions indicated by circles in (a) and (c), respectively.

5.4 Comparison between Cu_2O nanoparticles synthesized by plasma and conventional electrolysis

We find three differences between the plasma and conventional electrolysis for the synthesis of Cu_2O nanoparticles. The first difference is the synthesis rate of Cu_2O, especially at a short ($\leq$ 2 min) delay time after the initiation of the electrolysis. The much higher synthesis rate of the plasma electrolysis than the conventional electrolysis is obtained by the much efficient transport of OH^- toward the anode. The efficient transport of OH^- in the plasma electrolysis is due to the induction of a liquid flow by the plasma-liquid interaction [27].

The second difference is the minimum NaCl concentration at which Cu_2O nanoparticles can be synthesized. In the conventional electrolysis, we did not observe Cu_2O at an NaCl concentration of 0.25 M, as shown in figure 5.7(c), whereas as shown in figure 4.2(c), Cu_2O was produced at the same NaCl concentration in the plasma electrolysis. This difference could be related with the reduction ability in the plasma electrolysis. It is reported that solvated electrons and atomic hydrogen are produced by the plasma-liquid interaction, and they can work as reduction agents in the liquid in the plasma electrolysis [28]. However, it is impossible to expect the transports of solvated electrons and atomic hydrogen to the anode, since they are short-lived species. At the moment, we cannot point out the concrete reduction agents which work around the anode area, if the synthesis of Cu_2O at a low NaCl concentration is owing to the reduction ability of the plasma electrolysis.

The third difference is found in size and the shape of synthesized nanoparticles. As shown in figure 5.8 and figure 4.3, the plasma electrolysis synthesized larger-size octahedron Cu_2O than the conventional electrolysis. The fractional abundances of fibers and flakes were greater in the conventional electrolysis at the same NaCl concentration. In addition, the crystallinity of the fiber structures was completely different, as shown in figure 4.4 and figure 5.9. The mechanism which causes the difference in the morphology and the crystallinity of synthesized nanoparticles is left as an issue in the future work.

5.5 Conclusion

We have proposed the synthesis mechanism of Cu_2O nanoparticles by the atmospheric-pressure plasma electrolysis in the NaCl solution. The results indicate that the Cl^- concentration and the pH value of the electrolyte dominate the synthesis of Cu_2O nanoparticles. Cu^+ ions which are released via the anodic dissolution of Cu combine with Cl^- to form $CuCl_2^-$ at the surface of the Cu plate. Meanwhile, OH^- ions produced by the plasma irradiation are soon transported toward the Cu anode. When OH^- ions reach the surface of the Cu plate, the formation of Cu_2O occurs by the reaction between $CuCl_2^-$ and OH^-. A high NaCl concentration, the efficient generation of OH^-, and the fast transport of OH^- are the important factors for the efficient formation of Cu_2O. The results also indicate that the plasma electrolysis is not a unique method to synthesize Cu_2O nanoparticles. Cu_2O nanoparticles can also be formed by conventional electrolysis. The differences between the plasma and conventional electrolysis are the synthesis rate, the minimum NaCl concentration, and the size and the shape of synthesized nanoparticles.

References

[1] T. Shirafuji, J. Ueda, A. Nakamura, S.P. Cho, N. Saito, O. Takai, Jpn. J. Appl. Phys. **52** 126202 (2013)

[2] P. Pootawang, N. Saito, O. Takai, Mater. Lett. **65** 1037 (20110

[3] Z. Kelgenbaeva, E. Omurzak, S. Takebe, Z. Abdullaeva, S. Sulaimankulova, C. Iwamoto, T. Mashimo, Jpn. J. Appl. Phys. **52** 11NJ02 (2013)

[4] Z. Abdullaeua, E. Omurzak, C. Iwamoto, H.S. Ganapathy, S. Sulaimankulova, L.L. Chen, T. Mashimo, Carbon **50** 1776 (2012)

[5] Z. Kelgenbaeva, E. Omurzak, S. Takebe, S. Sulaimankulova, Z. Abdullaeva, C. Iwamoto, T. Mashimo, J. Nanopart. Res. **16** 2603 (2014)

[6] G. Saito, S. Hosokai, M. Tsubota, T. Akiyama, J. Appl. Phys. **110** 023302 (2011)

[7] G. Saito, S. Hosokai, T. Akiyama, Mater. Chem. Phys. **130** 79 (2011)

[8] C.M. Du, M.D. Xiao, Sci. Rep. **4** 7339 (2014)

[9] J.D. Liu, Q. Chen, J.S. Li, Q. Xiong, G.H. Yue, X.H. Zhang, S.Z. Yang, Q.H. Liu, J. Phys. D Appl. Phys. **49** 275201 (2016)

[10] T. Hagino, H. Kondo, K. Ishikawa, H. Kano, M. Sekine, M. Hori, Appl. Phys. Express **5** 035101 (2012)

[11] N. Shirai, S. Uchida, and F. Tochikubo, Jpn. J. Appl. Phys., 53, 046202 (2014).

[12] S. Ghosh,a R. Hawtof,a P. Rumbach,b D. B. Go,b,c R. Akolkar,a,* and R. M. Sankaran, Journal of The Electrochemical Society, 164 (13) D818-D824 (2017)

[13] V. S. Santosh K. Kondeti, Urvashi Gangal, Shurik Yatom, and Peter J. Bruggeman, J. Vac. Sci. Technol. A 35, 061302 (2017).

[14] J Patel1, L Nemcov ˇ a´2,3, P Maguire1, W G Graham2 and D Mariotti, Nanotechnology 24 245604(2013).

[15] Bruggeman P J et al., Plasma Sources Sci. Technol. **25** 053002 (2016).

[16] Liu J D, He B B, Chen Q, Liu H, Li J S, Xiong Q, Zhang X H, Yang S Z, Yue G H, and Liu Q H, Electrochemica Acta **222** 1677 (2016).

[17] Liu J D, He B B, Wang X, Chen Q, and Yue G H, Eur. Phys. J. D **73**: 11 (2019).

[18] Jiandi Liu, Naoki Shirai and Koichi Sasaki, which has been accepted by J. Phys. D: Appl. Phys., https://doi.org/10.1088/1361-6463/abca2a.

[19] Kear G, Barker B D, and Walsh F C 2004 Corros. Sci. 46 109

[20] H.P. Lee, K. Nobe, J. Electrochem. Soc. 132 (1985) 1031.

[21] H.P. Lee, K. Nobe, J. Electrochem. Soc. 133 (1986) 2035.

[22] A.L. Bacarella, J.C. Griess, J. Electrochem. Soc. 120 (1973) 459.

[23] W.H. Smyrl, J. Electrochem. Soc. 132 (1985) 1555.

[24] A.V. Benedetti, P.T.A. Sumodjo, K. Nobe, P.L. Cabot, W.G. Proud, Electrochim. Acta 40 (1995) 2657.

[25] C. Deslouis, B. Tribollet, G. Mengoli, M.M. Musiani, J. Appl. Electrochem. 18 (1988) 374.

[26] M. Kabasakaloglu, T. Kiyak, O. Sendil, A. Asan, Appl. Surf. Sci. 193 (2002) 167.

[27] Rumbach P, Griggs N, Sankaran R M and David B G, IEEE Trans Plasma Sci **42** 2610 (2014).

[28] Rumbach P, Bartels D M, Sankaran R M and David B G, Nat. Commun. **6** 7248 (2015)

APPENDIX EXPERIMENTS

As described in chapter 1, using a solution containing metallic ions as electrolyte has been widely studied in the synthesis of novel metal nanoparticles including Au and Ag nanoparticles. In this method, the metallic ions which are contained in solution can be directly reduced to zero valent metal as $M^{n+} + ne^- = M$, and then form metal nanoparticles. In the case of the Au nanoparticles, Au(III) ions were reduced to Au(0) by H_2O_2 produced via the rapid combination of OH radicals. In the case of the Ag nanoparticles synthesized by plasma-liquid interactions, the Ag^+ ions are directly reduced by solvated electrons or H radicals to Ag^0 and finally form Ag nanoparticles. Therefore, it is also possible that the electrons (including solvated electrons) can reduce the Cu^{2+} ions to Cu^0 theoretically.

In order to confirm this speculation, an experiment was carried out. The apparatus of the experiment was similar to the aforementioned experiments. The cathode was still a helium plasma while the anode was a Pt plate. The electrolyte was a $CuCl_2$ solution with different concentrations: 1.0 mM, 2.5 mM, 5.0 mM and 10 mM.

The photographs of reactors at 5 min after the initiation of the discharge was shown in figure S1. In the case of 1.0 mM $CuCl_2$ solution, the solution was kept blue and nothing was formed as shown in figure S1(a). The case of 2.5 mM $CuCl_2$ solution was similar to the case of 1.0 mM $CuCl_2$ solution. Things became different when the concentration of $CuCl_2$ solution increased to 5.0 mM. Some insoluble precipitates were formed in the solution as shown in figure S1(c). Larger amounts of precipitates could be observed in the case of 10 mM $CuCl_2$ solution.

In order to clarify the composition of the produced precipitates, five times of the experiments of using 10 mM $CuCl_2$ solution was carried out to prepare sufficient samples for XRD measurement. The result is shown in figure S2. According to the XRD pattern, it was obvious that the sample was a mixture of several compositions. In addition, it's difficult to distinguish which peaks belong to which kind of material. This result indicates that it is more complicated in the case of transition metal synthesis via plasma electrolysis than noble metal. However, we are still unclear about why pure Cu nanoparticles can't be synthesized by this method.

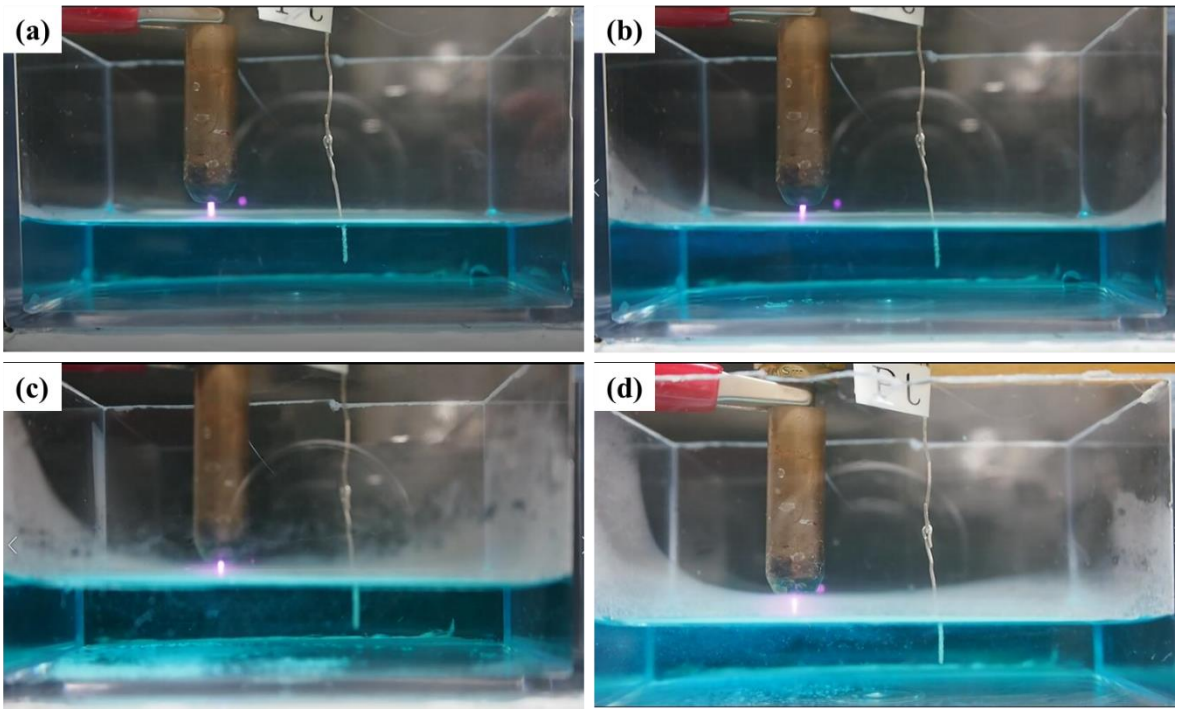

Figure S1. Photographs of reactors at 5 min after the initiation of the discharge. The concentrations of $CuCl_2$ solution are: (a) 1.0 mM, (b) 2.5 mM, (c) 5.0 mM and (d) 10 mM.

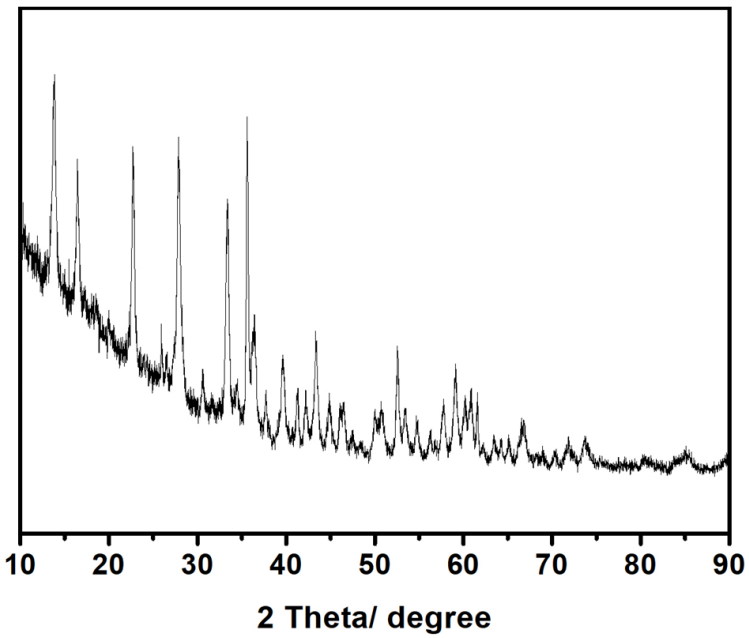

Figure S2. XRD patterns of synthesized products at $CuCl_2$ concentration of 10 mM.

Chapter 6 General Conclusions

Chapter 6 General Conclusions

6.1 Achievement of this study

In this dissertation, the author has successfully synthesized Cu_2O nanoparticles by using atmospheric-pressure plasma electrolysis. On this basis, the effects of additive surfactants were investigated. In order to clarify the synthesis mechanism of Cu_2O nanoparticles, the influence factors which affect the synthesis process were also explored. Based on the experimental results, the author has proposed the appropriate synthesis mechanism. The conclusions of the present work are summarized as follows.

In Chapter 2, a simple atmospheric-pressure argon plasma electrolysis system was used to synthesize Cu_2O nanoparticles in the presence of glucose. The XRD and SEM results showed that the Cu_2O nanoparticles were successfully synthesized which proved the powerful property of the plasma electrolysis. During the plasma treatment, the pH value was changed depending on the compositions of the solution. The influence of the glucose concentration on the crystallinity and shape of the final products was also investigated. The glucose played an important role as the capping agent which could tune the crystallinity and the phase. Amorphous Cu_2O crystalline, Cu_2O nanoparticles and a mixture of Cu_2O nanoparticles and $Cu_2Cl(OH)_3$ were synthesized under the conditions corresponding to high, medium, and low concentrations of glucose, respectively.

In Chapter 3, the effects of the addtive surfactants, glucose, ascorbic acid and cetyltrimethylammonium bromide (CTAB), on the shapes and sizes of the obtained products were experimentally investigated. In the case of glucose, the product formed without surfactant or with low glucose concentration was made of polyhedral and star-like samples. The products formed at high glucose concentration consisted of small-sized nanoparticles and a few sphere-like structures formed by small-sized nanoparticles. In the case of ascorbic acid, as the ascorbic acid concentration increased, the morphologies of products evolved from polyhedral with surfaces littered with small-size nanoparticles, polyhedra with coarse surfaces, polyhedra with smooth surfaces, to small-sized nanoparticles. In the case of CTAB, as the CTAB concentration increased, the morphologies of products evolved from a polyhedron shape, irregular shape, core-shell sphere shape, to spherical shape. The photocatalytic abilities of the produced products were also tested by visible-light photocatalytic degradation of organic dye methyl orange (MO). The results showed that the surfactant of glucose (2.0 mM) was favorable for

obtaining Cu_2O nanoparticles with high absorption efficiency of MO molecules, while the surfactant of ascorbic acid (2.0 mM) favored the formation of Cu_2O nanoparticles with strong visible-light photocatalytic activity on the MO degradation. And the synthesized Cu_2O nanospheres by using CTAB showed good photocatalytic activity on MO degradation.

In Chapter 4, the study on the several factors which affect the synthesis of Cu_2O nanoparticles was carried out. Different from chapter 2 and 3, the solution in this work was NaCl solution without any additives. The effects of the concentration of NaCl solution, the concentration of dissolved oxygen, the electrolyte temperature and the pH value of electrolyte, were investigated. The results indicate that some of them affect the synthesis, but some do not. A higher concentration of NaCl solution is more suitable for the formation of Cu_2O. The concentration of dissolved oxygen does not affect the synthesis of Cu_2O. The higher electrolyte temperature can improve the crystallinity of the final products. A high concentration of OH^- around the anode Cu plate is an important factor for the synthesis of Cu_2O nanoparticles. The most important is that we observe the production of Cu_2O in the vicinity of the anode plate even though the plasma is used as the cathode in the electrolysis system which exceeds our expectation. We originally expected that the reduction of $Cu_2(OH)_2^{2+}$ which was driven by solvated electrons and/or atomic hydrogen at the plasma-liquid interface was the key for the synthesis of Cu_2O. This phenomenon makes us reconsider the synthesis mechanism of Cu_2O.

In chapter 5, we proposed the possible synthesis mechanism of the Cu_2O nanoparticles on the basis of the experimental results. The synthesis mechanism indicates that the Cl^- concentration and the pH value of the electrolyte dominate the synthesis of Cu_2O nanoparticles. A high NaCl concentration, the efficient generation of OH^-, and the fast transport of OH^- are the important factors for the efficient formation of Cu_2O. The experiment results also indicate that the plasma electrolysis is not a unique method to synthesize Cu_2O nanoparticles. We observed the formation of Cu_2O nanoparticles by the conventional electrolysis. Therefore, the comparison between conventional electrolysis and plasma electrolysis was also explored. We found the differences between the obtained products synthesized by conventional electrolysis and plasma electrolysis. They were the synthesis rate, the minimum NaCl concentration, and the size and the shape of synthesized nanoparticles.

In this dissertation, we have proved that it is possible to synthesize Cu_2O nanoparticles by using plasma electrolysis and investigated various kinds of parameters which affect the synthesis products. We proposed the synthesis mechanism of Cu_2O nanoparticles on the basis of the experimental results

and found the Cu_2O nanoparticles could also be formed by the conventional electrolysis.

6.2 Challenges and outlook for the future

In this thesis, a simple plasma-liquid interactions system was used to synthesize Cu_2O nanoparticles. In this system, argon or helium plasma was used as a cathode while Cu plate was used as the anode. The electrolyte was NaCl solutions with different concentrations. In the initial stage, we believed the possibility of synthesizing copper and copper oxide nanoparticles by using plasma-liquid interaction systems because it can produce various kinds of high reactive species. Amounts of research on the Au and Ag nanoparticles synthesis have proved their powerful ability for nanomaterial synthesis. However, the experiments demonstrate that it is different in the case of transition metal nanoparticles compared with the case of noble metal.

We proposed the synthesis mechanism of Cu_2O nanoparticles on the basis of the experimental results and our knowledge on anodic dissolution of Cu. However, there were still some shortcomings on the synthesis of Cu_2O nanoparticles. Even though we have investigated the influence factors on the synthesis of Cu_2O nanoparticles, the formation of byproduct $Cu_2(OH)_3Cl$ is still a problem. The other challenge is that the sizes and shapes of the formed products are not homogeneous. In order to obtain Cu_2O nanoparticles with controlled sizes and shapes, the further experiments need to be done by adjusting both the plasma and liquid parameters.

On the other hand, the proposed synthesis mechanism can also be used to explain the synthesis of transition metal and metal oxide nanoparticles synthesized by plasma-liquid interactions systems such as Iron and Aluminum. Because they are belonging to the transition metal which means they have some similar properties.

ACHIVEMENTS

List of publications

[1] Jiandi Liu, Naoki Shirai and Koichi Sasaki: “Synthesis mechanism of cuprous oxide nanoparticles by atmospheric-pressure plasma electrolysis” Journal of Physics D: Applied Physics, https://doi.org/10.1088/1361-6463/abca2a

[2] Jiandi Liu, Qiang Chen, Junshuai Li, Qing Xiong, Guanghui Yue, Xianhui Zhang, Size Yang and Qing Huo Liu: “Facile synthesis of cuprous oxide nanoparticles by plasma electrochemistry” Journal of Physics D: Applied Physics, vol. 49, No. 27, pp. 275201 (2016)

[3] Jiandi Liu, Bangbang He, Qiang Chen, Hai Liu, Junshuai Li, Qing Xiong, Xianhui Zhang, Size Yang, Guanghui Yue, Qing Huo Liu: “Plasma electrochemical synthesis of cuprous oxide nanoparticles and their visible-light photocatalytic effect” Electrochimica Acta, vol. 222, pp. 1677-1681 (2016)

[4] Jiandi Liu, Bangbang He, Xin Wang, Qiang Chen, and Guanghui Yue: “Morphology-controlled synthesis of cuprous oxide nanoparticles by plasma electrochemistry and its photocatalytic activity” The European Physical Journal D, volume 73, No. 11 (2019)

List of presentation in international conference

[1] Jiandi Liu, Naoki Shirai, and Koichi Sasaki: “Effect of dissolved oxygen on the synthesis of copper oxide nanoparticles by atmospheric pressure plasma electrolysis”, 71th Annual Gaseous Electronics Conference, Portland, USA, 2018

[2] Jiandi Liu, Naoki Shirai, and Koichi Sasaki: “Effect of current on the synthesis of copper oxide nanoparticles by atmospheric-pressure plasma electrolysis”, XXXIV International Conference on Phenomena in Ionized Gases (XXXIV ICPIG) and the 10th International Conference on Reactive Plasmas (ICRP-10), Sapporo, Japan, 2019

[3] Jiandi Liu, Naoki Shirai, and Koichi Sasaki: “Influence of the pH value on the mechanism of cuprous oxide synthesis by atmospheric-pressure-plasma electrolysis”, The 11th Asia-Pacific International Symposium on the Basics and Applications of Plasma Technology (APSPT-11), Kanazawa, Japan, 2019

List of presentation in domestic conference

[1] Jiandi Liu, Naoki Shirai, and Koichi Sasaki: “Effect of dissolved oxygen on the synthesis of copper oxide nanoparticles by atmospheric-pressure plasma electrolysis”, 36th Symposium on Plasma Processing (SPP36) / The 31th Symposium on Plasma Science for Materials (SPSM31), Kochi, Japan, 2019

[2] Jiandi Liu, Naoki Shirai, and Koichi Sasaki: “Effect of electrolyte volume on the synthesis of copper oxide nanoparticles by atmospheric-pressure plasma electrolysis”, the 66th JSAP Spring Meeting, Tokyo, Japan, 2019

[3] Jiandi Liu, Naoki Shirai, and Koichi Sasaki: “Effect of pH on the synthesis of cuprous oxide nanoparticles by atmospheric-pressure plasma electrolysis”, the 80th JSAP Autumn Meeting, Sapporo, Japan, 2019

[4] Jiandi Liu, Naoki Shirai, and Koichi Sasaki: “Comparation between plasma electrolysis and conventional electrolysis on the synthesis of copper oxide nanoparticles”, the 67th JSAP Spring Meeting, Tokyo, Japan, 2020

ACKNOWLEDGEMENT

This thesis is based on the study carried out under the direction and supervision of Professor Koichi Sasaki and Associate Professor Naoki Shirai, at Graduate School of Engineering, Division of Quantum Science and Engineering, Hokkaido University. The author would like to express his deepest gratitude to their generous guidance and invaluable suggestions.

The author is also grateful to Associate Professor Qiang Chen, at Fujian Provincial Key Laboratory of Plasma and Magnetic Resonance, Institute of Electromagnetics and Acoustics, Department of Electronic Science, Xiamen University, and Associate Professor Guanghui Yue, at Department of Materials Science and Engineering, College of Materials, Xiamen University.

The author would like to appreciate the great help and kindly encouragement of all the members of Professor Sasaki's laboratory.

Finally, the author wishes to thank his family for their continuous encouragement.